Journal of Physics D: Applied Physics

ROADMAP • OPEN ACCESS

The 2026 thermionic converters roadmap

To cite this article: Alessandro Bellucci *et al* 2026 *J. Phys. D: Appl. Phys.* **59** 263001

Journal of Physics D: Applied Physics

Check for updates

OPEN ACCESS

RECEIVED
26 May 2025

REVISED
21 February 2026

ACCEPTED FOR PUBLICATION
17 April 2026

PUBLISHED
2 July 2026

ROADMAP

The 2026 thermionic converters roadmap

Alessandro Bellucci[1,22,*], Daniele M Trucchi[1,22], Gideon Segev[2,22], Ryan Jacobs[3], Dane Morgan[3], John Booske[3], Muhammad M Hasan[4], Ramiz Zulkharnay[5], Neil A Fox[5], Paul W May[5], L K Ang[6], Chace Franey[7], Mohammad Ghashami[8], Alessio Mezzi[9], Jared W Schwede[10], Nicolas A Loubet[11], Katie Bezdjian[11], Esther López[11], Alejandro Datas[11], Mohammadamin Jalili[12], Alireza Nojeh[12], Ehsanur Rahman[13], Xin Zhang[14], Peter Schindler[15], Elizabeth D Juette[16], Van P Carey[16], Jean-Pierre Fleurial[17], Matteo Mastellone[1], Guanghua Zheng[18], Lili Wang[19], Gang Xiao[20] and Hao Qiu[21]

[1] CNR-ISM, Consiglio Nazionale delle Ricerche-Istituto di Struttura della Materia sez. Montelibretti, DiaTHEMA Lab, Via Salaria km 29.300, 00015 Monterotondo Scalo (RM), Italy
[2] School of Electrical Engineering, Tel-Aviv University, Tel-Aviv, PO Box 39040, Tel Aviv 6997801, Israel
[3] University of Wisconsin-Madison, 500 Lincoln Dr, Madison, WI 53706, United States of America
[4] School of Applied Sciences and Technology, Shahjalal University of Science and Technology, Sylhet, Bangladesh
[5] School of Chemistry, University of Bristol, Bristol BS8 1TS, United Kingdom
[6] Singapore University of Technology and Design, 8 Somapah Road, Singapore 487372, Singapore
[7] University of Nebraska-Lincoln, 1400 R St, Lincoln, NE 68588, United States of America
[8] University of Illinois Chicago, 840 S Wood St Ste 920SN, Chicago, IL 60612, United States of America
[9] CNR-ISMN, Consiglio Nazionale delle Ricerche-Istituto per lo Studio dei Materiali Nanostrutturati, Via Salaria km 29.300, 00015 Monterotondo Scalo (RM), Italy
[10] Spark Thermionics, Inc., 1036 Ashby Ave, Berkeley, CA 94710, United States of America
[11] Universidad Politécnica de Madrid, Instituto de Energía Solar, Avenida Complutense, 30, 28040 Madrid, Spain
[12] The University of British Columbia, Vancouver, BC V6T 1Z4, Canada
[13] Department of Electrical and Electronic Engineering, Bangladesh University of Engineering and Technology, Dhaka 1000, Bangladesh
[14] School of Science, Jiangnan University, Wuxi 214122, People's Republic of China
[15] Northeastern University, Department of Mechanical and Industrial Engineering, Boston, MA, United States of America
[16] University of California, Berkeley, 101 Sproul Hall, Berkeley, CA 94720, United States of America
[17] Jet Propulsion Laboratory, California Institute of Technology, 4800 Oak Grove Dr, Pasadena, CA 91109, United States of America
[18] Institute of Energy, Hangzhou Dianzi University, Hangzhou 310018, People's Republic of China
[19] Zhejiang Technical Institute of Economics, Hangzhou 310018, People's Republic of China
[20] Zhejiang University, 866 Yuhangtang Rd, Hangzhou 310058, People's Republic of China
[21] Shandong University, 79, ShandaSouthRd, Jinan, Shandong, People's Republic of China
[22] Guest Editors of the Roadmap.
[*] Author to whom any correspondence should be addressed.

E-mail: alessandro.bellucci@cnr.it, danielemaria.trucchi@cnr.it and gideons1@post.tau.ac.il

Keywords: work function, device efficiency, thermal-to-electrical power, plasma-filled converter, thermionic energy conversion, electron emission, electrode spacing

Abstract

Thermionic technologies are based on electron emission from a material occurring at high temperatures, following the physical mechanism discovered by Richardson at the beginning of the 20th century. Although thermionic emitters were successfully used to produce commercial electronic devices, sensors, and electron sources, the large potential of this technology for the development of energetically active devices for space and terrestrial applications is still unexploited, since several challenges remain unresolved to enable practical implementation of competitive energy converters. This roadmap aims to collect the main efforts of the research and industrial community focused on thermionic technologies, covering aspects related to active materials, components and system engineering for the development of related devices. Additionally, contributions related to the progress of promising approaches for the prediction and design of the systems, as well as hybridization with other technologies or physical mechanisms, are also considered. The scope is to provide a guide for researchers and developers who are experienced on this topic—but also who are starting to work with it—by analytically describing state-of-the-art, technological challenges and future paths for a full development of thermionic technologies.

Contents

Acronyms

2D	Two-dimensional
3D	Three-dimensional
AC	Alternating Current
AES	Auger Electron Spectroscopy
AI	Artificial Intelligence
ALD	Atomic Layer Deposition
CB	Conduction Band
CFD	Computational Fluid Dynamics
CL	Child–Langmuir
CNT	Carbon NanoTube
CSP	Concentrated Solar Power
CVD	Chemical Vapor Deposition
DC	Direct Current
DFT	Density Functional Theory
EDA	Electronic Design Automation
ETL	Electron Transport Layer
FE	Field Emission
FEM	Finite Element Method
FL	Fermi Level
FN	Fowler–Nordheim
HTL	Hole Transport Layer
ITO	Indium Tin Oxide
IV	Current–Voltage
KPFM	Kelvin Probe Force Microscopy
LCOE	Levelized Cost of Electricity
ML	Machine Learning
MLIP	Machine Learning Interatomic Potential
MEMS	Micro-Electro-Mechanical Systems
NEA	Negative Electron Affinity
NFTPV	Near-Field Thermophotovoltaics
NSC	Negative Space Charge
PDE	Partial Differential Equations
PE	PhotoEmission
PEA	Positive Electron Affinity
PETE	Photon-Enhanced Thermionic Emission
PIC	Particle-In-Cell
PINN	Physics-Informed Neural Network
PV	Photovoltaic
RLD	Richardson–Laue–Dushman
SCLE	Space Charge Limited Emission
TE	Thermionic Emission
TEC	Thermionic Energy Converter
TEG	ThermoElectric Generator
ThEEM	Thermionic Electron Emission Microscopy
TIPV	Thermionic–Photovoltaic
TPV	Thermophotovoltaic

UPS	Ultraviolet Photoelectron Spectroscopy
VB	Valence Band
VL	Valence Level
VED	Vacuum Electronic Device
XPS	X-ray Photoelectron Spectroscopy
USSR	Union of Soviet Socialist Republics
WF	Work Function

1. Introduction

Alessandro Bellucci[1], *Gideon Segev*[2] *and Daniele M. Trucchi*[1,*]

[1]CNR-Istituto di Struttura della Materia (CNR-ISM), Italy
[2]School of Electrical and Computer Engineering, University of Tel Aviv, Israel

E-mail: danielemaria.trucchi@cnr.it

Status

Thermionic emission (TE) was historically used as the main mechanism operating in commercial devices such as electron guns for scanning electron microscopy, vacuum sensors or electronic components [1]. The potential of technologies based on TE for active energy generators, such as thermal-to-electrical energy converters, introduced and rationalized in renowned books of Hatsopoulos and Gyftopoulos [2], remains a scientific challenge that has yet to be fully resolved. In the 1960s, the 'Space Race' drove significant advancements in this field, searching for practical, steady-state, and compact power supplies to be applied also in the nuclear sector [3, 4]. However, after the end of the 'Cold War', such efforts disappeared. While TE represents an emerging and competitive solution for power generators from thermal and concentrated solar energy [5, 6], it has yet to achieve large market penetration in these areas.

In principle, the architecture of a thermionic energy converter (TEC) is straightforward: two parallel plates, where a hot cathode emits electrons, and a cold anode collects them. The output power on a load depends on the net electrical current flowing between the electrodes, which follows the Richardson–Dushman law for each one, and on the established voltage, which is, in principle, determined by the work function (WF) difference between the cathode and anode.

The main obstacle lies in the difficulty of developing systems composed of robust materials with the proper finely controlled surface properties. Vacuum TECs represent the most potential efficient solution with respect to vapor-diodes developed in the past. However, achieving an efficient device presents several challenges, including maintaining proper vacuum conditions to avoid degradation of electrodes' surface properties, fabricating a robust vacuum encapsulation technology and dielectric microspacers, controlling anode temperature to reduce electrons' counter-emission, and designing a device geometry that concentrates heat flow on the cathode while minimizing thermal losses.

Previous comprehensive reviews have addressed thermionic energy conversion from both device- and materials-oriented perspectives, providing an important foundation for the field [5, 7]. In contrast, the present roadmap focuses on the most recent advances and emerging directions developed over the past decade, with particular emphasis on new material platforms, advanced modeling approaches, hybrid device architectures, and system-level integration challenges. Finally, this roadmap aims mainly to identify the technological open issues and rationalize the key advancements performed by the scientific community in the past few years in the field of TE technologies, highlighting the predominant research directions in material science, device modeling, and system optimization.

Current and future challenges

Considering the key aspects introduced in the previous paragraph, the development of highly electron-emissive materials with low WF is arguably the most critical challenge for the practical implementation of thermionic technology. Historically, refractory metals such as tungsten, molybdenum, and rhenium have been used in thermionic devices due to their stability and suitability for operation at high temperatures ($\gg$1200 °C). However, these materials exhibit high WF values (>4 eV) and require surface engineering to enhance their electron emission capability. To address this issue, alkali-metal compounds based on cesium (Cs) and barium (Ba) have commonly been deposited on the surface to lower the WF. Even though these coatings have successfully reduced effective WF values even down to 1 eV [8], they suffer from low thermal stability, requiring a dynamic approach for stable coverage and long lifetimes. Alternatively, scandate cathodes, which have been extensively investigated for vacuum electronic devices (VEDs), remain highly relevant to thermionic energy conversion due to their exceptionally low effective WF and high current density [9–11]. However, their long-term stability, operational complexity, and compatibility with compact and sealed converter architectures continue to motivate the exploration of alternative material platforms. Consequently, research to develop durable materials with suitable surface properties remains a pressing need.

Perovskites and rare-earth hexaborides have emerged as promising candidates and represent the focus of sections 2 and 3 of this roadmap, respectively. A more challenging but potentially groundbreaking alternative involves the use of diamond thin films, which can be surface-functionalized to achieve negative electron affinity (NEA), thereby enhancing electron emission efficiency (section 4).

On the other hand, 2D materials (e.g. graphene [12]) present an intriguing opportunity for TE technologies, as they do not conform to classical physics governing bulk systems. As discussed in section 5, their enhanced properties stimulate challenges and opportunities for future advancements in the field.

Section 6 focuses on the importance of engineering the electrodes' surface, which is a very important challenge for the optimization of overall device performance.

However, in the material development route, the use of advanced characterization techniques allows for a quantitative and refined assessment of material surface properties. In thermionics, surface properties and their evolution in temperature, particularly the WF or the electron affinity in case of semiconductors, play a crucial role. Section 7 is dedicated to exploring the most suitable techniques for accurate surface characterization of thermionic systems.

Advances in Science and Technology to Meet Challenges

A critical component for TECs is optimization of the inter-electrode spacing, either by analyzing the effect of cesium vapor filling or by developing vacuum dielectric microspacers. This aspect is examined in detail in sections 8 and 9, respectively, of this roadmap.

Modeling and simulations are powerful tools to optimize the performance of technological devices, providing insights into how to address key challenges and move toward practical implementation. This is even more important for thermionic technologies, which combine at the same time thermal, mechanical, and electrical operating aspects. As discussed in section 10, zero-dimensional and one-dimensional (1D) models are fundamental for analyzing TECs under non-ideal conditions, such as in the presence of space-charge effects, as well as for assessing thermodynamic parameters to determine the optimal conditions for achieving maximum performance (section 11).

The selection of suitable materials for thermionic applications is increasingly benefiting from machine learning (ML). ML-driven approaches offer a significant advantage in accelerating and enhancing the development of cathode and anode materials, as detailed in section 12. Additionally, ML-based methods can be employed to predict and validate the performance of thermionic devices (section 13), providing valuable support in overcoming the challenges associated with thermionic technology.

Another crucial aspect in advancing thermionic technology and achieving competitive performance is its integration with other physical processes for energy conversion. One of the most interesting strategies is photon-enhanced TE (PETE) (section 14), which leverages both photoelectric and thermalization effects to significantly enhance electron emission when a radiation energy is converted [13]. Alternatively, hybridizing thermionic converters with photovoltaic (PV) anodes [14], as discussed in section 15, utilizing both energy carriers (photons and electrons) for thermal-to-electrical conversion, represents a major technological advancement aimed at overcoming the performance limitations of standalone thermionic devices. Additionally, although not specifically addressed in this roadmap, the combination of thermionic generators with thermoelectric converters—electrically independent but thermally coupled in series—represents a promising approach [15–17]. This configuration enables the recovery of heat released at the thermionic anode without compromising the overall performance of the TEC.

Concluding remarks

The widespread deployment of thermionic technologies still remains a demanding challenge, as several critical aspects still require advancement to reach a mature technological stage. This roadmap reports key contributions and concepts in the field to bridge this gap, with a particular focus on applications for thermionic energy conversion. A dedicated discussion explores the potential economic and environmental implications of these technologies (section 16). Finally, section 17 outlines the future directions of thermionics, envisioning the next steps once ongoing scientific and technological efforts lead to the development of high-efficiency devices.

2. Perovskites as next generation thermionic emitter materials

Ryan Jacobs, Dane Morgan and John Booske*

University of Wisconsin-Madison

E-mail: ddmorgan@wisc.edu

Keywords: perovskite oxides, surface terminations, machine learning

Status

Discovering new materials with high electrical conductivity, robust stability under high vacuum conditions, and low WF to enable copious electron emission at high temperature is central to development of next generation thermionics such as energy converters and high power VEDs [18]. Perovskite oxides were first proposed as promising candidates for TE applications in 2016. Prior to this time, perovskites such as $Ba_{0.65}Sr_{0.35}TiO_3$ were used as an insulating coating on Si field emission (FE) cathode tips, and were found to enhance the emission, quantified by reduction in the turn-on electric field to induce FE, by lowering the WF [19, 20]. Perovskites are particularly interesting for thermionics because their crystal structure can produce surfaces with intrinsically polar layers (see figure 1(A)), enabling creation of low WF as a monolithic material without the addition of volatile dipole layers characteristic of dispenser cathodes typically used in VEDs [11] or cesiated semiconductors used in TECs [5]. Density functional theory (DFT) calculations elucidate trends in (001) AO-terminated (e.g. SrO) and BO_2-terminated (e.g. VO_2) perovskite surfaces, and predicted that the (001) SrO-terminated surface of $SrVO_3$ should have a low WF of about 2 eV (see figure 1(B)) [21, 22]. This initial computational work on perovskites for thermionics also revealed that a bulk electronic structure feature, the O p-band center, correlates with the surface-sensitive value of the WF. This correlation enabled follow-on work where high-throughput DFT-based screening was used to enumerate other promising stable, low WF materials. Details are discussed in [18] and references therein.

By 2022, Lin and coworkers had experimentally synthesized $SrVO_3$ and demonstrated that bulk, sintered polycrystalline pellets of $SrVO_3$ exhibited TE with an effective WF in the range of 2.3–2.7 eV (see figure 2(A)) [23]. The polycrystalline surface has a distribution of WFs which result in so-called patch-field effects. Patch-field effects occur because surface patches with different WFs electrostatically interact with each other, resulting in an effective WF higher than the lowest local WF present on the surface [24]. The experimental results of [23] were consistent with a fraction of the emitting surface having an approximate 2 eV WF, although the precise termination microstructure of the emitting surfaces was not explicitly determined in this work.

Two additional studies by Sheikh *et al* [25, 26] from 2024 have extended our confidence in, and understanding of, $SrVO_3$ for TE. The first study described more detailed tests of polycrystalline $SrVO_3$ emission performance, which support the potential of this material for commercial thermionic device application [25]. The results showed that $SrVO_3$ emission was both stable during continuous pulsed emission periods of one hour and reversible as temperature was ramped up and down between 1050 °C–1275 °C, two essential features of a well-performing thermionic cathode. Interestingly, they found that the emission performance for some samples improved over time (see figure 2(B)), suggesting a 'burn-in' property where the emission evolved toward higher current densities over a period of a few hundred hours. The evidence suggested this behavior resulted from changing surface chemistry during operation, where the emitting surface was found to be Sr-enriched after the emission tests. Further study on $SrVO_3$ emission stability, such as examining the kinetics of Sr enrichment, evaporation rate and equilibrium vapor pressure of various species would be highly beneficial to better understand the emission stability. In the second study, Sheikh *et al* used thermionic electron emission microscopy (ThEEM) and high electric field ultraviolet photoelectric spectroscopy (UPS) and obtained the first direct experimental evidence of a low, 2 eV WF surface on $SrVO_3$ (see figure 2(C)) [26]. The use of high field was crucial to overcome the patch-field effects and expose the low WF surface. Meanwhile, the ThEEM data revealed the significant patchiness of the emitting surface (see figure 2(D)).

Current and future challenges

We see three major challenges that must be overcome to realize the full potential of perovskite materials for thermionics. The first challenge involves understanding the source of inconsistency of emission results. As a concrete example, the emission data for polycrystalline $SrVO_3$ from Lin *et al* show most samples having effective WFs in the 2.5–2.9 eV range, with two samples close to 2.3 eV. In thermionic

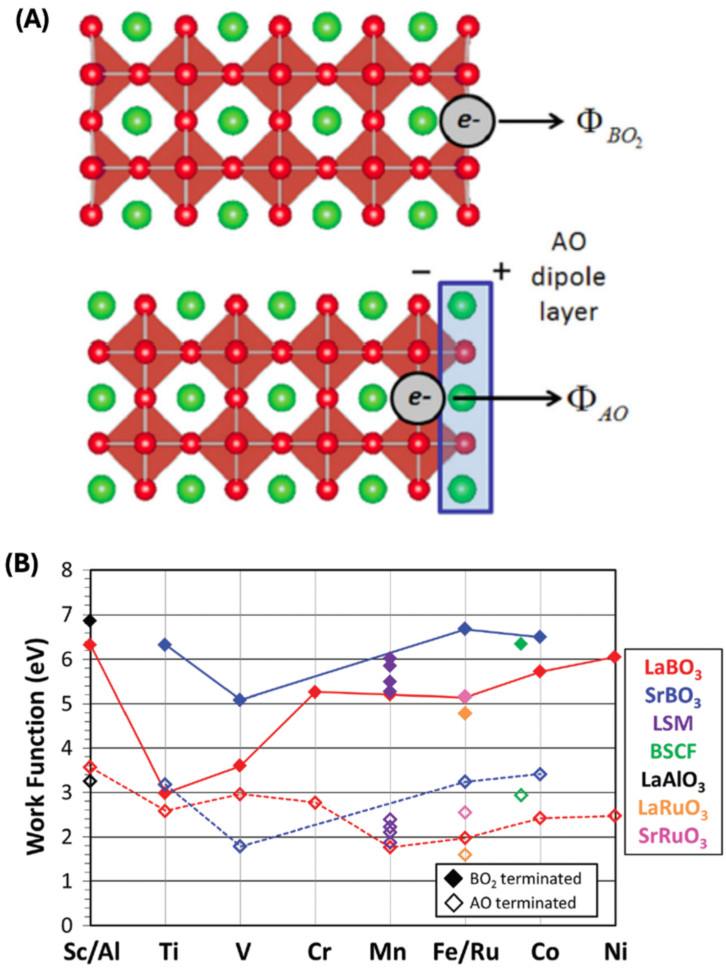

Figure 1. (A) Structure of perovskite $SrVO_3$ (green = Sr, red = O, octahedral centers = V) with (001) orientation showing intrinsic dipole effect. (B) DFT-calculated work functions of AO and BO_2-terminated (001) perovskite surfaces [21]. John Wiley & Sons. {Copyright © 2016 WILEY-VCH Verlag GmbH & Co. KGaA, Weinheim}.

devices, a few tenths of an eV in WF reduction results in exponentially more current at a given operating temperature, and understanding the materials processing (e.g. sintering temperature, time, and ambient gas composition) and sample manufacturing factors (e.g. sintering method, powder pressing pressure and sample dimension) behind such differences in emission performance are key to ensuring reliable emission operation.

The second challenge is related to the first challenge and involves a present lack of understanding of the interplay of surface processing and the resulting atomic-scale surface terminations present on the material. Optimal performance will require establishing an understanding of which surfaces are present on the emitting surface, the processing parameters necessary to obtain the desired surfaces, and how those surfaces may evolve over the lifetime of the emitter.

The third challenge is how best to assess other potentially promising perovskite materials. The bulk of research so far has been on $SrVO_3$, with some limited study of $BaMoO_3$ showing promising emission but significant stability issues such as observed phase transformation and loss of Ba [27]. However, the compositional flexibility of perovskites means there are potentially millions of compositions to explore. High-throughput DFT has been used to shed light on trends and suggest other promising materials from a space of a few thousand. However, having more quantitative and faster evaluation of potential material performance to guide experimental assessment and optimization of the most promising materials is still needed.

Advances in science and technology to meet challenges

The first two challenges above are likely solvable through recent advancements in high-throughput experiments and the development of autonomous research labs. Understanding both the performance inconsistencies and processing-structure-performance relationships could likely be obtained by navigating the high dimensional processing space in the most efficient way using, e.g. active learning

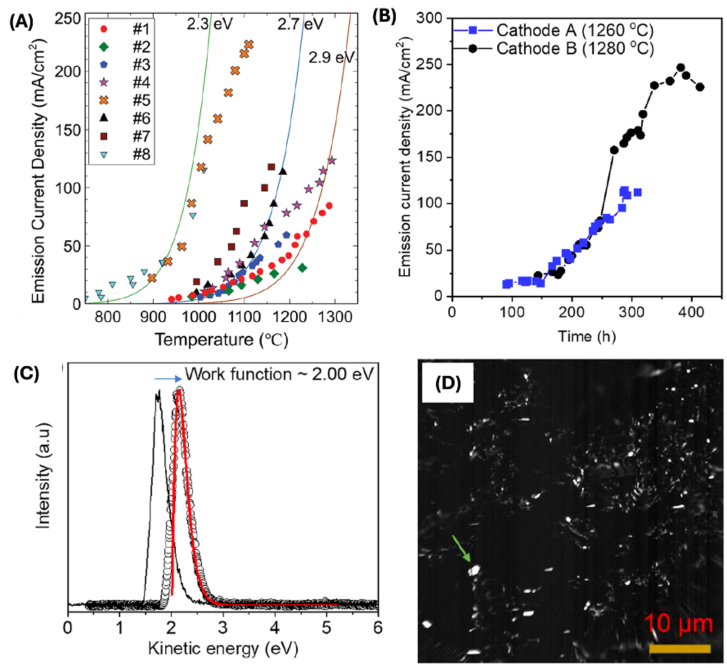

Figure 2. (A) Thermionic emission measurements of $SrVO_3$ (points) with Richardson–Dushman effective work functions (solid lines). (B) Time-dependence of $SrVO_3$ emission for two different samples. (C) High electric field UPS data showing 2 eV work function of $SrVO_3$. (D) ThEEM data at 900 °C showing patchy emission surface. Reproduced with permission from [23]. CC BY-NC-ND 4.0. Reproduced from [25]. CC BY 4.0. Reproduced from [26]. CC BY 4.0.

approaches [28, 29]. As an example, the autonomous lab could be tasked with minimizing the WF in a TE test as a function of variables like sintering temperature, time, pressing pressure, sintering gas ambient, and so on.

The third challenge can be solved by making use of advancements in ML for predicting materials properties and accelerating atomistic simulations (cf section 12). DFT calculations of WF are computationally expensive, and recent work from Schindler *et al* [30] developed an ML model with a novel featurization scheme enabling WF predictions of a particular surface orientation and termination of a material. Using this ML model, one can quickly and semi-quantitatively screen through materials orders of magnitude faster than performing DFT. In addition, recently developed universal ML interatomic potentials (MLIPs) [31, 32] can be used to study surface stability, dynamics, and reactions with environmental factors (e.g. water) shedding additional light on surface structure and chemistry at length and time scales inaccessible with conventional DFT approaches. The continuing maturation of materials databases and ML in materials science [33] holds great promise for accelerating our understanding of complex chemical processes and their impact on materials properties, not only for perovskites, but also to discover totally new classes of materials promising for next-generation thermionic devices.

Concluding remarks

This roadmap provides a succinct overview of the development history of perovskite oxide materials as new thermionic materials, from their inception as a DFT-predicted low WF curiosity to an experimentally demonstrated reality of a promising thermionic emitter. The present state of experimental findings shows emission properties consistent with the initial DFT predictions and sufficiently promising to warrant extensive additional investigation to overcome the key challenges holding back perovskites like $SrVO_3$ from use in commercial thermionic applications. Ongoing innovations in ML and artificial intelligence (AI), and their successful integration into materials research, will be key for understanding the complex processing-structure-performance relationships reflective of the rich chemistry indicative of perovskite materials, and for improving the engineering of these materials to enable electron emitters that emit copiously with consistently low WF and are stable and cheap to produce for next generation thermionic applications.

3. Hexaborides materials for thermionic cathodes

Muhammad M Hasan

School of Applied Sciences and Technology, Shahjalal University of Science and Technology, Sylhet, Bangladesh

E-mail: muhammad.hasan-ipe@sust.edu

Keywords: rare-earth hexaborides, perovskites, work function, current density

Status

In the last several decades, rare-earth and alkaline-earth hexaborides have been extensively studied as potential thermionic emissive materials. They currently show promise for a variety of applications, such as electron emitters, thermionic cathodes for ion and Hall thrusters, thermoelectric materials, coatings, single-photon detectors, and superconductors [34, 35]. Lafferty [34] first reported low WF values (2.6–3.45 eV) of several hexaborides, including CaB_6, SrB_6, BaB_6, CeB_6, LaB_6, etc, during TE. A variety of single and mixed hexaborides ((La, Ba)B_6, (La, Ce)B_6, etc) as single crystals were reported to have relatively lower WF during TE measurements [36, 37]. Recent studies investigating thermionic properties of rare-earth single hexaborides [38–40] and mixed hexaborides [8, 41–43] as solid discs confirm the possibility of achieving lower WF values and higher current densities using these materials. Considering the recent trends of thermionic cathodes, rare-earth hexaborides are found attractive for high-temperature applications due to their high melting points and high-temperature stability. Additionally, these hexaborides exhibit low vapor pressures of their metal species at elevated temperatures (1000 °C–1600 °C), resulting in a low evaporation rate [35, 44]. To date, among rare-earth hexaborides, lanthanum hexaboride (LaB_6) has been identified as the most efficient thermionic material [8, 34, 38–40]. It can produce a stable and high direct current (DC) due to its excellent chemical stability, low WF, high melting point, high electrical conductivity, and long service life. Moreover, it is well-suited for high-temperature applications, where TE can be exploited for solar energy harvesting with a TEC.

LaB_6 shows strong potential as a thermionic emitter owing to its low WF in the range of 2.64–2.93 eV as determined by thermionic tests conducted at a temperature between 1000 °C–1600 °C [34, 36, 39, 45–47]. The summary of the thermionic properties for promising hexaborides, including LaB_6, is given in table 1. Cerium hexaboride (CeB_6) and Gadolinium hexaboride (GdB_6) are also promising as thermionic cathodes owing to their low evaporation rates and low vapor pressures at elevated temperatures under high vacuum. The measured WFs of CeB_6 and GdB_6 emitters have been reported as 2.50 ± 0.09 eV and 2.42 ± 0.09 eV, respectively [40]. In addition, a hexaboride solid solution of $(La_{0.13}Ba_{0.69})B_6$ has been found to have an exceptionally low WF of 1.03 eV and a low emission constant of 8.44×10^{-6} A cm^{-2} K^{-2}, resulting in low DC output [8]. Therefore, materials exhibiting very low WFs and emission constants, such as mixed hexaborides, show strong potential for use as collectors rather than emitters in TEC applications. A eutectic system of LaB_6/VB_2 can be a promising option for high-performance thermionic emitters because of its low WF (1.10 eV) at temperatures below 1273 K [48]. A recent research work reveals that nanocrystalline $(La_{0.25}Ce_{0.25}Nd_{0.25}Eu_{0.25})B_6$ exhibits a remarkably low WF (2.83 eV) and an enhanced current density of 48.3 A·cm^{-2} at 1873 K [41]. Recently, hexaboride–perovskite composite cathodes, namely LaB_6–$BaHfO_3$ (20 wt%) and GdB_6–$BaHfO_3$ (20 wt%), have been reported to exhibit WF values of 2.21 ± 0.13 eV and 1.68 ± 0.03 eV, respectively [49]. These composite cathodes open a new avenue for investigating low-work-function materials with enhanced chemical stability and lifetimes by using perovskites as functional materials.

Current and Future Challenges

The main challenge in developing an efficient TEC lies in developing cathodes—both emitters and collectors—with low WFs. To ensure TEC operation within a practical temperature range, it is essential to develop cathode materials with reduced WFs. Selecting a thermionic cathode that combines a low WF with a high Richardson constant allows for high and stable current densities at operating temperatures, thereby enhancing the power output of the TEC. In a TEC, the collector/anode material needs to have a lower WF to increase the voltage difference between the cathode and anode, thereby maximizing power output. Additionally, a significantly lower Richardson (emission) constant for the anode operating at the lowest maintainable temperature is desirable to minimize back-electron emission [8]. Most of

Table 1. Thermionic properties of hexaborides.

Hexaborides	Work function (eV)	Emission constant (A cm^{-2}K^2)	Temp. (°C)	Maximum current density (A cm^{-2})	References
LaB_6	2.64–2.93	11.5–29	1000–1600	1.55–8.5	[34, 36, 39, 45–47]
CeB_6/GdB_6	2.50–3.02	1.48–3.6	1000–1600	3.1	[36, 40]
$(La_{0.31}Ba_{0.69})B_6$	1.03	8.44×10^{-6}	1000–1200	—	[8]
LaB_6/GdB_6–$BaHfO_3$ (20 wt%)	1.68–2.21	0.01–5.7	1000–1200	—	[49]

the past investigations dealt with pulsed emission phenomena at high temperatures to evaluate thermionic properties; therefore, the measurement of WF and emission constant for bulk hexaboride materials using steady and long-lasting DC emission is still worth considering as a future research approach. Current challenges for potential future applications of TE cathodes are to gain the stability of a micro-gap between the emitter and collector of a TEC and emitted DC current under ultra-high vacuum conditions and to eliminate oxygen contamination and/or cathode poisoning. The presence of a monolayer of a positive metallic element like Ba is thought to lower the WF of any emissive materials [34, 49]. The mixed hexaboride-perovskites (e.g. $BaHfO_3$, $BaZrO_3$, $SrVO_3$ etc) cathodes imparting Ba monolayer have rarely been investigated as thermionic cathodes [23]. Furthermore, nanostructured hexaborides, like other nanoscale materials, are promising candidates for TE cathodes [45].

Advances in science and technology to meet challenges

The necessary development of ultra-high vacuum environment for a TEC or a Schottky device [39] to perform TE testing is critically important. Current advances in science and technology are equipping present researchers with state-of-art technologies. In addition, the mechanism of TE at exceptionally high temperatures is difficult to be fully understood without suitable *in-situ* characterizations. This challenge is expected to be addressed by newly developed devices. Characterization techniques such as photoemission (PE) electron microscopy and ThEEM, x-ray photoelectron spectroscopy (XPS) are now-a-days available to be utilized for better understanding of TE mechanism and surface modifications of emissive materials during TE.

Concluding remarks

For many technologies, especially for electron emitters used in TECs and high-power vacuum electronics such as traveling wave tubes, magnetrons, x-ray tubes, cathode ray tubes, and electron microscopes, etc, engineering a material's WF is crucial. An important step forward in the design of electron emitters would be the discovery and engineering of novel materials like versatile hexaborides with intrinsic, stable, low WFs that are achievable without volatile surface species. Overall, the research to date has shown that rare-earth single and composite hexaborides with two components have superior thermionic emissive potential. Thermionic cathodes based on rare-earth hexaborides, particularly LaB_6, CeB_6, etc, exhibit strong anti-poisoning properties and high emission stability at elevated temperatures compared to tungsten or oxide cathodes. However, some barriers like oxide poisoning towards stable DC emission are still to be delicately addressed. Although there is immense scientific and technological promise in developing composite borides with two or more rare-earth hexaborides that have combined structural and functional performance, few research works are seen. Furthermore, the hexaboride-perovskites, as the rarely investigated thermionic cathodes, open a new research field with potential applications in TECs.

4. Functionalized CVD diamond and other NEA materials for electron emission

*Ramiz Zulkharnay, Neil A Fox and Paul W May**

School of Chemistry, University of Bristol, United Kingdom

E-mail: Paul.May@bristol.ac.uk

Keywords: diamond, chemical vapor deposition, surface functionalization, thermionic emission, negative electron affinity

Status

Electron emission from the surface of a solid into a vacuum has been the foundation of vacuum tube devices for over a century. The efficiency of the emission process was significantly enhanced with the advent of NEA materials, first proposed in 1965 with photocathode materials like gallium arsenide (GaAs), which can exhibit NEA when modified with *p*-type doping and a thin caesium (Cs) capping layer [50]. Specifically, NEA occurs where the conduction band (CB) minimum of a semiconducting material lies above the vacuum level (VL), allowing electrons situated in the CB to escape into the vacuum without having to overcome an additional energy barrier (figure 3(a)). This exceptional property, found only in certain rare materials, can improve electron emission efficiency considerably, making NEA materials critical for applications such as secondary electron emitters, dynode detectors, field-effect transistors, x-ray sources, radiovoltaic cells, high-temperature and radiation-tolerant sensors, *etc.* For TE in particular, NEA materials facilitate efficient electron extraction from solid surfaces, significantly enhancing the performance of TECs. In a TEC, thermal energy excites electrons in a cathode from the valence band (VB) into the CB, which then readily escape the material surface to be collected by a nearby anode. If the two electrodes are electrically connected, current flows back to the cathode, generating electric power [51].

Over the decades, advancements in material science have led to the exploration of various semiconductor materials to find NEA behavior, particularly in the III–V family, such as GaN, GaP, GaAsP, GaAsSb, GaAlAs, InP, InGaAs, InAsP and InGaAsP, reviewed in detail in [53]. Other materials, including AlGaN, AlN, cubic boron nitride and hexagonal boron nitride + carbon nanotubes , also demonstrate NEA characteristics under specific conditions [51, 54]. However, these materials are limited by their lack of emission efficiency and poor long-term stability at elevated temperatures, which leads to degradation due to the adsorption of residual gases and ion back bombardment. These problems ultimately restrict the applicability of many materials in TE devices, where consistent emission is critical.

The early 2000s saw a surge of interest in chemical vapor deposition (CVD) of diamond due to its exceptional thermal conductivity, stability at elevated temperatures, and potential for high-efficiency electron emission, making it a promising candidate for such applications. As such, in this report we shall focus on NEA diamond, noting that other NEA materials have been reviewed in [5, 53].

Current and future challenges

Current research on NEA materials is predominantly focused on functionalized CVD diamond systems, as many of diamond's exceptional properties significantly surpass those of competing materials, such as rare-earth metal hexaborides (LaB_6, CeB_6 and SmB_6), which are primarily used as electron emission sources [5, 6, 51, 55]. Additionally, unlike metals or conventional NEA semiconductors, which typically require temperatures above 1500 °C to achieve TE with current densities below 1 mA cm^{-2}, hydrogen-terminated NEA diamond can initiate emission at temperatures as low as 500 °C, with emission currents that rapidly rise to values >10 mA cm^{-2} as temperatures approach ∼800 °C [51, 55]. However, due to their relatively low C–H bond energy, hydrogenated diamond surfaces remain stable only up to ∼800 °C; beyond this, hydrogen desorbs, eventually leaving a bare carbon surface with a positive electron affinity (PEA) (see figure 3(b)) and significantly reduced emission current. In addition, H-terminated diamond surfaces oxidize in ambient conditions within hours or days, and may undergo so-called surface transfer doping from airborne adsorbates, ultimately degrading the NEA [51]. Consequently, considerable effort has been devoted to identifying alternative diamond surface terminations that can maintain NEA properties but with enhanced thermal and ambient stability.

The NEA surface in diamond is believed to originate from the surface dipole that is generated when an element that is more electropositive than carbon, such as H, bonds directly to the surface C atoms. The dipole that is produced has its positive charge outermost, and this may help attract the electrons from the bulk towards, and eventually out of, the surface. Efforts to find alternatives to H termination

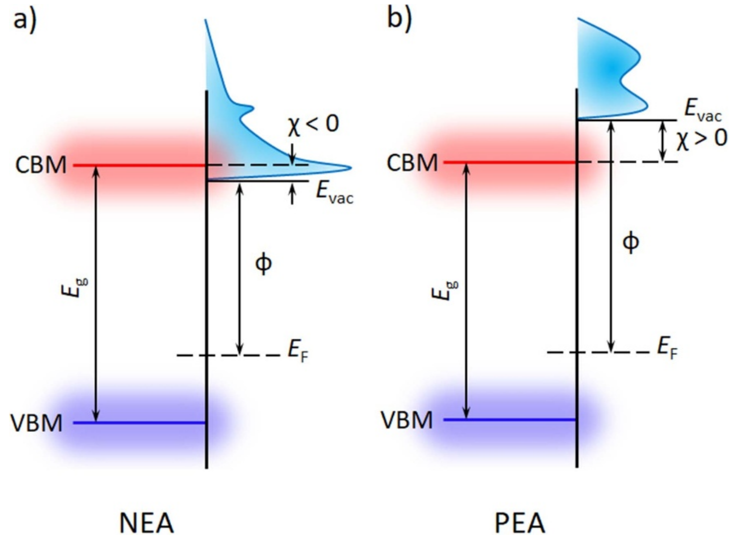

Figure 3. Schematic band diagram illustrating the electron affinity, χ and its relationship to the work function, ϕ, in relation to a fixed Fermi level, E_F, for various semiconductor systems with the density-of-states features for (a) NEA and (b) PEA. The valence band (VB) and conduction band (CB) are represented in blue and red, respectively. E_g and E_{vac} refer to the band gap and vacuum energy, respectively. Reproduced from [52]. CC BY 4.0.

have, therefore, focused upon highly electropositive metals, particularly from Groups 1 and 2, such as Li, Na, Cs, and Mg. NEA diamond surfaces have also been reported for other main group metal terminations (Al, Cu, Sn), several transition metals (Sc, Ti, V, Cr, Zn, Zr) and metalloids (B, Si, Ge) [51, 56]. Many of these M–C systems, indeed, show large NEA values with reasonable thermal stability, however, many metals do not form strong bonds with C, while others react preferentially with oxygen, making the M–C surface unstable in ambient air–potentially an issue when fabricating and handling these materials before packaging.

One potential solution to these challenges is pre-oxidizing the diamond surface before metal deposition. Although using electronegative oxygen for surface termination may seem counterintuitive, pairing it with a sufficiently electropositive metal can produce an M–O–C structure with a *net* NEA. The advantage here is that the metal is already partially oxidized, thus has a much lower tendency for further oxidation, which makes the surface less reactive toward ambient air.

Several such M–O–C configurations have been explored both experimentally and theoretically, revealing a few key insights applicable to both M–C and M–O–C surface structures. Results indicate that smaller metal adsorbates (e.g. Li) are preferable, as these atoms sit closer to the diamond surface, leading to stronger adsorption and better temperature stability. Additionally, metals with high electropositivity or those that readily ionize to form highly charged ions (e.g. Mg^{2+}, Al^{3+}, Sc^{3+}, Ti^{4+}) and form robust bonds with both C and O, are promising candidates for further exploration [56]. Recent reports indicate that Sc-terminated diamond holds the highest NEA values recorded to date for a metal adsorbed onto both bare and pre-oxidized diamond (100) surfaces (figure 4), measured at −1.45 eV and −1.02 eV, respectively, and are stable under ambient conditions, and in vacuum up to 900 °C [52, 57].

However, one of the challenges with pre-oxidizing the diamond surface in the M–O–C system is the formation of various oxygen-carbon bonding configurations, including ketone (C=O), bridging ether (C–O–C), hydroxyl (C–OH), as well as more complex groups like carboxylic acids and lactones. As a result, studies of the M–O–C system have been particularly challenging due to the limited understanding and control over the proportions of these various groups on oxygenated diamond surfaces. This complexity is further heightened by the tendency of certain metals (such as Al, Ti) to preferentially bond with oxygen, resulting in a mixed surface of M–O–C and M–C bonds that can exhibit both NEA and PEA (recall figure 3) [51, 56]. Other adsorbates preferentially bond to one of the possible O–C configurations, meaning a mixture of such configurations leads to reduced adsorption and poorer performance. For instance, Sc adsorbates preferentially bond to ketone groups, resulting in a surface with a large net NEA, a significant surface dipole and excellent thermal stability. Improving these properties, therefore, requires a novel surface-modification approach that disrupts carbon coordination and promotes ketone formation–ideally with 100% coverage. Although TE studies on Sc-terminated diamond have not yet been reported, Sc looks to be the most promising metallic adsorbate for this application so far. This may not be so surprising, as reports over the past decade studying the addition of Sc to other (non-diamond)

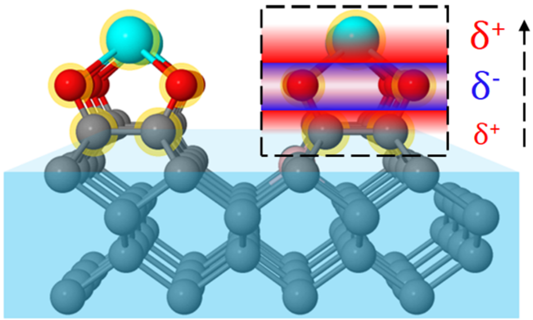

Figure 4. Conceptual dipole model of the ScO-terminated diamond (100) surface, showing outward-facing dipoles (black dashed arrow). The dashed square highlights the positively charged regions (red) and negatively charged regions (blue). Grey, red and cyan spheres are C, O and Sc atoms, respectively. Reproduced from [52]. CC BY 4.0.

thermionic cathodes suggest that Sc stabilizes the surface and reduces desorption, and may reduce the WF or extend the cathode lifespan [11].

In addition to M–O–C configurations, various other surface terminations relevant to diamond NEA have been investigated both experimentally and theoretically, as reviewed in [51]. Among these, the H-terminated BN-diamond (111) system appears highly promising, exhibiting the largest NEA value reported to date (−4.0 eV). However, the adsorption energy for this system is relatively low, and no experimental studies have yet been reported.

More broadly, even when large NEA values are predicted or experimentally achieved across a range of diamond surface terminations, practical electron emission remains constrained by bulk and interfacial limitations. A key challenge is the limited electron supply, arising from the difficulty of achieving high free-carrier concentrations due to the large activation energies of common dopants, particularly in *n*-type diamond [51]. Carrier injection from the bulk to the surface is further hindered by contact resistance, near-surface band bending, and carrier trapping or recombination at defects and grain boundaries, effects that are especially pronounced in CVD-grown films [58]. These challenges are compounded by the low electrical conductivity of CVD diamond, where poor dopant activation and compensation effects typically result in high resistivity, restricting current spreading and increasing Joule heating. A further limitation, common to many thermionic devices, is space-charge accumulation, arising from the build-up of slow-moving electrons near the cathode, which suppresses the electric field and hinders further electron emission [5, 51]. Addressing these coupled limitations will require advances in bulk doping, contact engineering, and charge-transport optimization, alongside continued development of stable NEA surface terminations.

Advances in science and technology to meet challenges

Building on the challenges outlined above, achieving stable, reproducible, and uniform surface coverage remains a central issue in the development of diamond-based thermionic emitters. As such, the problematic variability in O configuration on the oxidized diamond surface is being addressed by a number of approaches. First, a novel oxidation process using high-temperature annealing in water vapor has been reported to produce nearly 100% OH termination [59]. Suitable chemical treatment should allow such surfaces to be converted to near-100% coverage of the desired O configuration, e.g. ketone. Another approach is to use *in situ* exposure to molecular oxygen at atmospheric pressure to selectively convert undesirable O-bonding configurations to those required [60]. Finally, replacing the O-termination with N, to produce M–N–C structures has been reported so far only for Ti and Sc. *Ab initio* calculations suggest that these materials should also exhibit NEA with high-temperature stability [56]. The hope is that the N-terminated diamond might prove to be more reproducible and uniform than its O-terminated counterpart.

An alternative strategy is co-termination with complementary metal pairs. Certain metal pairs (e.g. Li–Sc or Mg–Sc) may have complementary characteristics that deliver NEA while enhancing thermal resilience. Preliminary *ab initio* atomistic simulations may help identify such ideal co-termination pairs and guide experimental optimization of the selection of metal pairs.

The space-charge problem can be mitigated by the addition of trace amounts of molecules such as CH_4 to the vacuum gap, which helps transport the electrons to the anode, or by application of a small bias to draw the electron cloud away from the cathode [51]. Furthermore, electron current can also be greatly enhanced by combining TE with PE (e.g. using UV light from solar radiation) in PETE devices [61], or by injecting electrons *via* beta-emission using the ^{14}C diamond cathode [62].

Concluding remarks

Advances in diamond and other NEA materials through optimized surface functionalization and doping techniques offer significant potential to enhance electron emission rates and improve air and thermal stability. Such NEA materials could find use in many terrestrial and space applications that demand high-performance electron sources, particularly TECs.

5. 2D materials for thermionic electrodes (theoretical models)

L K Ang

Singapore University of Technology and Design, 8 Somapah Road, Singapore 487372, Singapore

E-mail: ricky_ang@sutd.edu.sg

Keywords: electron emission models, 2D materials

Status

Electron emission from a material to free space or from one material to another via its interface is a fundamental process in science and engineering. Depending on the energy used to cause the electron emission or electron injection, it can be broadly characterized into 3 processes: TE (thermal energy), FE (quantum tunneling) and PE (photon absorption or optical tunneling). Regardless of the emission mechanism, the emission current density may become saturated by the space charge limited emission (SCLE). Basic models for these processes (TE, FE, PE, SCLE) have been captured in the Richardson–Laue–Dushman (RLD) equation, Fowler–Nordheim (FN) equation, Keldysh model for PE and Child–Langmuir (CL) equation. These equations are well-known concepts that they are commonly referred without the original papers.

Current and future challenges

Despite of decades in research in improving the classical electron emission models, it remains an active research area [63] especially with the emergence of two-dimensional (2D) materials such as graphene, transition metal dichalcogenides, semi-metals, topological insulators, black phosphorus, and many others. With these 2D materials and applications in engineering, the classical models are undergoing revision to account for the unique properties of 2D materials, as well as new operating regimes in nanometer dimensions and ultrashort time scales.

Here, we will briefly introduce the revision of the emission models due to 2D materials. These revisions are essential because the classical models had made simplified assumptions (based on bulk materials) that are no longer valid for 2D materials. The assumption of parabolic energy dispersion used in the old derivation is not valid that linear dispersion at low energy or specific unique band structure and density of states of the 2D materials should be included in the emission model consistently. The tunable Fermi energy level of 2D materials is also much smaller than metal that large Fermi energy used in the original derivation may not valid. Due to the geometrical shape of the 2D materials, its electron emission becomes direction-dependent, where the electrons emitted horizontally from the edge (or lateral emission), or vertically from the surface (or vertical emission) of the 2D materials are different as the (wrong) isotropic assumption used in the derivation is questionable. Thus, we should consider these three factors in the development of valid electron emission models for 2D materials and compare with the traditional models.

Advances in science and technology to meet challenges

When a material is heated to a high temperature T, the thermal energy gives the electrons enough kinetic energy to escape the surface's barrier by over-barrier emission mechanism. For a classical three-dimensional (3D) bulk material like metal, this TE current density J is described by the classical RLD equation [63]:

$$J_{\mathrm{RLD}} = A_{\mathrm{RLD}} T^{\beta} \exp\left(-\phi / k_{\mathrm{B}} T\right), \tag{1}$$

where $\beta = 2$ (classical model), $A_{\mathrm{RLD}} = \left(qmk_{\mathrm{B}}^{2}\right) / \left(2\pi^{2}\hbar^{3}\right)$ is a constant $= 120.1735$ (A cm^{-2} K^{2}) in SI units, and $\phi = \Phi - \sqrt{4QF}$ is the field dependent WF. Here, q and m are the charge and mass of free electron, k_B is the Boltmann constant, $Q = \alpha\hbar c/4$, a is the Fine structure constant, $\hbar$ is the Plank constant divided by 2β, c is speed of light, k_{B} is the Boltzmann constant, Φ is the zero-field WF and F is the small applied electric field (below the FE regime). Here, we have adopted the same parameters and omitted old references as they are well documented [63]. For a simple triangle barrier, the FE current density is described by the FN equation [63]:

$$J_{\mathrm{FN}} = A_{\mathrm{FN}} F^{\beta} \exp\left(-B_{\mathrm{FN}} / F\right), \tag{2}$$

where $\beta = 2$ (classical model), $A_{\mathrm{FN}} = q / \left(16\pi^{2}\hbar\Phi\right)$ and $B_{\mathrm{FN}} = 4\sqrt{2m\Phi^{3}} / (3\hbar)$ are some numerical constants as a function of Φ. From equations (1) and (2), it is interesting to note that both classical RLD and FN equations follow a scaling of $\ln\left(J/T^{\beta}\right) \propto -1/T$ and $\ln\left(J/F^{\beta}\right) \propto -1/F$, with $\beta = 2$ for both thermionic and FE.

For 2D materials like single layer graphene, the energy dispersion is non-parabolic, the effect of the linear dispersion has modified the RLD equation to have a different scaling from the classical $\beta = 2$ (see below). For example, it was postulated to have $\beta = 3$ from 2 different approaches [64, 65] for TE from a free-standing graphene. The isotropic assumption in the simplified model [64] was questioned by a 3D model for graphene and CNT [66]. This limitation is resolved by a more consistent approach [67] to provide a general scaling for TE of 2D materials with $\beta = 3/2$ and $\beta = 1$ for lateral and vertical emission, respectively, which can be expressed as (for a broad class of 2D materials) [67]:

$$J_{2D}\,[\text{edge}] = A_{||} \times (k_B T)^{3/2} \times \exp\left(-\Phi/k_B T\right), \text{ and} \tag{3}$$

$$J_{2D}\,[\text{surface}] = A_{\perp} \times (k_B T)^{2} \times [1 + \Phi/k_B T] \times \exp\left(-\Phi/k_B T\right). \tag{4}$$

Here, the 2D materials dependent parameters ($A_{||}$ and $A_{\perp}$) can be referred to the details [67]. Equation (3) clearly show a scaling of $\beta = 3/2$ for thermionic *lateral* emission, which recovers a prior model [68]. This scaling also explains why many experiments have been using the 3/2-Arrhenius plotting to characterize various 2D materials lateral-contact in semiconductor devices for which the reversed IV characteristics is basically obeying the TE model. For $\Phi > k_B T$, equation (4) suggest $\beta = 1$ scaling for thermionic *vertical* emission.

A numerical full-band model [69] has been constructed showing that Dirac approximation used in [67] is valid only at near room temperature or low barrier less than 1 eV. The ratio between the Dirac model and full band model is ranged from 0.4 to 1.4 for $\Phi = 0.5$–5 eV and $T = 300$–1000 K. For a graphene with fixed barrier height, this ratio is not sensitive to temperature, which suggests that the analytical equations derived from the Dirac approximation can be fitted by a numerical value calculated from the full band model. Similar to the TE for 2D materials, FE can also be expressed in a general form of [70]

$$J_{FN}\,[2D] = C \times F^{\beta} \exp\left(-D/F\right), \tag{5}$$

where parameters C and D depend on the direction of emission (edge or surface) and 2D materials.

A *vertical* FE model [70] for various 2D semi-metals (graphene and its few-layer, nodal point semimetal, Dirac semimetal and others) has reported same $\beta = 1$ scaling (like thermionic surface emission) at the limit of low temperature $T \to 0$ (or 300 K). An optical tunneling (or AC FE) model [71] for both edge and surface emission are shown to have analytical equations: $\beta = 3/2$ (lateral emission) and $\beta = 1$ (vertical emission) for a large class of 2D materials. The prediction is benchmarked with DFT simulation and an experiment using graphene as cathode. Both $\beta = 3/2$ (lateral emission) and $\beta = 1$ (vertical emission), which is different from the traditional $\beta = 2$ scaling, has been recently verified experimentally [72]. The $\beta = 3/2$ (edge) scaling also agrees with a quantum model based on Bardeen transfer Hamiltonian formalism for graphene [73]. Finally, by combining the effects of thermal and FE, a scaling of $\beta = 3$ is also shown for 3D Dirac and Weyl semimetals [74], which is yet to be verified experimentally. Combining PE and TE, a thermal-photo combined emission model [75] for graphene is in reasonably good agreement with the recent experiment [76]. For thermionic cathode operating at high current regime [77], space charge effects are important [78]. However, the transition from the pure TE models for 2D materials to SCLE is yet to be constructed. In terms of other applications, 2D materials based thermionic cathodes will have the potential to be compact thermionic-based solar and thermal energy converters [5, 6, 15, 79].

Concluding remarks

These models are not only important for basic emission physics, but also as charge injection models to determine the electrical contact resistance, which is one of the key issues in using 2D materials in engineering devices. The analytical scaling of emission models for 2D materials can be readily implemented as sources of electron injection in simulation tools, such as particle-in-cell (PIC) code, EDA tools, and electron gun code used in many areas. These findings will encourage more developments in both formulation and experimental verifications of electron emission for other quantum materials to be studied.

Multi-dimensional models (beyond the 1D models presented here) must be developed to include practical effects such as variation of WFs, surface roughness, non-uniform emission and effects of impurities or dopants. It is also likely that a general emission model of 2D materials to account for field, thermal and photo-emission in a single framework can be constructed at least numerically. Finally, among the emission process, photo-electron emission under light-excitation on different 2D materials is relatively less explored. Due to high WF, a pure graphene is not suitable for efficient TE, thus engineered graphene surface with lower WF is needed.

6. Engineering of electrode surfaces to enhance TEC performance

Chace Franey[1] *and Mohammad Ghashami*[2,*]

[1]University of Nebraska-Lincoln
[2]University of Illinois Chicago

E-mail: ghashami@uic.edu

Keywords: electrode surface engineering, micro/nanostructured emitters, surface-driven enhancement of thermionic emission

Status

Engineering the surfaces of TEC electrodes is a potent yet underexplored strategy for improving device performance. Surface engineering in this context refers to processes aimed at altering the surface topography of the electrode, employing techniques such as laser surface processing, plasma etching, and chemical deposition. There are two primary approaches through which surface engineering can boost TEC performance. The first is to enhance emission through microstructured emitters. Introducing sharp microscale features to the emitter surface increases the effective emitting area and lowers the local potential barrier at the features' apexes due to geometric field enhancement. This modification can lead to field-enhanced TE (via Schottky barrier lowering) and improved current density. The second approach focuses on reducing electron reflection at the collector. Modifying the collector surface to reduce electron reflection enhances its ability to absorb incoming electrons and decreases the buildup of negative space charge (NSC) by minimizing the number of electrons returning to the interelectrode gap. While studies on both methods have shown promising results, significant gaps remain in experimental validation and computational simulation, which are crucial for assessing feasibility and optimizing designs.

Microstructured emitters: Microstructured emitter surfaces have been extensively studied in FE applications, where sharp tips enhance local electric fields and facilitate field-enhanced TE due to the Schottky effect [63]. In TECs with sub-micron vacuum gaps where the potential profile between the electrodes is almost a straight line (as shown in figure 5(a)), similar microstructures can theoretically enhance TE by increasing the local electric field and reducing the potential barrier at the emitter surface, as shown in figure 5(b). Although TECs operate at much lower voltage biases than field emitters, the small interelectrode distances result in appreciable electric fields even at lower voltages, allowing for some degree of Schottky barrier lowering. In the Richardson-Schottky framework, the field enters through a barrier reduction $\varphi \propto \sqrt{E}$, so the emission enhancement is not linear in E but occurs through the exponential factor $J = AT^2 \exp\left[-\left(\varphi - \Delta\varphi\right)/k_{\mathrm{B}}T\right]$ (equation (1) in [80]). For TEC-relevant field in microgaps ($E \sim 10^5$–10^6 V m^{-1}), $\Delta\varphi$ is typically only ≈0.01–0.04 eV, indicating that Schottky lowering is often a secondary effect relative to surface-area enhancement [80]. However, in TECs, maximum power output is typically achieved when the emitter and collector are held at similar potentials, minimizing the electric field between electrodes and thus limiting the influence of Schottky barrier lowering. Consequently, the primary benefit of microstructures in TECs may be the increase in effective emitting surface area rather than field enhancement effects. The current density is increased proportionally to the increase in surface area, and, therefore, the power density of the TEC is also increased. Computational and analytical studies have highlighted the significance of surface area enhancement [80, 81], although some experimental investigations have overlooked this aspect [82].

It is important to note that increasing the emitting surface area also intensifies near-field thermal radiation between the electrodes when the gap distance is less than the characteristic thermal wavelength [83, 84]. Therefore, near-field radiation's simultaneous increase with power density means that the microstructures' effects on efficiency are limited.

Reducing electron reflection at the collector: Reducing electron reflection on the collector has received less attention despite potentially being the cause for discrepancies between experimental results and theoretical predictions of TEC performance. Electron reflection can contribute to NSC buildup by returning electrons to the interelectrode gap. The nature of electron reflection—specular versus diffuse—is critical in this context [83]. Specular reflection sends electrons directly back into the gap, exacerbating NSC, whereas diffuse reflection reduces the likelihood of electrons re-entering the gap, as some of their kinetic energy perpendicular to the collector surface is dissipated. Both surface roughness and microstructural

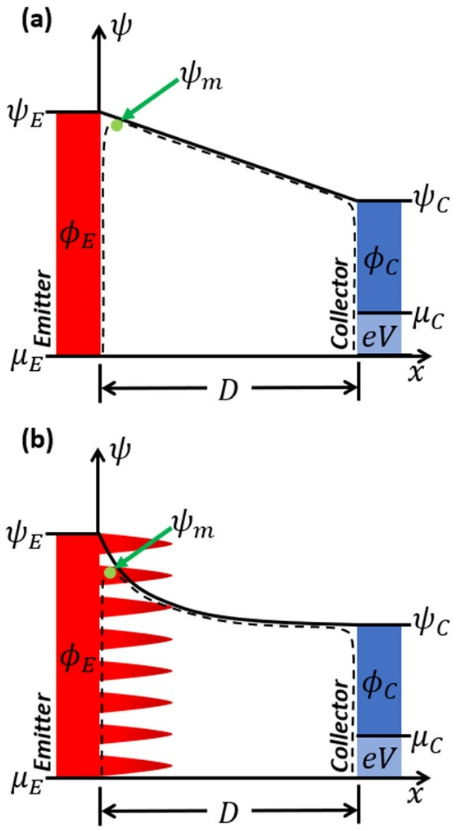

Figure 5. (a), (b) Energy diagrams showing the expected potential profile (a) before the addition of emitter microstructures, and (b) after the addition of emitter microstructures, where **e** is the unit charge, **V** is the applied voltage, **D** is the plane-to-plane interelectrode gap distance, $\phi_{\mathbf{i}}$ is the electrodes' WFs, $\boldsymbol{\mu}_{\mathbf{i}}$ is the electrodes' Fermi levels, $\boldsymbol{\psi}_{\mathbf{i}}$ is the electrodes' potentials, and $\boldsymbol{\psi}_{\mathbf{m}}$ is the maximum potential. Subscript $\mathbf{i} = \mathbf{E}$ stands for the emitter and subscript $\mathbf{i} = \mathbf{C}$ stands for the collector. Reprinted (figure) with permission from [81], Copyright (2024) by the American Physical Society.

disorder (e.g. nanocrystallinity) can promote diffuse reflection [85, 86]. For instance, cesiated nanocrystalline Cr films absorb about 96% of low-energy electrons, compared with 79% for epitaxial Cr(110) films ($a \sim 17\%$ percentage-point increase in absorption), even though their macroscopic roughness is similar [86]. Thus, tailoring collector surfaces whether by introducing controlled roughness, suppressing crystallinity, or applying low-WF coatings, offers a promising route to mitigate NSC and enhance TEC performance.

Current and future challenges

Although previous investigations of surface engineering have offered valuable insights into its ability to improve TEC performance, future studies are needed to fully realize the benefits of electrode surface engineering in TECs. One of the main challenges is experimentally validating the effects of microstructures on the emitter surface under actual TEC operating conditions. Most studies measure the impact of microstructures under high electric fields akin to FE scenarios and extrapolate the results to TEC conditions [82, 87]. This approach does not adequately decouple the effects of increased surface area and Schottky barrier lowering, making it difficult to develop accurate theoretical models.

Designing experiments that simulate TEC conditions with microstructured emitters and collectors separated by microscale gaps is necessary to obtain reliable data for model validation. However, maintaining a microscale gap while ensuring a significant temperature difference between the emitter and collector is challenging due to increase of near-field thermal radiation at small scales [88]. This radiation can lead to unwanted heat transfer that affects the temperature gradient essential for TEC operation. Moreover, current mathematical models may not account for NSC buildup between individual surface features, highlighting the need for comprehensive computational simulations to better understand these effects. Similarly, the unpredictability of electron reflection adds complexity to optimizing the collector surface. The influence of surface topography, crystal structure, and material properties on electron reflection is not fully understood, necessitating further experimental and computational studies.

Advances in science and technology to meet challenges

Recent advancements in materials science and nanofabrication technologies are paving the way to overcome challenges in TEC electrode surface engineering. For emitters, techniques like CVD enable the growth of vertically aligned carbon nanotube arrays and the integration of graphene or other 2D materials, which reduce WFs and enhance TE. Patterning metals such as tungsten into nanostructures via electron beam lithography creates sharp tips that boost local electric fields. Emerging methods like additive manufacturing and 3D nanoprinting allow the production of complex nanostructures tailored for maximum emission while mitigating unwanted thermal radiation.

For collectors, reducing electron reflection is achieved by surface modifications that promote diffuse reflection and enhance electron absorption. Techniques such as plasma etching and laser texturing introduce nanoscale roughness [89], while thin films of low WF materials like cesium or alkali metal oxides can be applied via atomic layer deposition. Utilizing materials with low secondary electron emission coefficients, such as titanium nitride or boron-doped diamond, further minimizes NSC effects and improves collector performance.

Advances in computational modeling and ML are critical for optimizing these engineered surfaces. Quantum mechanical simulations predict material properties to guide electrode design, while multiphysics simulations provide insights into the interplay between electron emission, heat transfer, and structural stability. ML algorithms expedite the exploration of vast design parameters, predicting performance outcomes based on simulation and experimental data. By leveraging these technological advancements, researchers can design electrodes with tailored surface structures and compositions that significantly enhance TE and reduce electron reflection, bringing TEC technology closer to practical applications in high-efficiency energy conversion.

Concluding remarks

Electrode surface engineering holds significant promise for enhancing TEC performance, yet substantial knowledge gaps remain. Both strategies—implementing microstructured emitters to increase surface area and reduce potential barriers and modifying collector surfaces to minimize electron reflection—require further experimental validation and advanced computational modeling to optimize their practical implementation. Addressing these challenges could lead to significant improvements in thermionic energy conversion efficiency and power density, potentially making TECs more viable for practical applications in waste heat recovery, concentrated solar power (CSP), and other areas where high-temperature heat sources are available.

7. Characterization methods of low WF coatings

Alessio Mezzi

National Research Council - Institute for the Study of Nanostructured Materials (CNR-ISMN)

E-mail: alessio.mezzi@cnr.it

Keywords: work function, UPS, electron spectroscopies

Status

The conventional definition of WF is the minimum amount of thermodynamic work required to remove an electron from inside of a solid and place it at rest at a point in free space, positioned ideally at infinity, outside the surface [90]. In practice, the WF is the energy difference between the VL and the Fermi level (FL), being an intrinsic surface property of a material. The WF is very relevant in phenomena involving electron transfer between different materials in contact, or from a material to a vacuum [91]. The main applications in which WF plays a critical role are TE and photoelectric effect, which determine the amount of the emitted electrons [18], as well as in the FE, which determines the amount and direction of emitted electrons in the presence of a strong external electric field. In addition, WF is a good indicator of the surface energy and the electronic structure of materials, revealing important information on surface properties such as adsorption, corrosion, catalysis, etc [90].

The growing interest in green energy storage devices (PV and thermionic) has attracted the attention of many researchers to the development of low WF devices. The study of the WF can be carried out by theoretical calculations [92, 93, 94], however, the experimental approach is preferred since its value is not fixed, for a given material, but depends on various factors such as surface chemical composition, structure, roughness, geometry, local charge distribution, etc.

Basically, the characterization techniques can be roughly classified in two categories, the first based on electron emission processes and the second based on the comparison between the WF of various materials [91]. The most popular techniques are: (1) TE: the WF is measured by providing thermal energy to the material. When sufficient thermal energy is provided to remove electrons from the surface, an electron current is induced and can be measured. This method is described by the RLD equation. It is possible to extrapolate the WF value by measuring the temperature and thermoionic current density and fitting the RLD equation to experimental data [18]. This method can be used to study the WF of many metals (e.g. W, Mo and Ta) and compounds (e.g. LaB_6, BaO and BaF), however, they must be characterized by a high-melting-point and discrete robustness at high temperatures since a sufficient electron current emission occurs at high temperatures (>1000 K); (2) FE: the electrons are removed by tunneling as a consequence of applying a strong electric field. The emission current is proportional to the intensity of the electric field, as described by the FN equation, which includes current density and WF [93]. In practice, WF is calculated by measuring the FE current and the applied voltage. In this method, the materials should be shaped into a sharp tip, to enhance the FE [92]; (3) photoelectron emission (PE): this method is based on the photoelectric effects, namely photons excite electrons from the outer electronic levels. The WF is calculated using the cut-off threshold in the spectrum (e.g. UPS) [90, 95]. PE can be performed to investigate electrical conductors (e.g. Ag, Ag, Cu, etc) and semiconductors (e.g. Si, GaAs, etc), while it cannot be used to investigate bulk insulators, as the charging effect hinders emission of photo-electrons; (4) contact potential difference: it relies on the electrostatic potential difference that occurs when two dissimilar conductive materials, in thermal equilibrium, are brought in contact or electric connection. It is a non-destructive method to investigate WF, in which a conductive probe (reference) is into contact with material whose WF is to be determined. (e.g. Kelvin probe force microscopy-KPFM) [96].

For a comprehensive comparison of WF characterization techniques—covering advantages, limitations, and representative material systems—the reader is referred to [96, 97]. Generally, these characterization techniques have advantages and drawbacks in monitoring the WF value, depending on the material and the type of information required (e.g. local or average WF). However, the most popular characterization techniques are recognized to be UPS and Kelvin probe; UPS is considered more reliable for calculating the absolute WF, while KPFM is faster and more cost-effective technique [98]. Both techniques are surface sensitive, able to investigate few layers of the materials, up to 1 nm. As it concerns UPS, it is generally assembled in apparatus dedicated also for XPS or Auger electron spectroscopy (AES). This is a very powerful tool for characterizing materials, because it allows the WF value to be linked to the surface

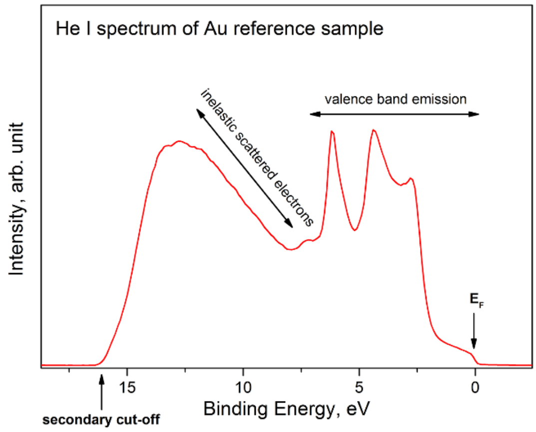

Figure 6. Typical UPS spectrum of reference gold foil, acquired using our apparatus equipped with a He I source ($h\nu = 21.2$ eV).

chemical composition. This can drive research activities towards the optimization of the WFs by identifying the best conditions for improving the surface properties of the materials by etching or thermal treatments or by covering them with other materials. For this reason, the rest of the article will be focused on exploring the methodology and results obtained by UPS and XPS techniques.

Current and future challenges

UPS is a relatively simple technique in which a He lamp is used as a source of photons to excite photoelectrons. Two photon energies can be selected from this source: $h\nu = 21.2$ eV (He I) and 41.2 eV (He II). The investigations of the WF are generally performed using the He I line, while He II line is generally used to study the VB structure. Figure 6 shows a typical spectrum (He I line) acquired from a pure gold (99.9 wt%) reference foil. This spectrum can be divided in three zones: (1) VB emission; (2) inelastic scattered electrons; and (3) secondary electrons threshold (or secondary cut-off).

In the He I spectrum of a grounded conducting metal, the position of the FL can be found at the zero point of the binding energy scale. While the WF is calculated by measuring the energy of the cut-off, and applying the formula (6):

$$\mathrm{WF}\ (\varphi) = h\nu\,(\mathrm{He\ I}) - E_{\text{cut-off}}. \tag{6}$$

Using to this formula, the WF of many metals and semiconductors can be calculated. However, this technique is not applicable to insulator, because the positive charge created on the surface of the sample by the PE process cannot be neutralized, compromising the spectrum acquisition. Fortunately, this phenomenon is avoided in the study of metals and semiconductors, because the sample is in electric contact with the apparatus by a metallic clip.

However, there is another important detail to consider during an UPS measurement, namely, the low kinetic energy cut-off of the apparatus overlaps with the energy cut-off of the sample, which compromises the WF detection. In order to avoid this contribution, a negative bias voltages is applied to the sample. In this way, different bias are applied and the WF is extrapolated at 0 V of bias from the $E_{\text{cut-off}}$ vs $V^{1/2}$ plot, since the WF depends on the bias as a quadratic function (figure 7) [99].

The combined use of UPS and XPS characterizations was successfully employed to minimize the WF value of borides and nitrides coatings for applications in the cathodes of thermoionic- PV device [100]. The analyses revealed that the coatings were characterized by the presence of oxy-borides and oxy-nitrides, as well as by a no-stoichiometric composition, showing an excess of metals. Coatings with low WF in the range 3.2 ÷ 3.4 eV were produced by adjusting the deposition parameters and increasing the concentration of borides and nitrides in the coatings [101]. Further reduction of the WF up to 2.8 eV was achieved by deposition using a femtosecond laser beam, which induced the nanostructuration of the boride films. Interestingly, the obtained value was comparable to that obtained by thermionic characterization (WF = 2.6 eV) [45].

In our studies, we have recognized that the thickness of the deposited coating is an important parameter when a surface dipole is formed that must be considered in the design of the device, as it strongly affects the absolute WF value. This was evidenced by the investigation of barium fluoride and scandium oxides. The obtained results showed that the lowest WF was achieved with a thickness of the film of 2 nm, WF = 2.0–2.7 eV for barium fluoride and scandium oxide, respectively [102, 103]. Interestingly,

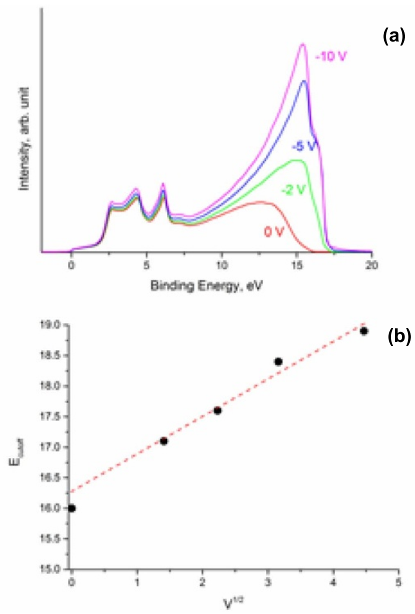

Figure 7. (a) Comparison of He I spectra of reference foil gold acquired using our apparatus and applying a bias of 0 V, −2 V, −5 V and −10 V; (b) E_{cut}-off vs $V^{1/2}$ plot.

a further decrease in thickness leads to an increase in the WF value, giving rise to a characteristic curve. This phenomenon can be explained by considering that for ultra-thin films, the contribution of the substrate to the WF becomes dominant [102].

Advances in science and technology to meet challenges

A further development of the electron spectroscopies (UPS and XPS) for the investigation of the WF could involve the study of materials at temperature above the room temperature, at which spectra are usually collected. In this way, the obtained values could be comparable with those obtained by the thermionic method, and it would eventually be possible to understand how degradation mechanism can damage the materials. For instance, this is of particular interest in the investigation of the perovskites. It is well known that they are very sensitive to the increase of the temperature and tend to degrade at relatively low temperature (∼150 °C), which is a drawback when using them for PV devices. Thus, in this case, the electron spectroscopies may help in the preparation of much more robust perovskites.

Concluding remarks

The growing interest in the development of devices characterized by materials with low WF has focused attention on the method used to detect it. Among all the characterization techniques, UPS offers a versatile and sufficiently accurate method to calculate WF value. Moreover, by combining UPS with XPS or AES, it is possible to study how to modify the deposition parameters to optimize the WF value.

8. Thermionic devices using cesium

Jared W Schwede

Spark Thermionics, Inc.

E-mail: jared.schwede@sparkthermionics.com

Keywords: cesium, plasma, microgap

Status

Cesium-based thermionic energy conversion devices achieved ∼10 W cm^{-2}, up to ∼15% efficiency, and up to 5 year lifetime in the 1960s. However, the capabilities and challenges of cesium-based thermionic devices appear underappreciated in contemporary literature. Recently, Campbell *et al* proposed criteria for practical thermionic conversion, requiring at least >1 W cm^{-2} and therefore in practice emitter temperatures >1300 K [5]. Cesium-based thermionic devices have routinely met these criteria, and as described here can form a solid baseline for future efforts in thermionic conversion.

In a TEC, electrons evaporate from a hot electrode, the emitter, into a vacuum gap and are collected by a cooler electrode, the collector, to generate electric current (figure 8(a)). Two elements are essential for practical thermionic energy conversion: (1) a method to mitigate space charge in the gap, and (2) low electrode WFs for practical operating temperatures. Cesium historically performed multiple roles in thermionic devices. Electronic space charge could be mitigated by a cesium plasma requiring as low as a ∼0.5 eV overpotential across the gap, while WF of electrodes in cesium vapor is to first order solely dependent on the 'bare' WF of the electrode and ratio of its temperature to the temperature of a cesium reservoir, figure 8(b) [104]. Subsequent work proposed tighter predictions using cesium pressure [105], although neither set of correlations capture WFs across the full coverage range. Due to this dynamic cesium coverage, the bulk emitter and collector electrodes could be selected for Cs compatibility and long-term stability, and today, as in 1967, 'no fundamental life limiting mechanism for thermionic converters is presently known' [106]. Ground-based testing demonstrated over five year lifetime with a 1700 °C emitter and 800 °C collector [107], while nuclear thermionic TOPAZ satellites from the USSR provided several kilowatts of electrical power for up to one year in space [108]. Characteristic ranges of performance are shown in figure 8(c) [106].

Despite these successes, cesium-based thermionic devices have seen challenges moving beyond this historical performance. As described in the following sections, developments in materials, fabrication, and computational capabilities in the intervening years create opportunities to improve upon these proven Cs-based devices.

Current and future challenges

The high-level performance of thermionic devices is often characterized by the 'back voltage' V_B (also called 'barrier index'), which is the sum of the collector WF and required voltage in the gap required to mitigate space charge, shown schematically in figure 8(a). Historical Cs-based back voltages were on the order of ∼2–2.2 eV, with associated emitter temperatures >1400 K, figure 9(a). Improving thermionic devices requires (1) reducing the voltage required to mitigate space charge in the gap and/or (2) further reducing the collector WF. This section is focused on space charge; selected methods for WF reduction appear elsewhere in the roadmap and/or will be briefly outlined in the following section.

Several techniques have been suggested for reducing the voltage required for space charge mitigation below the historical ∼0.5 eV. For instance, both temporally varied (e.g. pulsed diodes or triodes) and spatially varied (e.g. 'hybrid mode') plasma concepts have been proposed [109, 110]. Development of advanced plasma-based mitigation has been difficult in part because formulating complete descriptions of the plasma was challenging. As shown in figure 9(b), while literature models can adequately agree with experimental current–voltage (IV) curves in technologically relevant regions to guide conventional plasma diode design, these models nonetheless diverge from experimental data beyond the 'transition point' where plasma cannot be sustained, which is also the voltage region where advanced plasma methods would be expected to operate. Other areas important for performance such as an imperfect correlation of output voltage with independently measured collector WF have also been suggested in literature to be related to factors not always included in standard plasma modeling, for instance back emission or negative ion emission [111].

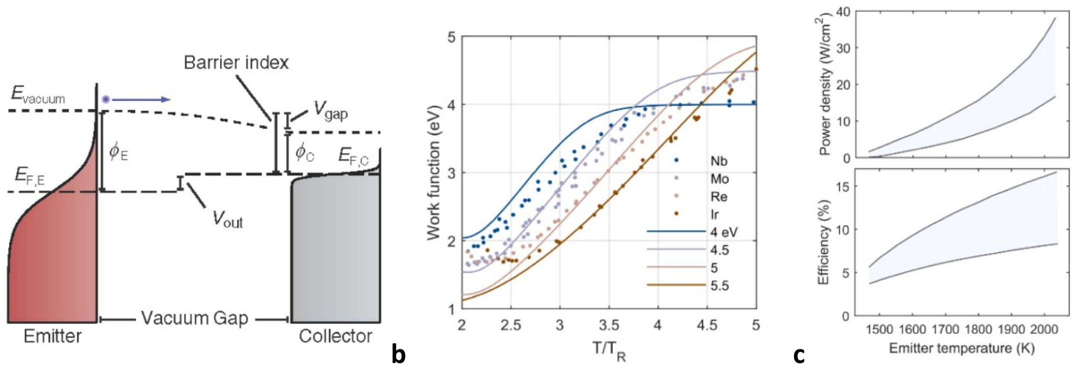

Figure 8. (a) Operating principle of thermionic energy conversion. Essential elements are low work function electrodes and a method to mitigate space charge in the gap with minimal voltage loss. (b) 'Rasor plots' of work function vs ratio of electrode to Cs reservoir temperature. Dots are experimental data. Lines are updated correlations courtesy of J. McVey using 416 K reference as in [104]. (c) Historical plasma power density and efficiency from [106].

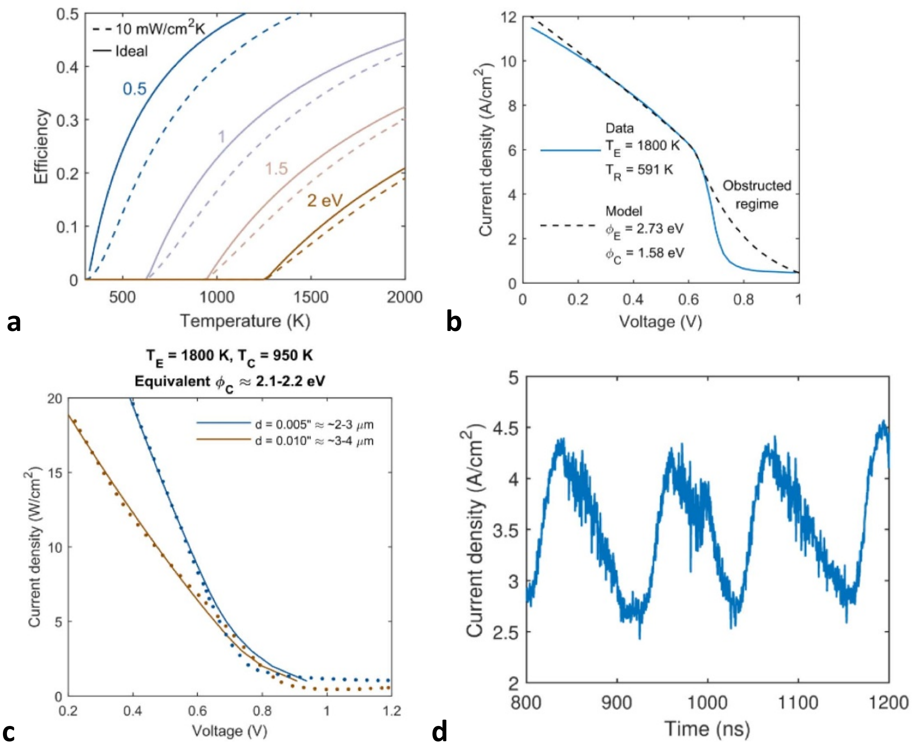

Figure 9. (a) Efficiency vs emitter temperature and barrier index. Radiation and lead resistance are included in the solid lines. Conductance of 10 mW cm^{2}K^{-1} is included in dashed lines. (b) The divergence of theory in the plasma 'obstructed mode' has remained unexplained. Electrode work functions are chosen manually for illustration to emphasize divergence in the obstructed mode compared to [105]. (c) Plasma curves with reservoir optimized from [105] compared to microgap fits ∼2–3 and ∼3–4 μm. (d) Long-duration PIC simulations with highly simplified and accelerated ionization and recombination showed surprising time-dependent behavior.

Another well-known route to mitigating space charge is to reduce the gap size to a few microns or less. In contrast to plasma devices, modeling of microgap systems is well addressed in literature, including complicating factors like electron reflection [83], back emission from the collector, or ion emission from the emitter [105], which can become important at high temperatures. It should be appreciated that in microgap devices, space charge in the gap tends to control current flow above a threshold emission, and operation is only mildly dependent on emitter WF below a threshold value. An effective gap electrical resistance can be estimated by examining the slope of the current–voltage curve at the 'critical point', the crossover between the space-charge-limited regime and the retarding regime, where the maximum motive is just outside the collector. In the limit of high injected current, the gap electrical conductance can be written as:

$$\mathrm{d}J/\mathrm{d}V = {\xi_{\mathrm{crit}}}^2 \varepsilon_0 (kT_\mathrm{E}/2\pi\, m_\mathrm{e})^{1/2}/d^2, \text{ where } \xi_{\mathrm{crit}} = 2.553\,89. \quad (7)$$

It can be illustrative to compare this simplified relation to the well-known Child's law which calculates the limiting current vs accelerating voltage while ignoring thermal effects:

$$\mathrm{d}J/\mathrm{d}V = 2\,\varepsilon_0/3\;(2\,q_\mathrm{e}V/m_\mathrm{e})^{1/2}/d^2. \quad (8)$$

The primary difference between equations (7) and (8) besides numerical prefactors is that the Child Law's total accelerating energy $q_\mathrm{e}V$ has been replaced with the emitted electron's thermal energy $\sim kT_\mathrm{E}$. Gap electrical resistance is weakly dependent on temperature but depends strongly on gap size.

This gap resistance illustrates a central challenge with the microgap approach compared to plasma. According to equation (7): at 1 μm and typical emitter temperatures, apparent resistance in the gap is $\sim$0.003 Ω cm^2, while at 10 μm, it is $\sim$0.3 Ω cm^2, too high considering current densities in plasma devices are often $\sim$10 A cm^{-2}. For comparison, figure 9(c) features reference plasma data that have been optimized for Cs reservoir temperature with mechanically straightforward gap sizes of $\sim$127 and 254 μm [105]. If fitted with microgap theory, these curves are equivalent to gap sizes of $\sim$2–3 μm and $\sim$3–4 μm, respectively, with an effective collector WF corresponding to the back voltage $\sim$2.1 eV. As a result, substantial improvements over plasma-based require microgap sizes in this same range, $\sim$1–4 μm.

Cesium-based microgap approaches also tend to feature larger parasitic heat pathways compared to plasma-based devices, such as an increase in Cs convection due to ballistic transport as well as thermal conductance of structural materials like micron-scale ceramic spacers. These parasitic heat flows imply that a microgap emitter may operate at a lower temperature than in a plasma device in the same environment, partially mitigating improvement in performance from reduction of V_B, figure 9(a). More generally, a thermionic converter should be designed within the context of the application's thermal environment: while current–voltage results in literature are typically reported at a constant temperature, the choice of current output—and thus the heat carried by electrons—can have a substantial impact on the emitter's temperature [112]. Parasitic pathways combined with practical operating temperatures tend to push the microgap approach to target even smaller gap sizes to maximize heat carried by electrons.

Historically, achieving such small gaps was challenging due to the large length scale difference between a $\sim\mu$m gap size and typical thermionic electrodes ($\sim$cm scale) using conventional machining. Prior work relied on thermal expansion effects or ceramic spacers to achieve gaps on the order of 10 μm [113, 114], see section 9 in this roadmap.

Advances in science and technology to meet challenges

Today, advances in science and technology are poised to meet these challenges. For plasma operation, advances in computation could yield large progress in modeling, while advances in microfabrication make micron-scale gap sizes realistic. In addition, further improving barrier index via collector WF reduction could be enabled with new materials approaches and deposition techniques.

Plasma modeling: Moving beyond demonstrated plasma performance has been hampered in part due to a lack of full description of plasma behavior, notably including a failure of models to adequately capture the 'obstructed' mode in standard current–voltage characteristics, figure 9(b). Fundamentally, this challenge is in part due to the vastly different timescales associated with the various processes in plasma-based devices, such as multi-step ionization and electron and ion transport, resulting in model simplifications in literature. Dramatic increase in computational power could now allow for a much more complete treatment of plasma processes, for instance using PIC codes. Lietz and colleagues performed kinetic simulations of cesium vapor thermionic converters that included tracking of 52 excited states of Cs in part to examine ionization and recombination processes [115]. Large differences in excited state populations were found compared to thermalized models used in literature, although it should be noted that the simulations did not reach steady state, which could have suppressed excited state populations. These simulations should be continued with much longer duration to reach steady state.

Long-duration PIC calculations have been performed using ionization/recombination models that were highly simplified and dramatically accelerated, allowing simulations to be run for long durations. In the 'ignited' regime believed to be well-captured by conventional modeling, the calculations showed oscillatory behavior in the output current and emitter sheath with periods up to 100s of ns, timescales that appeared to correspond to transport of cesium ions, figure 9(d). Existence of time-dependent effects is supported by unpublished work from J. McVey at Rasor Associates that examined comparatively large gaps and low cesium vapor pressure, effectively slowing plasma dynamics. In these experiments, an unexpected oscillatory behavior was recorded in the 'obstructed' regime between modes that featured (1) exponentially decreasing current with voltage, essentially matching the 'model' curve in figure 9(b), and (2) a negative resistance state. At more typical spacings and pressures, fast oscillatory behavior would likely be effectively averaged, which could give rise to the stereotypical *IV* curve shape.

These results suggest time-varying operation could potentially capture the full plasma *IV* curve: as voltage moves closer to the transition point, oscillations in the emitter sheath grow larger. Beyond a transition point, these oscillations become so large that plasma cannot be sustained, and the device rapidly drops out of the ignited mode. Recent fundamental work on plasma diodes by Campanell and colleagues considered the importance of backflow of electrons from the plasma on the potential near the emitter surface. In certain circumstances when the total plasma length was in an intermediate regime of a few electron mean free paths (common in cesium plasma diodes), oscillatory behavior was shown to develop, suggesting this behavior may be representative of a general property of plasma-surface interactions [116].

To confirm this hypothesis, previous PIC calculations should be repeated to ensure that time-dependent behavior was not indirectly introduced by model simplifications. If confirmed, these results could solve longstanding problems in thermionic analysis via incorporation of time-dependent effects and could enable successful description of proposed advanced modes of operation. Work in this area should first extend the work of Lietz, ensuring that detailed simulations of ionization and recombination reach full steady state. Results of these detailed simulations can then guide development of simplified but theoretically grounded models for processes like ionization and recombination, for instance by collapsing the number of excited levels in Cs. These reduced models can then be used for long-duration simulations that can examine both standard plasma as well as proposed concepts for further improving performance. These PIC results can then feed back into more rapid calculation approaches.

Microgap fabrication: Advances in microfabrication make it much more feasible to form micron-scale gaps. Recent progress in microgap devices was reviewed in Campbell *et al* in 2021. MEMS-inspired designs using mixed oxide low WF coatings resulted in proofs of principle measurements [117, 118]. More recently, by microfabricating ceramic spacers between electrodes, Cs devices with gap sizes of technical relevance (<4 μm) have been experimentally demonstrated with power outputs >1 W cm^{-2} [119] that meet the Campbell criteria [5]. While mechanical stability of spacers and electrodes remain important design considerations, primary goals for continued work in this area should be to (1) further reduce gap sizes, (2) increase operational temperature if the application can accommodate it, and (3) minimize spacer thermal conductance.

As shown by Campbell *et al*, reducing spacer thermal conductance below $\sim$10 mW cm^{-2} K is critical for overall performance [5]. Careful and reliable experimental determination of spacer thermal conductance is therefore of upmost importance.

Low WF materials: Several methods to effectively reduce WF appear elsewhere in this roadmap. A broad class of techniques (PETE, combined thermionic and PV effects, back-gating graphene, etc) exploit a decoupling of the WF coating at the surface (electron injection) from the relevant FL in the bulk material or contact (electron extraction). Many of these methods for effective WF reduction can be compatible with cesium-based devices. Here we briefly touch on methods to further improve the WF coating at the surface.

Historically, reducing collector WF in plasma-based cesium devices was focused on incorporating an electronegative element, most commonly oxygen, which is well known to result in WFs with Cs in UHV environments $\sim$1 eV. Challenges with this approach have involved stabilizing oxygen; desired vapor pressures for oxygen-containing species are usually orders of magnitude lower than Cs pressure. It should be noted that most literature explorations of Cs–O-based devices were performed prior to the development of advanced deposition techniques like ALD, which could greatly expand the possibilities of practical coatings. Rasor and colleagues reported success in stabilization using a combined oxygen-cesium reservoir based on porous nickel, resulting in a back voltage of $\sim$1.8 eV and efficiency of 20% [120]. WFs as low as 0.95 eV have been reported in Cs devices, levels that were proposed to be related to the development of ordered graphite/graphene layers [121]. If these results are replicated and shown to be compatible with either advanced plasma mitigation or microgaps, such WFs could enable efficiencies approaching 40%, figure 9(a).

Recent theoretical results also suggest potential advances for Cs-based devices. Chou and colleagues successfully simulated the WF of metals with Cs coverage using DFT and developed an orbital overlap model based on their results [122]. A promising program could combine this orbital overlap model with the simple correlations on WF shown in figure 8(b), with the potential to fully describe WF behavior across the full coverage range. Another promising area to examine is the influence of Cs coverage on DFT-predicted materials with ultra-low or ultra-high WFs—see section 12 in this roadmap.

Concluding remarks

Cesium-based devices remain the high-water mark in terms of thermionic conversion power density and reliability, and the author proposes these devices should serve as a baseline for future efforts. While it was historically challenging to improve upon these devices' performance, advances in computation, microfabrication, and materials strongly motivate revisiting this highly power dense technology.

9. Spacers for the inter-electrode gap in thermionic devices

Nicolas A Loubet, Katie Bezdjian, Esther López and Alejandro Datas*

Universidad Politécnica de Madrid, Instituto de Energía Solar, Avenida Complutense, 30, 28040 Madrid, Spain

E-mail: nicolas.loubet@upm.es

Keywords: spacers, microgap, ceramics

Status

One of the issues hindering the performance of thermionic devices is the formation of a cloud of electrons between the cathode and the anode. This phenomenon called space-charge effect, impedes the flow of electrons emitted by the cathode and prevents it from reaching the anode which in turns reduces the power production. Historically a Cs plasma has been used between the two electrodes to effectively reduce the space charge-effect but it resulted in a reduced overall system efficiency (reduced by 30%–50%) [5]. This reduction comes from the inherent power loss required to sustain the plasma as well as the plasma impeding some of the electron flow. As a result, those systems need to operate at high temperature to be efficient [109]. Other solutions to mitigate the space-charge effect includes the introduction of a grid in the gap, to tune the electric field in the gap and accelerate the flow of electrons has also been shown to be efficient in preventing the formation an electron cloud. However, similarly to plasma-based solutions, this approach requires power to function which negatively impacts the system efficiency. Section 6 of this roadmap also presents a way to address the space-charge effect problem by modifying the collector surface to decrease the number of electrons being reflected into the interelectrode space which could otherwise participate to the formation of a cloud of electrons. The most conceptually simple solution, by comparison to the solution mentioned above, consists in maintaining a micron-sized gap between both electrodes in high vacuum conditions. Indeed, both theoretical and experimental works showed that reducing the inter-electrode gap to less than 10 μm can reduce the space-charge drastically as the limited interelectrode space prevents electrons from interacting with each other to form a cloud [123]. Maintaining this inter-electrode gap can be achieved through piezoelectric actuators or MEMS but both of these solutions rely on external structures that can be sensitive to thermal stress and have been limited so far to small active areas. By contrast a spacer-based approach, where a material is intercalated between the electrodes, is an effective way to maintain the inter-electrode distance, without additional energy consumption and has the potential to be scaled up to bigger areas. The first use of spacers in a thermionic converter was reported in 1963 by Beggs [124] who used three pieces of molybdenum foil on ceramic inserts to maintain a gap under 6 μm. Since then, spacers have taken many shapes: they can either be directly fabricated onto one of the electrodes through microfabrication techniques to obtain pillars of various designs (pyramids, columns) or be free standing (foils, rings, corrugated films). Figure 10 illustrates the current state of spacer based thermionic converters by showing the maximum emitter temperature reported in thermionics experiments (i.e. measured in each specific experimental setup) using spacers as a function of the area of the device, as well as the value of the inter-electrode gap (labels) and the spacer material (colors). The data presented in figure 10 were extracted from a review including both spacers for thermionics and thermophotovoltaics (TPVs) [125]. A division has been made between works focused on measuring the thermal resistance of the spacer and works where the spacer has been included in an actual thermionic device. A large range of temperature has been explored but only two reports achieved an area over 1 cm^2. As seen on figure 10, only two reports measured a thermionic current for temperatures above 1500 K which is the temperature around which thermionic converter could reach high efficiencies [5]. Most works achieved an interelectrode gap below 10 μm which is enough to limit the space-charge effect (see also section 8 of this roadmap) and above 500 nm, under which near-field radiative heat transfer could be prevalent and represent an important source of loss [5].

Current and future challenges

As seen in figure 10, most of the gaps achieved in thermionic devices are greater than 5 μm. This is coherent with previous works that claimed that the optimal inter-electrode distance is in the range of a few microns to fulfill a trade-off between the reduction of the space charge and the apparition of near-field thermal radiation that represents a source of heat loss to the system [123]. However, recent publication accounting for nanoscale charge and thermal interactions predicts optimal distances in the

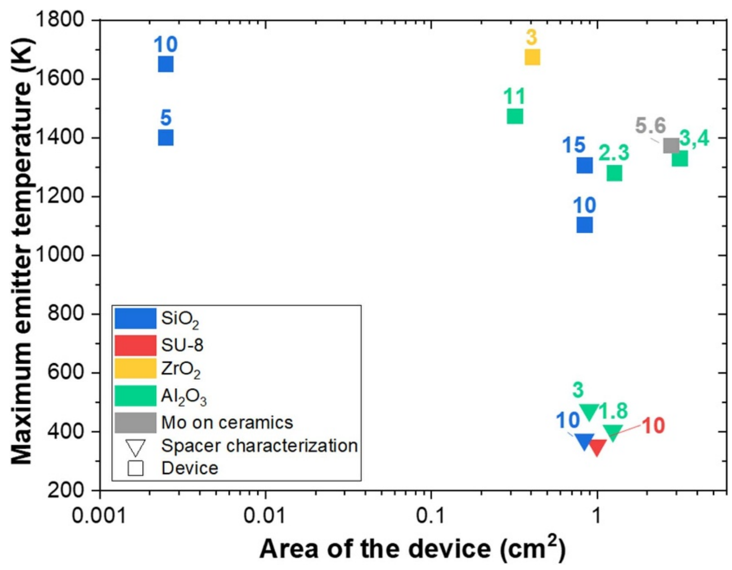

Figure 10. Maximum temperature of the emitter as a function of the area of the device, the label of each marker indicates the gap distance (in μm). A distinction is made between actual thermionic devices and works focused on the characterization of the spacers without achieving a device, data extracted from [125].

sub-micrometric range [79], meaning that efforts remain to reduce the inter-electrode distance and further enhance the performance of the thermionic generator.

Currently, a few spacer designs have been used to realize the inter-electrode gap in thermionics devices. A few of them were characterized for thermal resistance first and later introduced and tested in operational devices [119, 126–128]. Approaches used in thermionic devices are presented in figure 11. So far, only posts and beads have been employed to achieve nanometric scale inter-electrode distances applied to TPVs [129–131] but the corrugated film presented by Nicaise *et al* [128] and Campbell *et al* [119] can be potentially scaled down. Spacers should meet additional requirements such as exhibiting a high thermal resistance to minimize the parasitic conduction of heat between the electrodes, and being electrically isolating to prevent short-circuits. Moreover, spacers must be mechanically and chemically stable over repeated cycling at the high temperatures (>800 °C) required for TE to avoid potential failures such as stress induced cracking and diffusion between the spacer material and the electrodes. External pressure is often applied to the electrodes to correct any bowing which means that the spacer should be sufficiently robust and covering enough area to prevent breakage and shorting [132]. In this regard, the surface coverage of the spacer is an important parameter to consider: if it is too high it can lead to high conduction losses but if it is too low it could potentially weaken the robustness of the device. The thermal expansion of each component of the generator, including spacers, should also be considered as deformation could lead to breakage of the spacers and short-circuit [133]. Thermal and electrical resistances, as well as stability at high temperature, are all key parameters to take into account when selecting a spacer material. A table listing some of those properties can be found in literature [125]. All these requirements explain why ceramics such as alumina and silicon dioxide have been widely utilized as a spacer material but their bulk thermal conductivity remains relatively high compared to other less explored ceramics which could lead to high conduction losses [125]. Furthermore, the thermal resistance of spacers has not been heavily characterized in literature and only a few works focused on the issue (see figure 10) [126, 128, 134]. Finally scaling up the area of the electrodes while maintaining and reducing the gap is another challenge that remains to be addressed as seen in figure 10.

Advances in science and technology to meet challenges

Current fabrication techniques can achieve features of the order of microns but advances in spacers applied to thermionics are currently limited because of the poor characterization of the thermal resistance and the limited testing of devices featuring spacers in literature. To address conduction heat losses, Littau *et al* [134] have used alumina microspheres to maintain the gap, the distance being fixed by the diameter of the sphere. They noted that the gap distance was highly sensitive to potential dispersion in the spheres' diameters. The minimal contact area of the spheres with the electrodes allowed to increase

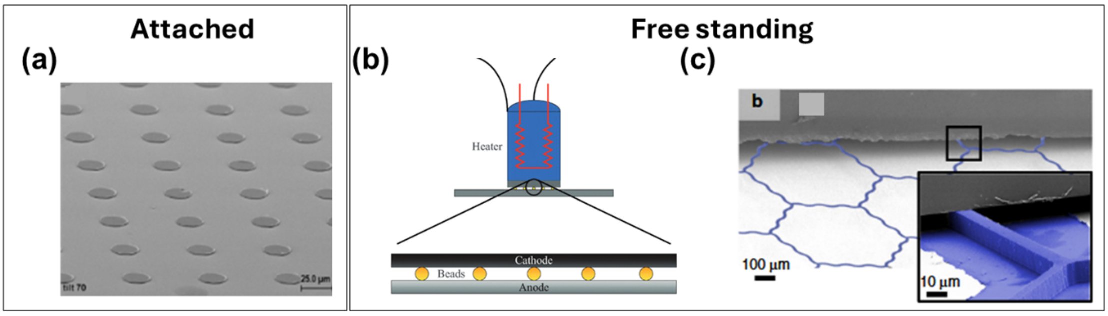

Figure 11. Examples of different spacers solutions: (a) Zirconia posts as presented in [132] (b) Alumina beads as presented in [16] and (c) Corrugated film as presented in [128, 132]. John Wiley & Sons. {Copyright © 2021 WILEY-VCH Verlag GmbH & Co. KGaA, Weinheim}. Reproduced from [134] with permission from the Royal Society of Chemistry. Reproduced from [128]. CC BY 4.0.

the interfacial resistance and reduce the conduction losses. However, these spheres could present a reliability issue because they moved during operation and could potentially create grooves on the electrodes. Belbachir *et al* [126, 127], extensively studied pyramidal posts made of silicon dioxide to maintain a 10 μm gap. They showed that the actual thermal resistance was significantly lower than the one approximated by a Fourier's law that considered only the bulk thermal conductivity of silicon dioxide. This highlighted the importance of characterizing properly the thermal resistance of the spacers to accurately determine the heat losses. When the pyramids had a sharper tip, an increase in thermal resistance was observed, emphasizing that the design of the spacer can be as important as the intrinsic properties of the material to reduce heat losses. More recently, Nicaise *et al* [128] and Campell *et al* [119] proposed a removable spacer in the form of a corrugated film with a honeycomb pattern made of either alumina or alumina, hafnia and zirconia multilayers achieving a thermal resistance on the order of $\sim$100 cm^2 K W^{-1}. Simulations showed that a thermal resistance above 100 cm^2 K W^{-1} is a threshold to reach high efficiencies, consequently the corrugated film spacers are very promising [5]. Current research shows that to mitigate the conduction losses there are several pathways that are not mutually exclusive. Developing or implementing materials with low thermal and electrical conductivity such as zirconia or multilayered ceramics [128, 132, 135] could enable spacers that greatly reduce conduction losses compared to silicon dioxide and alumina that are currently predominant. The design could also be tuned to further increase the interfacial thermal resistance, for instance, through removable spacers or embedded long posts [136] that have a long conduction path without sacrificing the gap distance but also by introducing additional rugosity to the contact area [119]. Regardless of the pathway chosen to reduce parasitic losses, the need for thorough characterization of the spacers remains. To this end, calorimetry measurements can help characterize the spacer thermal resistance and simulation can help in designing mechanically robust spacers that limit the conduction [132].

Concluding remarks

Implementation of inter-electrode gap is key to mitigate the space-charge effect and achieve high efficiency and power density. To this end the development of mechanically stable spacer with high thermal resistance is essential to limit the heat conduction losses inevitably introduced by the spacer material. Using multilayered ceramics or low conductivity materials and designing the spacers with high interfacial resistance by introducing rugosity and/or making them free standing could address this issue, as long as the solution is scalable to bigger areas. However, implementation of spacers requires thermal resistance characterization as well as testing of the spacers in real conditions of use of a thermionic generator.

10. Space-charge in thermionic energy conversion

*Mohammadamin Jalili and Alireza Nojeh**

The University of British Columbia, Vancouver, BC V6T 1Z4, Canada

E-mail: alireza.nojeh@ubc.ca

Keywords: heat engine, thermionic, space-charge, multiphysics

Status

As static heat engines, TECs are viewed as near-perfect thermodynamic machines and are expected to deliver high energy conversion performance. For example, considering a wide range of predictive studies from over the decades, an overall power conversion efficiency of around 50% seems to be a good, albeit ambitious, ballpark to aspire to. However, in practice efficiencies have remained below 20%, and typically around 10%—values that were already achieved in the mid-20th century (figure 12). Given the variety of device architectures and operational parameters, it is not possible to attribute this difference between theory and practice entirely to a single cause, but all indications are that, in vacuum TECs, the space-charge effect—the opposition to electron emission and transport due to the Coulomb repulsion of the electrons in the gap between the cathode and the anode—is a major contributor, either directly or indirectly. Since even a modest improvement to energy efficiency can lead to significant socio-economic benefits, addressing the space-charge effect emerges as a critical need in TEC research and development.

Current and future challenges

The space-charge effect may be mitigated using various approaches, but the challenge is that an energy cost is inevitably incurred as a result, which in turn decreases the TEC device's performance. Plasma-based TECs incorporate positive ions, most commonly of cesium, in the vacuum gap between the cathode and the anode to neutralize the negative electron cloud [109]. Another method involves employing a positively-charged grid as a gate electrode. This creates an electric field accelerating the electrons away from the cathode; a magnetic field can be added to help guide the electrons through the gate openings, effectively increasing the gate's transparency to electrons [137]. Although practical, these approaches come with an efficiency penalty due to the electrical energy required to maintain the plasma or the gate voltage. Furthermore, both the positive ions and the gate can themselves interfere with electron transport. A conceptually simpler method to mitigate the space-charge effect is to reduce the distance between cathode and anode to the micrometer scale and below. However, near-field radiative heat transfer between the electrodes can then lead to significant thermal energy loss.

All the above approaches are nonetheless promising and have seen experimental demonstrations and systematic progress (figure 12) [5]. More recently, advancements in microgap TECs have been demonstrated through innovative fabrication techniques. For instance, in one study, photolithography, lift-off, and reactive sputtering were used to fabricate ZrO_2 and Al_2O_3 microspacers, which were then incorporated into a thermionic-PV (TIPV) device to assess their practical application [132]. These microspacers enabled the device to achieve a vacuum gap as small as 3 μm and improved energy conversion performance. This work is also an example of the development of materials capable of withstanding the high temperatures involved in TECs while maintaining precise design parameters, which is an ongoing challenge.

Given the trade-offs involved in mitigating space-charge, progress in TECS will ultimately require the ability to engineer and optimize devices, for example by balancing losses due to the space-charge effect against interelectrode radiative heat transfer in microgap TECs. This demands a thorough understanding of the various loss mechanisms at play, which in turn necessitates accurate physical models with quantitatively reliable predictive power. The CL model provided a basic understanding of the space-charge effect in a vacuum diode, and theory has since been developed significantly [138]. In the context of TECs, increasingly there is a need to incorporate the appropriate space-charge formulations into larger, all-encompassing models that capture the various pieces of physics at play in a given device. Progress toward such multiphysics modeling of TECs has accelerated in recent years. An example is the inclusion of space-charge interactions and near-field radiative coupling together with semiconductor physics in a self-consistent energy balance framework for the analysis of microgap TECs in hybrid energy converters [139]. Similar calculations have also been carried out for devices incorporating new materials, such as a sub-microgap cesium-based TEC with a graphene anode [140]. There has also been progress in

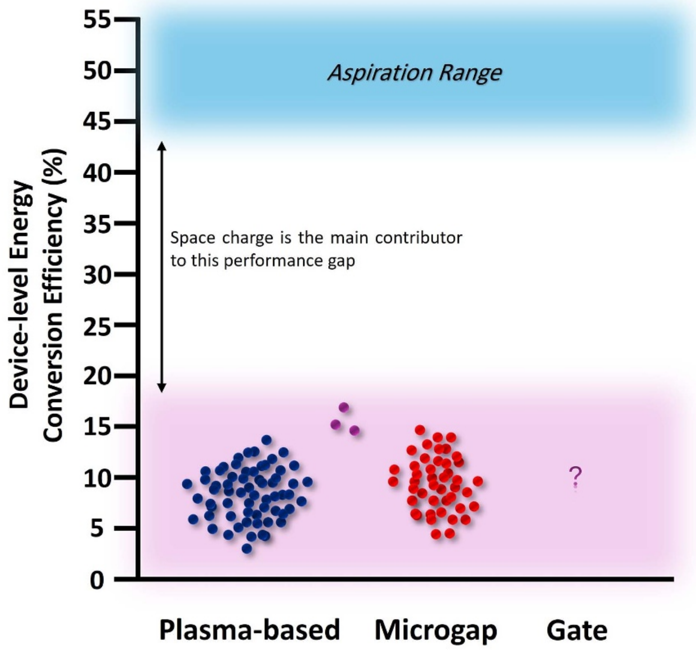

Figure 12. A representation of thermionic energy conversion efficiencies (the ratio of the output power density to the total input heat flux to the emitter) experimentally achieved for the most common methods of mitigating space charge, compared to an estimation of what is expected to be possible based on theoritical studies. The filled circles do not represent exact values, but rough ranges, and their number is an indication of the degree of attention that each method has received. The question mark represents the lack of experimental data for gated devices.

employing simulation codes from the rich tradition of VED and accelerator physics research in the study of space-charge in TECs and their optimization [141].

Numerical simulations, such as in the above examples, provide great predictive ability; in general, such simulations may involve PIC methods for space-charge dynamics, density function theory for predicting material properties, and finite element methods (FEMs) for thermo-mechanical analysis, but the need for powerful analytical models is also ever-present, as these can enhance insight and guide invention and design. Improved models capable of capturing a range of physical phenomena are often crucial since basic and traditional models may fall short in terms of quantitative accuracy. An example of such limitations has been the inability to capture the smooth transition between temperature-limited and full-space-charge-limited regimes, which restricts a model's applicability to cathodes operating under real conditions. As a step forward, a unified approach that integrates 3D space-charge effects, patch fields, and Schottky barrier lowering was developed [142]. This physics-based model enables the prediction of the emission current from a polycrystalline cathode with known surface grain orientations and WFs, and provides insights into the relationship between the microscopic structure of the cathode and its emission behavior.

Advances in science and technology to meet challenges

The last two decades have seen a revival of interest in TECs, and progress has been encouraging and accelerating. Looking ahead, efforts along several directions appear necessary in order to make TECs into a viable technology.

The individual material properties of both the cathode and the anode are critical: high-temperature stability, thermal expansion, thermal conductivity, electrical conductivity, WF, electron reflectivity, optical emissivity, and the temperature dependence of these properties. There is thus a need for continued development of new materials and fabrication techniques, as well as improved characterization methods particularly for measurements at high temperatures, which present specific additional challenges. On all these fronts, it may be possible to learn significantly from the technologies involved in mechanical heat engines, which have reached a high level of maturity; for instance, the knowledge of high-temperature superalloys, thermal barrier coatings, or advanced brazing techniques developed for gas turbines may help address some of the existing challenges of TECs.

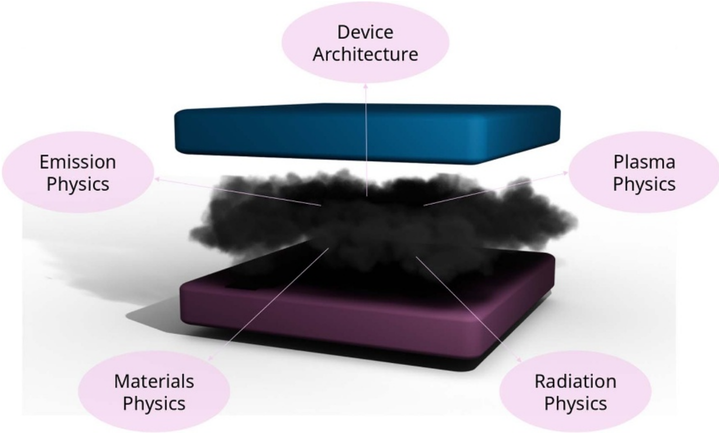

Figure 13. Simple depiction of a thermionic device with space charge between the cathode and the anode. Methods to mitigate the space-charge effect add new engineering requirements and physical phenomena to the device or couple existing phenomena with each other, significantly complicating the overall problem. In a sense, space-charge has been a dark cloud hanging over thermionic energy converters, slowing progress for more than half a century.

Beyond establishing the individual material properties in isolation, it is necessary to study how these interact and affect each other in a device under operating conditions—where the need to mitigate space-charge interactions leads to various physical phenomena becoming intertwined (figure 13)—and how to improve each property while minimally affecting the others. For example, maintaining a microscale gap at high temperatures imposes requirements on mechanical characteristics, which may have consequences for other properties.

The advances in materials and fabrication processes in other domains, such as micro/nanofabrication, present new opportunities for space-charge mitigation. Reduced dimensionality and strong correlations in nanostructures and quantum materials enable new degrees of freedom to engineer structural, thermal, electrical, and optical properties; even thermal emission laws in these materials may differ compared to those in bulk materials, offering possibly advantageous forms of temperature dependence. However, these opportunities also come with new challenges and call for more advanced characterization techniques. In this regard, much may be borrowed from the sophisticated characterization techniques employed in condensed-matter physics research.

As with other electron devices, TEC progress can also benefit from innovative device ideas and architectures. Using plasmonics, enhancing thermal emission with photoexcitation, and hybridizing TECs with other solid-state energy converters are examples of such innovations [5]. At its core, thermionic conversion is about electron energy engineering: pumping electrons from a low-energy reservoir to a higher one with minimal over-excitation (which would ultimately dissipate as waste). An example embodiment of this goal is the field-emission heat engine [143]. Such energy engineering calls for the application of advanced electron and photon spectroscopy methods not only for materials characterization, but also for the *in-situ* study of the entire device.

On the theoretical side, there is much room for further advancing the existing approaches based on semi-classical electron emission and transport combined with other physical mechanisms, in both analytical and numerical domains. At the same time, significant progress in computational physics and chemistry, notably in the form of first-principles quantum-mechanical simulations, can enable material properties by design. Naturally, AI methods can also play an important role in accelerating these theoretical studies, for instance through data driven surrogate models that capture coupled effects such as space-charge, materials physics, and radiative heat transfer, enabling rapid multiphysics design and optimization, in addition to helping analyze large experimental datasets.

Concluding remarks

Ultimately, from a device engineering point of view, we believe that, regardless of the presence of a vacuum gap, TECs should be regarded as complex solid-state devices, and designed, characterized, and studied in the same manner as that of electronic devices used in information technologies—as elaborate multiphysics problems that incorporate increasingly more physics using increasingly better models. In parallel, it will be important not to lose sight of the high-level trends that are better understood based on simpler analytical models, whose further development and improvement will remain continually relevant.

11. Thermodynamic approaches of thermionic-based converters

Ehsanur Rahman[1,*] *and Xin Zhang*[2]

[1]Department of Electrical and Electronic Engineering, Bangladesh University of Engineering and Technology, Dhaka 1000, Bangladesh
[2]School of Science, Jiangnan University, Wuxi 214122, People's Republic of China

E-mail: ehsaneee@eee.buet.ac.bd

Keywords: thermodynamics, modeling, hybridization

Status

Thermodynamic approaches are indispensable to the advancement of TECs, which are solid-state devices converting heat into electricity via TE. Due to their simplicity, scalability and high conversion efficiency potential, TECs have drawn significant attention for diverse applications ranging from powering space crafts to electrification of remote off-grid areas. However, various practical challenges such as space charge effects, thermal management, material limitations, and sub-optimal coupling of energy conversion processes have prevented TECs from reaching closer to their promising theoretical limit [5]. To overcome these challenges, researchers are using advanced thermodynamic methodologies such as synergistic integration of multiphysics modeling, material innovation, and hybrid system architectures. Self-consistent thermodynamic framework that integrates electron transport, radiative heat transfer, and space charge dynamics, has enabled precise predictions of device behavior under operational conditions [112]. Iterative computational models coupling charge transport with heat transport have provided deeper insights into electron cloud interactions and heat loss mechanisms in microscale gaps, informing photon/electron recycling strategies and spacer optimization. Data-driven techniques such as ML and computational tools such as the FEM further support these advances, accelerating the discovery of high-performance electrode materials, thermally stable interfaces, and spacer designs [144]. In addition to improving TEC efficiency, the integration of these devices with secondary thermodynamic cycles, such as thermoelectrics (TEGs), TPVs, and Brayton cycle, has emerged as a promising strategy for waste heat recovery [54]. Laboratory-scale prototypes, such as hybrid systems combined with thermionic converters, have demonstrated the feasibility of multi-stage energy extraction. These innovations highlight the potential of TECs to operate in synergy with other energy systems, enhancing overall energy conversion efficiency. Data-driven techniques and computational advancements could further refine the interplay of thermal, electrical, and radiative processes, particularly in extreme thermal environments.

Current and future challenges

The main challenges in thermionic-based converters that the thermodynamics approach needs to model and solve can be categorized into the following broad areas:

- **Space charge effects**: Space charge effects cause electrons to accumulate in the interelectrode gap, creating a negative potential barrier that can limit electron flow and thus reduce the overall efficiency of the TEC. This phenomenon is particularly pronounced in TECs with large vacuum gaps, where the Coulombic repulsion between emitted electrons becomes significant.
- **Thermal management**: Efficient heat transfer is critical for maintaining the large temperature gradient required for thermionic conversion. However, thermal conduction through spacer materials, radiative losses, and non-uniform temperature distributions can degrade performance. Fabricating microscale mechanically robust and thermally insulating spacers and optimizing thermal balance are key challenges.
- **Material limitations**: TEC electrode materials simultaneously require low WF, high electron emission efficiency and high temperature stability. Achieving all these criteria in a single electrode remains a long-term challenge in TECs. Moreover, spacers which are used for mechanical support must be made of materials with low thermal conductivity and high mechanical and electrical integrity.
- **Integration with other thermodynamic cycles**: The high temperature operation of TECs generates waste heat that could be utilized in secondary energy conversion cycles. However, designing efficient multi-stage cascade systems that integrate TECs with other thermodynamic cycles, such as

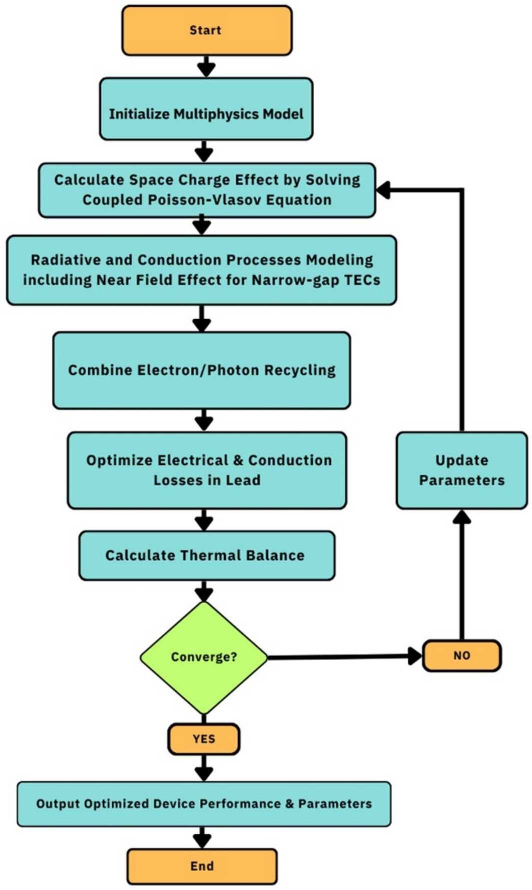

Figure 14. Self-consistent iterative multiphysics-based thermodynamic computational framework for TEC optimization.

thermoelectrics [16], TPVs [145], or Brayton cycles [146], requires careful thermodynamic modeling, precise thermal zoning, and optimization. For example, efficient TPV conversion required spectral matching between emitters and PV cells, thereby complicating the system design. Similarly, the thermodynamic figure of merit of the thermoelectric device is optimized at a specific temperature gradient depending on the thermoelectric material properties.

Advances in science and technology to meet challenges

Recent advances in thermodynamic approaches have provided innovative solutions to the above-mentioned challenges to implementing a high-performance TEC and paving the way for their broader application. Key developments include:

- **Multiphysics-based self-consistent iterative modeling**: The operation of a TEC device involves complex interaction among various mechanisms such as space charge effects, thermal balance, and radiative exchange processes. Self-consistent multiphysics based iterative models incorporate space charge effects, heat conduction or convection, near field enhancement of radiative coupling and electron and photon recycling to provide a comprehensive framework for optimizing device performance [147], as shown in figure 14. Such a complex model could provide unprecedented physical insights into the operational mechanism of the device and its performance optimization.
- **Near-field thermal radiation coupling**: At sub-micron gap scale, coupling of evanescent electromagnetic waves which are either generated by frustrated total internal reflection or resonance of surface plasmon or surface phonon polaritons can significantly increase the strength of radiative exchange between the TEC electrodes. This is known as the near field effect of thermal radiation. Incorporating near-field effects into thermodynamic models using fluctuating electrodynamics has provided useful insights into the design of TECs with enhanced radiative coupling [112]. Moreover, while near-field coupling effect can present itself as an unintentional by-product of space charge mitigation in TECs, this coupling can also be carefully applied to innovative thermionic-TPV hybrid devices [148] or thermo-photo-thermionic devices [139] for improved energy conversion performance.

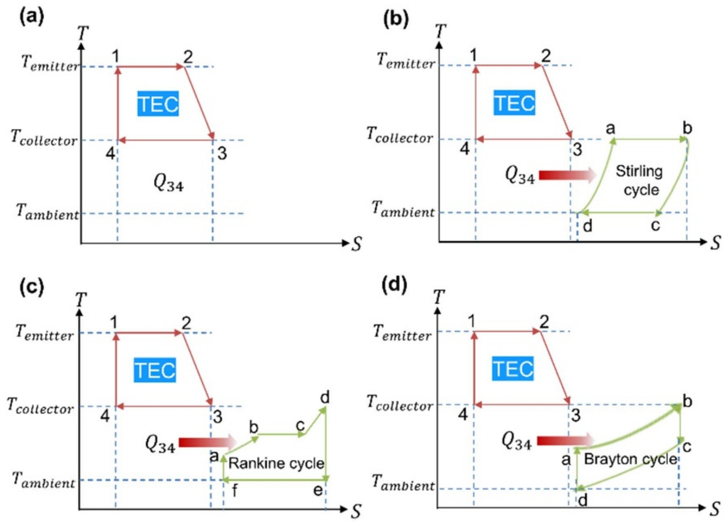

Figure 15. The temperature–entropy (T–S) diagrams of (a) TEC alone, (b) TEC-Stirling hybrid system, (c) TEC-Rankine hybrid system, and (d) TEC-Brayton hybrid system.

- **Advanced computational modeling for combined cycles**: Thermodynamic modeling has been extended to explore cascading energy conversion systems combining TECs with other heat engines. Notably, integrated systems with TECs as the top stage and thermoelectric generators [16], thermoradiative [149] or TPV cells [145] as the bottom stage have been conceived to optimize waste heat recovery. In addition, past literature has shown the feasibility of combining TEC with well-established thermal cycles such as steam and gas turbines [150], Stirling engines [151], Rankine cycle [152] or Brayton cycle [146] to further improve the power output and efficiency of the whole system. Figures 15(b)–(d) depict temperature entropy diagrams for the combined Stirling, Rankine and Brayton systems, respectively, representing the three practical bottom thermodynamic cycles. Multi-objective optimization of these integrated systems can be performed using advanced thermodynamic tools that help balance factors such as efficiency, complexity and cost.

- **Space charge mitigation via NEA**: Electrode materials with NEA have been shown to mitigate space charge effects [153]. Such electrodes emit only sufficiently energetic electrons that can traverse the interelectrode space without creating a coulomb blockage. This could lead to a compact and reliable TEC device that does not require additional mechanisms for space charge mitigation such as cesium vapor or accelerating gate electrode. Thermodynamic models that incorporate the physics of space charge mitigation with NEA could guide the design of such compact TECs with optimized electrode spacing and material properties.

- **FEMs for thermal management**: FEMs have been extensively employed to study thermal conduction in spacer materials and design the structure of thermally insulating spacers [128]. Through microscopic heat transfer simulation, FEM helps identify mechanically robust spacer geometries and materials that could minimize thermal losses. These insights have led to the development of advanced spacer designs that could improve thermal balance and overall device efficiency.

- **Data-driven AI for material development**: AI and ML techniques can be instrumental in the search for novel TEC electrode materials and optimal device structure [154–156], as shown in this roadmap in sections 12 and 13. By analyzing large datasets of material properties, AI-driven methods can help identify candidate TEC materials with desirable characteristics such as high efficiencies of thermal electron emission, low WF, high Richardson constants, and stability at high temperatures. In future, such methods can also accelerate the discovery of thermally stable NEA coatings for space charge mitigation.

Concluding remarks

In summary, advanced thermodynamic frameworks spanning from single-stage thermionic converters to multistage hybrid systems have significantly advanced the development of thermionic converters by elucidating the effects of key limiting factors such as space charge effects, irreversible thermal radiation losses, and thermal conduction losses on device performance. These models provide physical insight into operational limitations and device physics, enabling precise optimization of device structure, thermal gradients, and photon/electron recycling. For example, finite-time thermodynamic analysis quantifies the trade-off between power density and efficiency in hybrid TEC-TEG and TEC-TPV systems, while multiphysics field modeling addresses the interactions and trade-offs between space charge effects and near-field radiation in submicron gaps. These advances, combined with data-driven materials development and advanced computational tools, can dramatically improve device efficiency and facilitate its integration with multistage energy conversion systems. In addition, integrating TEC with other thermodynamic cycles is a viable approach to maximizing waste heat recovery and achieving higher efficiencies. Looking ahead, future thermodynamic work should focus on three key areas to realize the full potential of thermionic converters. First, thermodynamic modeling must be expanded to higher dimensions to incorporate spatiotemporal gradients such as non-uniform emission sites and charge carrier dynamics. Second, computational efficiency must be enhanced through AI-accelerated solvers and reduced-order modeling to manage the computational load of complex multiphysics simulations. Finally, unifying thermodynamic models with real-time sensor data will enable predictive maintenance and adaptive control, accelerating the deployment of TECs in extreme environments such as space reactors and concentrated solar plants. By advancing these tools and addressing remaining challenges, the field can transition from iterative prototyping to commercial products, unlocking the full potential of TECs as efficient and reliable solutions for direct heat-to-electricity conversion.

12. Recent progress in data-driven discovery of stable low WF materials

Peter Schindler

Northeastern University, Department of Mechanical and Industrial Engineering, Boston, MA

E-mail: p.schindler@northeastern.edu

Keywords: machine learning interatomic potentials, density functional theory, surface reconstructions

Status

The discovery of new ultra-low WF surfaces that are stable at elevated temperatures would enable high conversion efficiencies in TECs and pave the way for next-generation electron emission devices [30]. The WF is the energy required to extract an electron from the surface of a material. In solid state physics terms, the WF is the energy difference between the vacuum energy level away from the surface and the Fermi energy level of the material. There are several approaches to determine the WF of a surface experimentally, including KPFM, ultraviolet photoelectron spectroscopy, and TE-based methods (cf section 7). Depending on the technique, utilized electric field, surface contamination, and spatial inhomogeneity of the surface, the measured WF may differ for the same surface [18]. Computational approaches are not only orders of magnitude faster in calculating the WF compared to experimental methods but also exhibit exact atomistic control to relate structure to property. While *ab initio* methods such as DFT reliably predict the WF of solid-state surfaces, their computational expense renders screening through a vast number of surfaces for promising candidates impractical. ML approaches show promise for enabling rapid screening of stable material surfaces with ultra-low WFs, and this section examines their potential in detail and discusses recent progress.

Current and future challenges

Predicting whether a material forms a stable surface with an ultra-low WF can be divided into two key tasks, as shown in figure 16: Task 1-*Identification of the most stable surface(s) of a given bulk material;* Task 2-*Prediction of the WF of a surface.*

The first task is typically evaluated by computing the cleavage or surface energy of various low-index Miller facets using DFT, where facets and terminations with lower energies are more stable and play a more prominent role in the Wulff construction. Beyond the Wulff construction, which serves as a model for the equilibrium shape and facet distribution of nanoparticles, surface terminations with the lowest cleavage energy for a given Miller index are also of relevance, even when that index does not correspond to the globally lowest energy among all orientations. Such terminations, which minimize the energy within a specific crystallographic orientation but not overall, are particularly important for epitaxially grown films with a preferred orientation, as well as for polycrystalline materials in which multiple distinct Miller indices may be exposed at the surface. The cleavage energy is exactly equal to the surface energy in the case of symmetric slabs (i.e. mirror or glide plane parallel to the surface or a two-fold rotation axis normal to the surface). For slabs lacking this symmetry, two times the cleavage energy poses an upper bound to the surface energy [30]. In addition to the computational expense of DFT, limiting the analysis to ideally cut Miller surfaces may overlook surface reconstructions, which can yield even lower surface energies than their ideal counterparts. The search space of possible surface reconstructions is vast, as is often illustrated by the notoriously known Si (111) reconstruction that requires a 7×7 supercell.

The second task can also be effectively addressed with DFT. A slab geometry padded with vacuum in the direction normal to the surface is utilized within DFT to obtain the electrostatic potential averaged parallel to the surface and the Fermi energy level of the material. The planar-averaged electrostatic potential energy a few Angstroms away from the surface is taken as the vacuum energy level (for polar surfaces, a dipole correction is required to flatten out the vacuum energy levels on each side of the slab). DFT at the gradient-corrected level (PBE exchange-correlation functional) has been shown to reliably predict WFs for elemental crystals, with a slight systematic underestimation, and errors compared to experimental values are typically below 0.3 eV for elemental crystals (all elements in groups 1–15 with atomic number $<$84, excluding B, Mn, N, P, and all lanthanides) [157] and around 0.15 eV for elemental metals (Al, Cu, Ru, Rh, Pd, Ag, Pt, and Au) [158]. Similar to Task 1, the computational expense of DFT is the main bottleneck in screening a vast range of possible surfaces for desirable WFs.

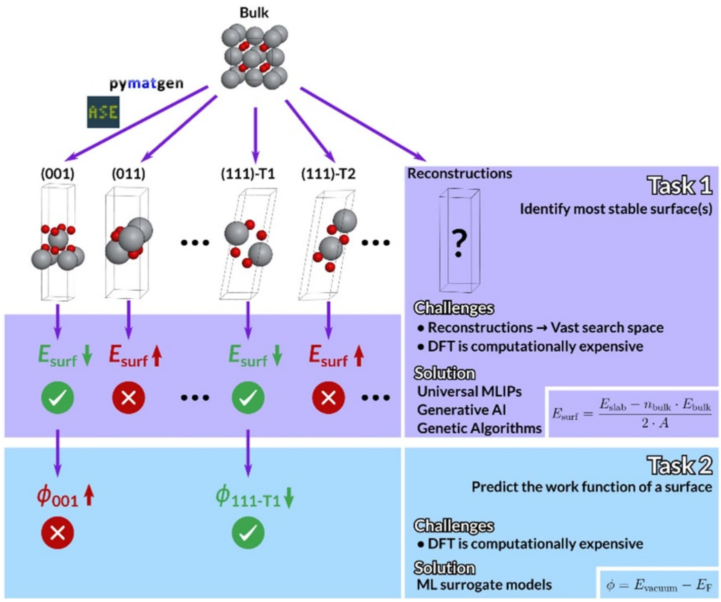

Figure 16. Overview illustration of the two tasks to identify stable, ultra-low work function surfaces from a given bulk crystal structure. Red arrows pointing upward and green arrows pointing downward refer to high and low values, respectively. E_{surf}, E_{slab}, E_{bulk}, E_{vacuum}, E_F, A, n_{bulk}, and ϕ refer to surface energy, total energy of the slab, total energy of the bulk, electrostatic energy level in the vacuum, Fermi energy level, surface area, number of bulk units in the slab, and work function, respectively. T stands for surface termination.

Advances in science and technology to meet challenges

For both tasks described above, ML has offered a solution to speed up surface stability and WF predictions by several orders of magnitude at near *ab initio* accuracy. ML models require accurate datasets encompassing a diverse range of materials with various chemistries and structures to effectively predict material properties. However, most major materials datasets, such as the Materials Project, primarily focus on bulk crystal properties, with the exception of the Open Catalysis 2020 dataset, which concentrates on surface adsorption calculations. Schindler *et al* established the largest database of cleavage energies (33 631) and WFs (58 332) for up to ternary metallic materials (3716) [30]. Prior to this work, these surface properties have only been reported for elemental crystals and 2D materials.

To address the first task, it is essential to develop methods that can rapidly predict cleavage or surface energies. In addition to the database above, the cleavage energy has also been calculated for 3033 intermetallic alloys. This data has been used to train a graph-based ML model with a mean absolute test error of 0.0071 eV Å^{-2} for cleavage energy predictions [159]. The rise of universal MLIPs has also enabled the prediction of the surface energy directly from total energy predictions of the bulk and slab. While earlier work suggested this is not yet accurate enough for reliable surface energy predictions and requires fine-tuning [160], a more recent benchmarking study shows that current state-of-the-art MLIPs can accurately predict the cleavage energy with a mean absolute percentage error below 6% and correctly identify the thermodynamically most stable surface termination in 87% of cases, without any explicit surface energy training or fine-tuning [161]. An ML framework can be particularly valuable in searching for potential surface reconstructions, which require an extensive and computationally prohibitive search of possible atomic configurations at the surface, typically performed using a genetic algorithm or other global optimization methods. For example, MLIPs within a Bayesian approach have enabled large-scale molecular dynamics simulations to describe the thermodynamics and time evolution of the low-index mesoscopic surface reconstructions of gold [162]. Another recent example is the use of generative diffusion models to sample stable surface structures and reconstructions [163].

To address the second task, a surrogate ML model needs to accurately predict the WF of a surface at a fraction of the computational cost. Schindler *et al* have developed a physics-motivated featurization approach for surfaces (utilizing elemental and structural information from the top three atomic layers near the surface) and have trained a random forest model to predict the WF with a mean absolute test error of 0.09 eV. This accuracy is comparable to the underlying DFT while being 5 orders of magnitude faster [30]. This WF ML model has been integrated with a new fully *ab initio* PE model to screen over 70 000 semiconducting materials, identifying novel, ultra-bright photocathode materials that are likely to be air-stable [164]. In follow-up work, the ML model has been benchmarked on its out-of-distribution generalization performance. While the model generalizes relatively well to unseen chemistries, the generalization error increases significantly when holding out unseen structural prototypes (i.e. space groups) [165]. A recent equivariant graph neural network model, FIRE-GNN, trained on the same surface dataset, outperforms the hand-featurized random forest model in terms of the mean absolute error (0.065 eV) and out-of-distribution generalization performance [166]. In recent literature, there are further ML surrogate models to predict the WF of two specific classes of materials, binary intermetallics (3526 surfaces) and 2D MXenes (275 materials). The mean absolute test errors for the two models are 0.118–0.25 eV utilizing a graph-based and a compositional featurization approach, respectively [167, 168].

Concluding remarks

The recent progress in ML surrogate models shows promise to enable rapid screening of new materials at the Pareto front that exhibit both high stability and low WFs. Moreover, universal MLIPs and generative AI approaches open an avenue toward identifying complex surface reconstructions critical to closing the gap between computational surface models and experimentally observed structures. These developments are likely to drive the discovery of next-generation electron emission devices and TEC anodes.

13. New methods for the prediction of performance of thermionic materials and devices

Elizabeth D Juette[1,*], *Van P Carey*[1] *and Jean-Pierre Fleurial*[2]

[1]University of California, Berkeley
[2]Jet Propulsion Laboratory, California Institute of Technology

E-mail: ejuette@berkeley.edu

Keywords: physics-informed neural networks, machine learning integrated performance prediction, multiphysics modeling

Status

Conventional thermionic device models frequently use a variation of the integral equations presented in [169], solved using iterative numerical methods for nonlinear systems. Vacuum diode models commonly assume collisionless, ballistic electron transport using the Vlasov–Poisson equation and can account for back-emission effects due to hot collector temperatures. Research efforts in the late 1980s and early 1990s developed modified variations of the conventional performance models to account for specular and diffuse reflection at boundaries within the device that is included in later publications on electrode material development [170]. These models require knowledge of material performance parameters, such as the emitter WF, that can be challenging to measure experimentally with sufficient accuracy at the operating temperatures.

To complement experimental measurements, material properties, such as the emitter WF, have been determined computationally using theoretical equations such as those presented by researchers such as Rasor and Warner in 1964 [104] and alternative analytical solutions presented by Hatsopoulos and Gyftopoulos [169]. Khoshaman and Nojeh presented a self-consistent particle-tracing method that does not rely on the analytical 1D solutions for devices operating in the space-charge limited regime with the presence of back-emission in their 2016 paper [171]. Researchers at Sandia National Labs examined layered microstructure electrodes using Monte Carlo approaches to examine coarsening and diffusion through the materials, used patch models for WFs and transmission coefficients in non-uniform electrode coatings, and presented the results of using DFT to predict WFs of technologically relevant materials [170]. Each of these studies includes a discussion of electron reflection and its impact and inclusion into 1D performance models. More recently, the impact of diffuse and specular electron reflection in thermionic devices has been studied numerically and with PIC simulations [83].

These conventional models provide an approximate performance prediction for developing thermionic technologies and rigorous computational models have provided reasonable predictive capabilities [172]. However, rising interest in thermionic technology for applications such as space nuclear power and propulsion systems also require high reliability and longevity for their energy conversion systems. If these devices are to be seriously considered for critical applications such as interplanetary space missions or lunar surface power, performance models should be grounded in real device data with lifetime performance prediction capabilities to provide a realistic picture of the feasibility of a particular device design. Thermionic converter performance is particularly sensitive to minute changes in material properties, such as the WF, which change with temperature and material structure. Leveraging advanced ML techniques and data-driven approaches in diode modeling can help provide a better understanding of modern thermionic diode technology's potential in both high-temperature terrestrial and space applications.

Current and future challenges

Modern thermionic diodes include novel designs with complexities such as interstitial gate electrodes, complex materials and coatings, interelectrode plasma, surface texturing, and solid-state (non-vacuum) diodes that require more complex performance models than microgap vacuum devices [172]. It is also necessary to have an accounting of thermal losses in a system-level model to understand device behavior and performance when integrated into a power system. However, performance models can struggle with accuracy due to the uncertainties associated with WF prediction and measurement and the sensitivity of thermionic diodes to small variations in performance variables. For example, a 2 μm shift in the gap width in a conventional microgap performance model can more than double a model's performance prediction by over or underpredicting the inhibiting space charge in the interelectrode space. Similarly, a 0.1 eV change in the collector WF can change a performance prediction by more than 20%. Sensitivity

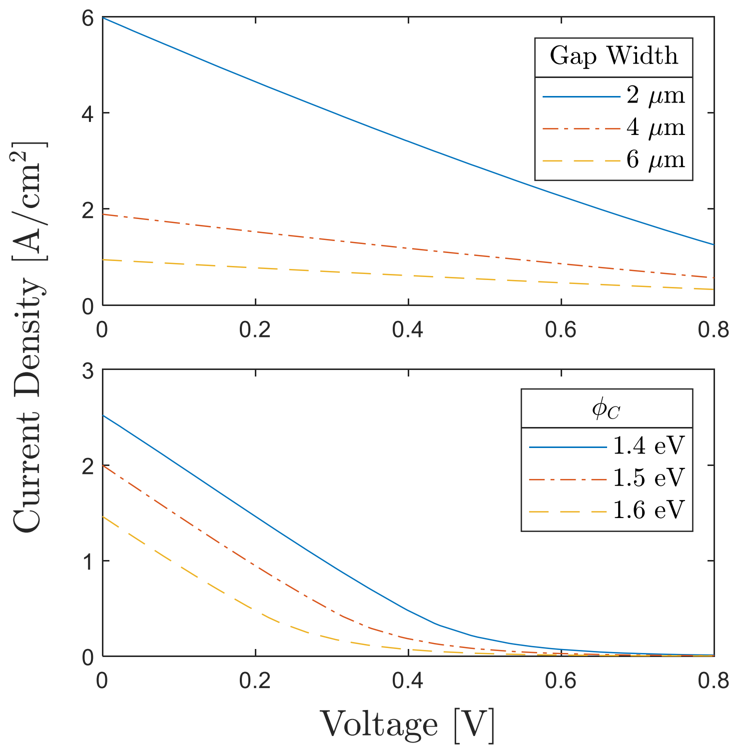

Figure 17. Current–voltage characteristics for a vacuum thermionic diode operating at varying gap widths and varying collector work functions. Decreasing the interelectrode gap width demonstrates an increase in output current density. Decreasing the collector work function shifts the performance curves towards higher voltages.

studies have demonstrated that an error in the emitter WF on the order of 0.1 eV can change the predicted output current by a full order of magnitude [173]. Figure 17 includes performance of a microgap diode with negligible back-emission and no electron reflection at diode interfaces and demonstrates the basic effects of small changes in device performance variables on the model prediction.

Recent and ongoing efforts have successfully used genetic algorithms to back-infer material properties from device performance data in microgap devices [173]. However, these models primarily focus on conventional parallel-plate vacuum diodes. Novel designs require more involved physics incorporated into the underlying model, further complicating the back-inferencing process to determine effective performance properties. Current and future challenges include accounting for all the relevant physics associated with these new devices while ensuring they are grounded by real device performance and developing data-driven modeling techniques that provide insight into the material and device behavior under real operating conditions. Further challenging existing modeling capabilities is the need for end-to-end system level models with insight into lifetime device performance under varying operating conditions [5].

As thermionic technology advances and interest grows in commercial device development, it is critical to have accurate performance predictive models and effective system models useful for practical case studies. Performance predictive models become increasingly complex for devices with cascaded designs, textured surfaces, intragap plasma, and other modern designs. As device designs become more complex, and proposed applications require significant resiliency in the energy conversion system, it becomes increasingly important to consider predicting performance using data-informed modeling frameworks.

Advances in science and technology to meet challenges

There have been significant improvements to computing power and the advancement of ML tools since the end of the thermionic fuel element verification program and subsequent reduction in thermionic R&D efforts in 1995 [174]. Since then, not only has ML evolved significantly, but also there has been a steady increase in innovative approaches to combining ML and physics. Recent studies have successfully applied these new techniques to legacy thermionic device performance data to gain a new perspective on device behavior [172]. Figure 18 illustrates the results of applying these techniques to back-infer material characteristics and the resulting model versus performance data. In this case, the mean absolute error of the model tailored to device data is less than 5%.

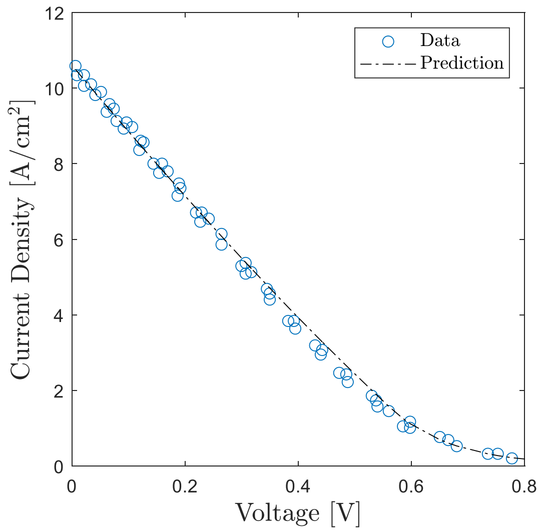

Figure 18. Comparison between performance data and vacuum diode performance model with back-inferred values of emitter work function, collector work function, and gap width. The mean absolute error between the data and the model is 4.8%.

As thermionic technology is considered more seriously for modern applications, it is advantageous to have system-level modeling capabilities, lifetime performance models, and transient behavior predictions. These complex systems are good candidates for Physics Informed Neural Networks (PINNs), which can be effective tools in performance prediction for complex non-linear systems with multiphysics constraints and has been increasingly leveraged in CFD studies. First introduced in 2019, PINNs are neural networks restricted by governing physics described by partial differential equations (PDEs) [175]. The PINNs effectiveness in solving classical quantum mechanics, fluids, and time varying nonlinear systems was demonstrated in the original presentation of the data-driven algorithm and is proposed as a valuable tool for data-driven performance forecasting and multi-physics/multi-scale simulation [175]. A 2023 study presents the flexibility of PINNs and the results of non-adaptive uniform and adaptive nonuniform sampling in solving PDEs, allowing for an efficient meshless physics-informed modeling [176]. Future work in thermionic material and device performance modeling should leverage these advanced computational tools, especially with the emerging high-performance device designs.

Advancing modeling capabilities through the merging of ML techniques with known physics can allow for the development of system, device, and materials models with governing equations dictated by real system behavior, allowing for improved predictive capabilities. Models should consider a study in transient behavior for long-duration diode operation at relevant temperatures, using a data-driven methodology that leverages emerging ML tools. Additionally, investigators should consider system level 3D multiphysics models where commercial software is merging with ML tools to enable more comprehensive and effective predictive capabilities.

Concluding remarks

Modern modeling capabilities include significantly more computing power for modeling complex materials and device geometries, and computer architectures designed specifically for leveraging ML. Emerging ML tools can be meshed with physical models to provide a new perspective and high-resolution prediction of material and device behavior. The emerging techniques such as PINNs and ML integrated multiphysics models present potential avenues for improving predictive capabilities and further proving the validity of thermionics as practical energy conversion devices. We are now in a new era for performance prediction of thermionic materials and devices and should explore the new tools available to provide a picture of modern thermionic converter capabilities during a device's lifetime.

14. Development of PETE converters

*Matteo Mastellone**, *Alessandro Bellucci and Daniele M. Trucchi*

CNR-Istituto di Struttura della Materia (CNR-ISM), Italy

E-mail: matteo.mastellone@cnr.it

Keywords: cathode semiconductor, photon absorption, device engineering

Status

Although the use of PV technology is widely diffused, its efficiency remains constrained by the intrinsic properties of semiconductor materials, particularly the bandgap of the active layer, which restricts sunlight absorption to a specific wavelength range. This constraint, particularly enhanced for wavelengths in the infrared spectrum, limits PV theoretical maximum efficiency for single-junction cells at 33.7% (Shockley–Queisser limit). In practice, real-world inefficiencies, such as absorption imperfections or material resistivity, further reduce performance due to material and device fabrication challenges.

TE can offer a complementary approach when the sunlight is concentrated by converting solar energy into thermal energy and then into electrical energy. Despite a high theoretical conversion efficiency far exceeding 30% [6], practical vacuum microgap TECs achieved efficiencies of about 10% at temperatures above 1300 K limited by the difficulties in balancing electrode WFs and operating temperatures [5].

Since the paper by Smestad introduced the concept of relying on both thermal and photon emission effects [177], PETE-based converters have emerged as a promising alternative that combines the benefits of both PV and TE mechanisms [13], aiming to overcome the limitations correlated to the independent converters. PETE uses photons to provide the energy needed to excite electrons in the CB of a semiconducting absorber, which are then thermionically emitted from its surface. The key innovation in PETE lies in the capability to harness both photon and thermal energy, allowing for more efficient conversion of sunlight into electrical energy. By simultaneously exploiting higher-energy solar photons for charge carriers' generation and lower-energy ones for thermal energy harvesting, PETE offers the potential for significantly higher conversion efficiencies compared to standing-alone traditional PV or TECs.

In TE, thermal excitation provides electrons with enough energy to overcome the emitter's WF, enabling emission and establishing a current flow, as described by the Richardson–Dushman equation. PETE enhances this process by also exploiting the photon absorption, where photons with energy $h\nu$ can excite electrons. The efficiency of PETE depends on the semiconducting cathode's capability to absorb photons and utilize their energy to surpass the electron affinity barrier, which is a far smaller quantity than the WF ruling the TE. The mechanism results in a more intense emission current than standard TECs at a given temperature. Additionally, the thermalization of excess photon energy and sub-bandgap absorption, usually known in PV as thermalization and absorption losses, contributes as heat sources, raising the cathode temperature and further boosting thermionic current density.

The cathode PETE current density is more conveniently written in terms of electron charge, e, electron density promoted in CB by radiation, n, average thermal velocity perpendicular to the surface v_x, cathode temperature, T, Boltzmann constant, k_B, and electron affinity, χ:

$$J_{th} = en\langle v_x\rangle e^{-\chi/k_B T}. \tag{9}$$

Photoexcitation, which determines an increase of the electrons' concentration in the conduction-band over the equilibrium value, together with the temperature increase, which facilitates the electron emission over the electron affinity barrier, contributes to the increase of the current density emitted from the PETE cathode with respect to that of a conventional thermionic cathode.

During the last decade, several theoretical analyses were carried out to estimate the conversion efficiency of PETE devices after the first estimation performed in 2010 by Schwede *et al* [13], predicting an efficiency larger than 40% for an incident solar radiation concentration of 1000 suns and a cathode temperature over 500 K. Subsequent analyses refined the model by including loss mechanisms that were not taken into account. In 2013, a model including the heat exchange between cathode and anode provided an overall efficiency of 38% at a concentration of 1000 suns under the assumption of optimal values of cathode's bandgap and electron affinity [178]. In 2016, Wang *et al* investigated a novel model of PETE device featuring a nanoscale vacuum gap. By incorporating the effects of quantum tunneling and image force correction, their study predicted that under solar concentration of 1000 suns, the

PETE device could achieve an efficiency of 48.6% when operating with a cathode temperature of 1321 K [179]. A refined thermodynamic model performed by Xiao *et al* [180], taking into account a detailed energy balance and entropy analysis, predicts a solar-to-electrical efficiency of 54.32% under 500-sun concentration.

Varpula and Prunnila established a more rigorous diffusion-emission theory that accounts for realistic semiconductor transport. Their model highlights the critical role of surface recombination and electron diffusion lengths in determining device performance, demonstrating that efficiency is highly sensitive to cathode temperature and electron affinity [181].

If combined with a secondary thermal cycle, the total system efficiency approaching 70% allows to exceed even the Carnot limit, as a validation that PETE converters mix advantages of photoelectronic and thermal machines [182].

Current and future challenges

PETE faces several significant challenges that hinder its current viability and necessitate future advancements across material science, engineering, and system integration. One of the primary obstacles lies in a refined optimization of the electrodes' surface properties. The cathode and anode for PETE converters should show low electron affinity and WF, respectively, to facilitate electron emission and collection. However, materials with such properties often lack other essential attributes, such as thermal stability or efficient photon absorption. Several proposed structures for PETE systems use III–V semiconductors [183] due to their excellent photon absorption properties and high electron diffusion lengths. However, these materials typically require alkali metal coatings, such as cesium, to achieve a low electron affinity suitable for electron emission [184]. Furthermore, these coatings are highly sensitive to high temperatures, leading to instability and degradation over time. Developing robust, thermally stable alternatives to alkali coatings is a critical topic of ongoing research to improve the durability and practicality of PETE devices.

The first proof-of-concept demonstration reported by Schwede *et al* on a Cs-coated p-type GaN cathode [13] was followed by a GaAs/AlGaAs heterostructure coated with Cs–O [185], which showed an external quantum efficiency of 1.4% at a cathode temperature of about 400 K, far from the high efficiencies of the theoretical model owing to a low escape probability for the emitting electrons. The explored temperatures of such a PETE cathode were <400 K owing to instability of the Cs–O coating. Alternatively, Reck *et al* [186] presented experimental results on heavily doped *p*-type and *n*-type silicon, which is a thermally-stable material. Even though the study exhibits a photon-induced enhancement of the emission current at temperatures below the onset of dark TE, the necessity of a Cs-coating prevents the cathode operations over 600 K in a vacuum environment. It is indisputable that to obtain efficient electrons' emission, the cathode should achieve high temperatures. This represents a critical challenge for PETE systems since it demands materials capable of withstanding prolonged thermal stress without degradation. A solution to provide higher operating temperatures is the use of materials compatible with thermally-stable coatings or chemical terminations. Synthetic diamond films have been proposed and explored, especially thanks to the robust hydrogen surface termination, that attributes low and even NEA, and the capability to withstand extreme temperatures under vacuum. Phosphorus-doped diamond has emerged as a compelling candidate for low-temperature thermionic applications due to its unique electronic structure. Koeck *et al* demonstrated an effective WF as low as 0.9 eV. This exceptionally low barrier allows for detectable TE at temperatures below 400 °C, significantly lower than traditional metallic emitters [187]. Additionally, nitrogen-doped and hydrogen-terminated diamond films were deposited on p-type Si substrates to provide low WF surface (1.9 eV) with operational stability up to 1000 K [188]. Such a configuration, combining a robust p-type Si absorber and an n-type diamond emitter, was tested under monochromatic irradiation in the wavelength range from 400 to 450 nm. The related cathodes provided a substantial increase in the photo-induced electron emission as the temperature increased up to 700 K. The injection of electrons at the silicon/diamond film interface is the relevant mechanism limiting the structure performance. Such a mechanism has been accurately investigated in [189]. An alternative *p*-type/intrinsic diamond structure has been developed, based on a monolithic photocathode consisting of a periodic nanostructured surface (i.e. black diamond technology [190]) as a sunlight absorber with a hydrogenated emitting surface [61]. Nanotechnology tools such as treatments with ultrashort lasers enable efficient photon absorption, which has a primary importance in the device efficiency. Development of ordered nanostructures on the active materials' surface or embedded in the bulk enhance photon capture and conversion aim to maximize the use of impinging solar energy, including infrared band wavelengths. Nanostructured surfaces can also enhance electron emission by optimized surface geometries [81]. Looking forward, the integration of 2D emerging materials [12] can

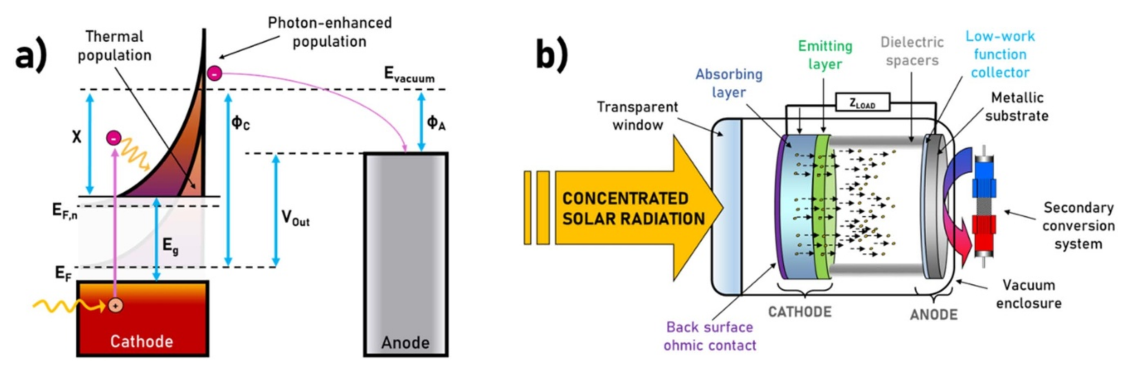

Figure 19. (a) Energy band diagram illustrating the PETE mechanism, where incident photons excite electrons to higher energy states, reducing the effective work function and facilitating thermionic emission. The combination of photon absorption and thermal excitation enhances electron emission efficiency. Reproduced from [13], with permission from Springer Nature. (b) Schematic representation of a parallel-plate PETE converter.

offer solutions for smart and compact converters, potentially offering a viable pathway for high-efficiency solar energy conversion in CSP systems.

One noteworthy alternative to the traditional configuration shown in figure 19(b) is the adoption of a side-illuminated architecture [191]. In this design, the illumination surface is decoupled from the emission surface, enabling more flexible thermal management and facilitating integration with a secondary thermal conversion cycle. By maintaining both electrodes at essentially the same temperature, this configuration can mitigate detrimental temperature gradients while allowing for more effective recovery of waste heat from the anode for subsequent energy conversion. Such features offer the potential to improve overall device performance and support the deployment of multiple PETE stages in series.

Another major challenge involves heat distribution. The cathode temperature needs to be uniform to ensure consistent electron emission across the entire surface. However, achieving this uniformity is complicated by several factors. Solar concentration typically creates hot spots, and the device's specific geometry can lead to uneven heating patterns. Furthermore, the edge effects and thermal gradients near the device boundaries can create cold zones that reduce overall efficiency. Another critical aspect is the thermal management of heat flow between the cathode and anode. The cathode needs to maintain its high temperature for emission, while the anode must operate at a relatively cooler temperature to effectively collect electrons and avoid their counter-emission. This temperature difference is essential for PETE operation, but maintaining it requires sophisticated thermal insulation techniques, such as dielectric microspacers between the two electrodes [132].

Moreover, continuous exposure to ultraviolet radiation can degrade active materials over time, reducing efficiency and operational life. Long-term studies and accelerated aging tests will be critical to identifying materials and designs capable of maintaining performance over extended periods.

Advances in science and technology to meet challenges

Innovations in vacuum-gap engineering and electrode spacing control should lead to improved device stability and more consistent performance under real-world conditions. One possible strategy is the development of dielectric microspacers between the two electrodes [132], which must guarantee thermal and electrical insulation, as well as avoid space-charge conditions. The latter is a common challenge with thermionic devices, since the architecture of the PETE device is the same of that of conventional thermionic converters.

The integration of a secondary thermal cycle after the PETE process represents another possible advancement in maximizing overall system efficiency. In this configuration, the residual thermal energy from the PETE device is collected and utilized in a subsequent thermal cycle. By implementing a secondary thermal stage, engineers have demonstrated the potential to boost total system efficiency up to 20% above standalone PETE systems [182]. The heat transfer from the PETE collector to the secondary thermal cycle can be optimized through specialized heat exchangers and working fluids designed to operate efficiently at these elevated temperatures. In this context, thermoelectric generators can be used for a fully solid-state combined technology. This dual-cycle approach not only improves overall energy conversion efficiency but also provides more flexible power generation options, as the secondary thermal cycle can continue to generate electricity even during periods of reduced solar irradiance, thereby enhancing the system's reliability and practical utility in real-world applications.

Concluding remarks

PETE technology stands at a crucial stage in its development, with recent advances in materials science, thermal management, and device architecture bringing it closer to a practical implementation. Although promising advancements are ongoing, current laboratory demonstrations have shown limited conversion efficiency values, due to several challenges remaining to be addressed. In particular, there is the need for optimizing material stability at operating high temperatures, engineering the device architecture, reducing manufacturing costs, and improving system integration with secondary thermal cycles. Looking ahead, the combination of emerging materials, nanotechnology tools, advanced thermal management strategies, and hybrid system design suggests a promising trajectory for PETE technology, potentially establishing it as a solid-state high-temperature solar cell to make economically competitive and scalable next-generation CSP systems [192].

15. Advances in hybrid TIPV energy converters

Alejandro Datas

Instituto de Energía Solar – Universidad Politécnica de Madrid

E-mail: a.datas@upm.es

Keywords: thermionics, photovoltaics, thermophotovoltaics, near-field

Status

Hybrid TIPV energy conversion, introduced in 2016 [193], optimizes TECs by simultaneously utilizing photon and electron energy fluxes, effectively reducing radiative thermal losses. This method is especially beneficial for submicron-gap vacuum TEC devices, where the small inter-electrode distance enhances photon tunneling and significantly increases radiative energy transfer. In TIPV, a transparent thermionic collector is placed on a PV cell, enabling photons emitted by the cathode to be absorbed by the PV cell, generating additional electricity.

The first experimental demonstration of a two-terminal TIPV device was reported in 2020 using GaAs-based PV devices [148] (figure 20(a)), followed by validations with InGaAs-based PV devices [194] graphene-on-silicon heterojunction [195], as well as three-terminal [196] (figure 20(b)) and four-terminal [197] (figure 20(c)) configurations. A related study in 2019 also demonstrated enhanced TEC performance by illuminating a GaAs collector with a 532 nm laser. However, the improvement was attributed to the generation of surface photovoltage, rather than to the TIPV effect [184]. Several conceptual TIPV converters have been also proposed and analyzed theoretically. Early works focused on analyzing sub-micron interelectrode distances to assess the impact of near-field radiative heat transfer on the overall TIPV performance [145, 198, 199]. Other investigations explored TIPV converters based on Schottky junctions [200], as well as designs incorporating a graphene collector and a filter between the collector and the PV cell [201], a configuration further examined for solar-powered TIPV applications [202]. Hybrid approaches have also been studied, including a solar photo- TIPV converter that integrates PETE with TIPV. In this design, high-energy solar photons enhance TE in a semi-transparent cathode, while low-energy photons and thermal radiation are absorbed by the PV cell [203, 204]. Additional advancements include the evaluation of a hybrid thermionic-thermoradiative cell, similar to the original TIPV concept, but with the PV cell operating in thermoradiative mode, generating power by emitting photons toward a colder ambient [205]. This idea was later expanded by integrating it with the PETE-TIPV hybrid to create an inner-cascade PV-thermionic-thermoradiative converter [206].

Current and future challenges

The optimal interelectrode distances for vacuum TECs have traditionally been set in the single-digit micrometer range. However, recent studies accounting for nanoscale charge and thermal interactions suggest that sub-micron gaps yield better performance [79]. At these distances, near-field thermal radiation becomes the dominant heat transfer mechanism, significantly increasing energy losses in conventional TEC. Therefore, as the technology advances toward smaller interelectrode distances, TIPV emerges as a solution to overcome the efficiency limitations of conventional vacuum TECs.

A common limitation in most reported experimental TIPV implementations is the very low thermionic current densities, attributed to a combination of excessively high cathode WFs and large interelectrode distances. Thus, a key challenge remains the integration of an efficient thermionic sub-device within a TIPV system, particularly by reducing the WFs and the inter-electrode distance to eliminate space charge effects and leverage near-field radiative energy transfer. Moreover, a unique challenge specific to TIPV converters is the requirement for a transparent thermionic collector, which must enable photons to pass through and reach the underlying PV cell. This dual requirement—high optical transparency and sufficient electrical conductivity—introduces a significant design trade-off that must be carefully addressed.

Additional challenges unique to TIPV converters stem from the interconnection between thermionic and PV sub-devices. Based on the interconnection scheme, TIPV systems can be categorized into three configurations (figure 21): two-terminal, three-terminal, and four-terminal:

In a two-terminal configuration [148, 194, 195], thermionic electrons are injected in the VB of a semiconductor, then pumped to the CB by the PV effect and finally extracted from the CB to produce useful energy before they are reinjected in the cathode. In this configuration, both sub-devices are connected in series and there is a unique current flow through the whole device. The main challenge of this

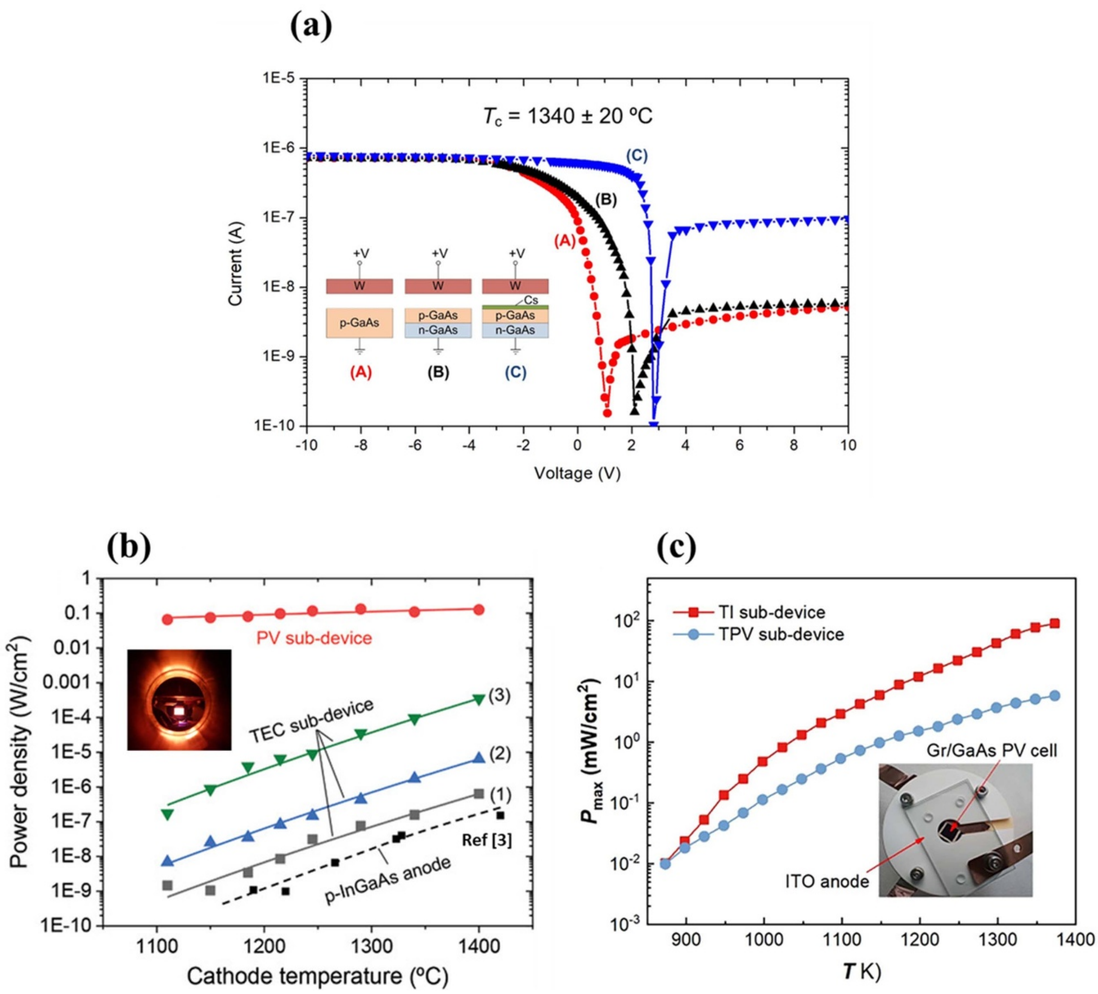

Figure 20. Experimental results for two-terminal [148] (a), three-terminal [196] (b), and four-terminal [197] (c) thermionic–photovoltaic (TIPV) converters. Reprinted with permission from [148]. Copyright (2020) American Chemical Society [196]. John Wiley & Sons. {Copyright © 2022 WILEY-VCH Verlag GmbH & Co. KGaA, Weinheim}. Reprinted from [197], Copyright (2023), with permission from Elsevier. (a) Current–voltage characteristics of a baseline thermionic converter (A) and two-terminal TIPV converters without (B) and with (C) Cs-coated anodes. (b) Power density of the photovoltaic and thermionic sub-devices in a three-terminal TIPV converter with different surface treatments: (1) none, (2) BaF_x anode, and (3) BaF_x anode with Sc_xO_y cathode. (c) Power density of the photovoltaic and thermionic sub-devices in a four-terminal TIPV converter.

configuration is that it prevents independent biasing of each sub device at their respective maximum power points. Current matching at maximum power point represents a very demanding condition that is only met at a particular thermionic cathode temperature, and it is also very sensitive to variations in the other device parameters (WF, interelectrode distance, etc). Another limitation of two-terminal configuration is that the injection of electrons in the VB requires the creation of a hole-selective contact (HTL in figure 21) at the surface of the semiconductor. Hole-selective contacts (e.g. p-type semiconductors) have their Fermi energy level pinned near the VB and typically exhibit higher WFs than electron-selective counterparts (e.g. n-type semiconductors). As a result, the TIPV device may experience a reduced thermionic voltage contribution.

In the three-terminal configuration [196], thermionic electrons are injected into either the valence or CB of a semiconductor and directly extracted from the same band before being reinjected into the cathode. Within the semiconductor, photogenerated electrons and holes are extracted from the conduction and VBs, respectively, as in conventional PV cells. In this setup, the band receiving the thermionic electrons serves as a shared channel for both the thermionic and PV processes. The key advantage of this configuration is the ability to independently bias both sub-devices while utilizing an electron-selective contact or ETL (figure 21) (e.g. an n-type semiconductor) with its Fermi energy pinned near the CB at the semiconductor surface to collect thermionic electrons. This enables the collector to have a lower WF, potentially increasing the thermionic voltage contribution of the TIPV device. However, a major challenge lies in interconnecting TIPV devices within a module, as this may require a sophisticated electrical scheme to convert the system into a two-terminal array.

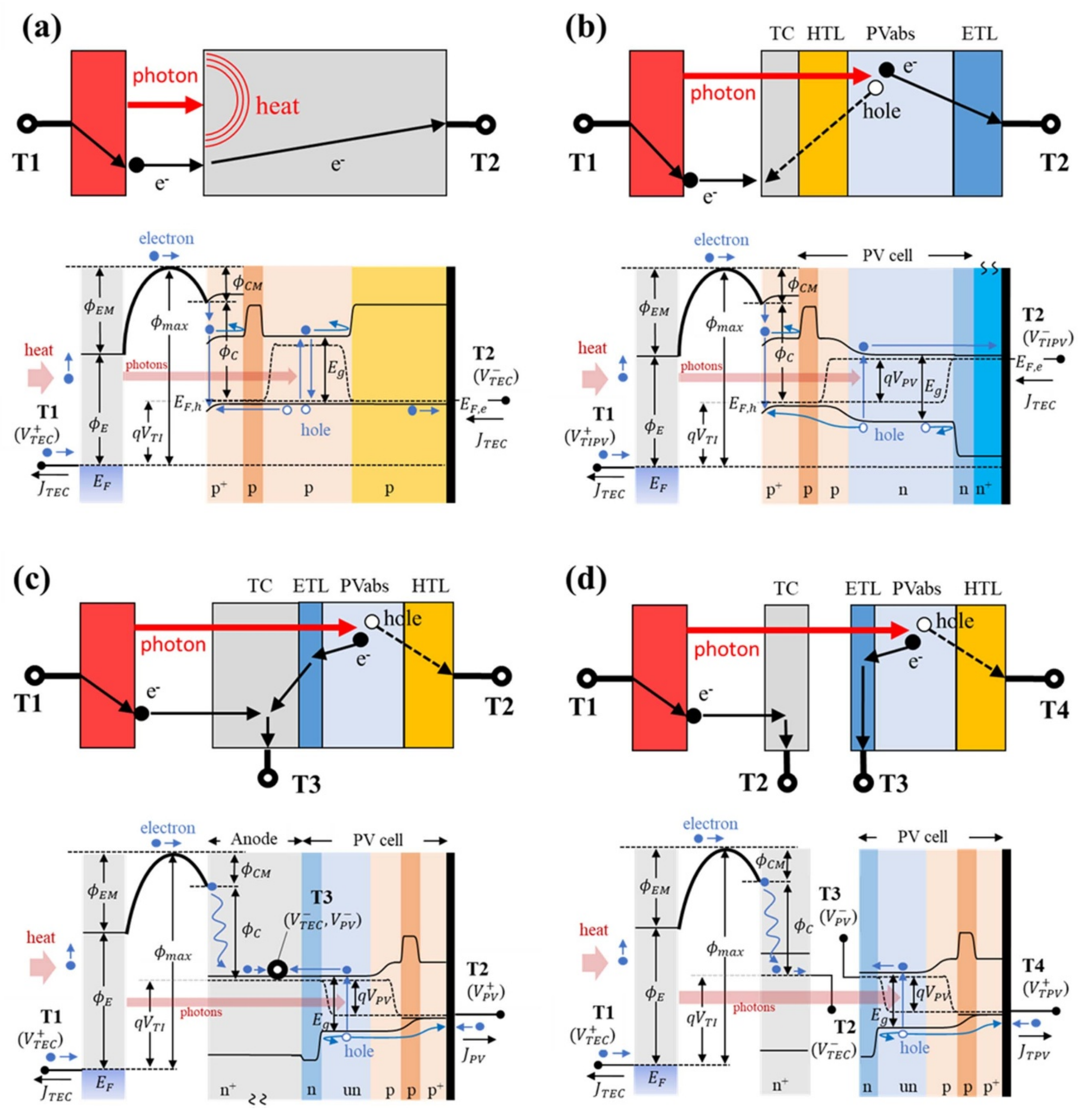

Figure 21. Schematics of a conventional TEC (a) and the three TIPV configurations: two-terminal (b), three-terminal (c), and four-terminal (d). TIPV systems consist of an emitter (thermionic cathode), a transparent collector (TC), and a PV cell, which includes a PV absorber (PVabs), a hole-transport layer (HTL), and an electron-transport layer (ETL). The band diagrams for each configuration are shown, indicating some key parameters, such as the emitter and collector workfunctions (ϕ_E and ϕ_C), interelectrode space-charge energy-barriers (ϕ_{EM} and ϕ_{CM}), bandgap energy of the PV absorber (E_g), quasi-Fermi energy levels for electrons ($E_{F,e}$) and holes ($E_{F,h}$), and internally generated voltage in the PV (V_{PV}) and thermionic (V_{TI}) stages.

In the four-terminal configuration [197], a TEC with a transparent collector is directly placed on top of a PV cell, with both devices maintaining their respective two-terminal structures. Similar to the three-terminal configuration, the primary advantage of this setup is that each sub-device can be biased at its maximum power point. However, the key advantage is the flexibility to interconnect the thermionic and PV stages independently, allowing for the formation of separate optimized arrays for each process. The main challenge of this configuration is the lateral extraction of current from the transparent thermionic collector. Achieving an optimal balance between transparency and high lateral electrical conductivity is crucial, as this trade-off may impose strict design constraints on the thermionic collector.

Advances in science and technology to meet challenges

As previously mentioned, a major challenge in all TIPV experimental demonstrations to date is the very low thermionic current densities. Addressing this challenge involves implementing similar strategies than in conventional TEC, such as the integration of advanced materials for TE and collection, and the implementation of solutions to eliminate the space charge effect, such as the establishment of micron- or sub-micron gap interelectrode distances. Solutions to address these challenges have been described in previous sections (all the sections included in Thermionic active materials and Device engineering parts) and, therefore, are not repeated here.

A key advancement required for TIPV technology is the development of transparent collectors. The concept of transparent collectors was proposed in the 1990s as a means to mitigate thermal radiation losses in conventional TEC [207]. Early solutions involved depositing ultra-thin metallic coatings onto transparent substrates, such as sapphire. Similar strategies have been implemented in TIPV experimental demonstrations, including ultra-thin film coatings of Cs [148], BaF [194, 196], and Ba-coated graphene [195] that where directly deposited onto PV cells, or indium tin oxide (ITO) coatings on borosilicate glass in the case of four-terminal TIPV realizations [197].

Other advancements are required depending on the specific TIPV configuration. For instance, in two-terminal TIPV configurations, a potential solution to mitigate the challenge of high collector WF—arising from Fermi-level pinning at the VB of the PV cell semiconductor surface—is the incorporation of tunnel junctions near the surface. A $n{+}{+}/p{+}{+}$ tunnel junction allows the PV cell to be terminated with an n-type material, even when electrons are injected into the VB of the PV absorber. Tunnel junctions have been widely developed for multijunction solar cells [208], where they facilitate electrical connection between sub-cells, and they could be readily adapted for TIPV systems. In four-terminal configurations, a potential solution to mitigate the lateral extraction of current from the transparent thermionic collector may involve the incorporation of thick metallic grids, as in [79], but this approach may be incompatible with sub-micron interelectrode gaps. Alternative solutions may include the use of thick transparent conducting films, such as ITO, as in [197].

Another challenge for sub-micron gap TIPV converters is optimizing PV energy conversion in the near-field regime [145, 198, 199]. At these distances, near-field thermal radiation can excite resonant optical modes, such as surface plasmon and photon polaritons, which may enhance or hinder PV efficiency depending on their alignment with the PV cell bandgap. Research in near-field TPVs (NFTPVs) has explored these challenges since the early 2000s [209], proposing various strategies to mitigate losses or exploit resonant effects. While a detailed discussion is beyond this work, further insights can be found in NFTPV literature [209]. Additionally, the impact of low-workfunction thermionic coatings on near-field radiative transfer remains an unexplored area with potential implications for TIPV performance.

Concluding remarks

Hybrid TIPV energy conversion presents a promising solution to overcoming the efficiency limitations of conventional TECs by simultaneously harnessing photon and electron energy fluxes. While recent advancements have demonstrated the feasibility of TIPV systems, experimental implementations still face significant challenges, primarily due to low thermionic current densities—an issue shared with conventional vacuum TECs. In addition to these common obstacles, TIPV technology presents unique challenges, including the development of transparent thermionic collectors and the reduction of interelectrode distances to the sub-micron scale to minimize space charge effects and enhance near-field radiative energy transfer. Various TIPV configurations—two-terminal, three-terminal, and four-terminal—have been proposed, each with specific challenges that require further research and optimization. Regardless of the chosen configuration, future advancements should focus on the integration of near field TPV concepts to optimize radiative energy transfer and maximize energy conversion.

16. Carbon footprint and economics of thermionic topping system

Guanghua Zheng[1,*] and Lili Wang[2]

[1]Institute of Energy, Hangzhou Dianzi University, Hangzhou 310018, People's Republic of China
[2]Zhejiang Technical Institute of Economics, Hangzhou 310018, People's Republic of China

E-mail: guanghuazheng@hdu.edu.cn

Keywords: efficiency, life cycle analysis, economic viability

Status

To combat global warming, nations have been actively transitioning their energy structures from centralized, large-scale, and high-emission systems to distributed, environmentally friendly integrated energy configurations. This shift toward sustainable technologies underscores the urgent need to improve power generation efficiency as a key strategy for reducing carbon emissions and capital investment [210]. TECs, initially developed for space applications, are emerging as a versatile solution for terrestrial energy systems. By utilizing a vacuum-separated cathode and anode, TEC could theoretically achieve impressive conversion efficiency of approximately 40%, offering a direct and advanced method for converting heat into electricity [54]. Their ability to harness high-temperature gradients between heat sources and the ambient makes them especially suitable as topping cycles in traditional thermal energy systems, such as fossil fuel-fired and CSP plants.

In fossil fuel-fired power plants, where thermal efficiency typically ranges between 30%–40%, integrating a thermionic topping cycle can significantly enhance overall system efficiency, exceeding 50% [150]. This improvement translates to a reduced fuel requirement per unit of electricity generated, effectively lowering carbon emissions per kilowatt-hour. Additionally, the reduced fuel consumption and associated operational emissions make the system more environmentally friendly and economically viable, particularly when combined with government incentives, such as subsidies or carbon credit schemes [211].

In the context of CSP, while electricity costs have fallen in recent decades, they remain higher compared to other renewables. Currently, the average cost of CSP systems is still 3–4 times that of wind power and 5–6 times that of PV systems. Despite this, CSP technology offers unique advantages, such as achieving solar concentrator ratios up to 3000, which can produce extremely high receiver temperatures of up to 2000 °C [212]. These temperatures exceed the operating limits of conventional heat engines but align well with TECs' capabilities. The high hot-side temperatures enable greater heat-to-electricity efficiency with combined with thermionic topping cycles, and consequently a reduction in carbon emissions, ultimately contributing to more competitive electricity pricing.

However, the integration of thermionic topping systems into these applications requires meticulous optimization, as shown in figure 22, considering carbon emissions, system costs, and their influence on overall energy system performance. This holistic roadmap focuses on the carbon footprint and economic feasibility of thermionic systems, addressing their environmental impact and the cost-effectiveness of integrating this advanced technology into integrated energy production frameworks.

Current and future challenges

The challenges in thermionic energy systems predominantly involve device fabrication and system integration, where energy-intensive manufacturing processes and material limitations significantly impact sustainability and performance. High capital expenditure stems from the use of high-purity materials like cesium (\$207.15 g^{-1}) and tungsten (\$19.54 kg^{-1}) processed via carbon-heavy techniques such as powder metallurgy and high-temperature sintering, alongside complex vacuum encapsulation processes. While advanced materials like nanostructured cathodes, e.g. LaB_6 films deposited via magnetron sputtering or electron-beam evaporation, reduce WFs to enhance conversion efficiency, their stringent thickness uniformity and crystallinity requirements escalate production costs. Similarly, graphene cathodes synthesized through CVD exhibit superior electron emission but generate substantial emissions of up to 500 g CO_2/g graphene due to methane pyrolysis and high-temperature processing [213]. Besides, vacuum encapsulation demands precise thermal expansion matching to prevent microcracking in traditional glass-to-metal seals (e.g. Kovar alloys), while advanced metal-ceramic seals endure high temperatures but cost 3–5 times more due to complex brazing. Emerging solutions like wafer-level bonding enable miniaturized vacuum cavities but require ultra-clean environments and harsh bonding temperatures.

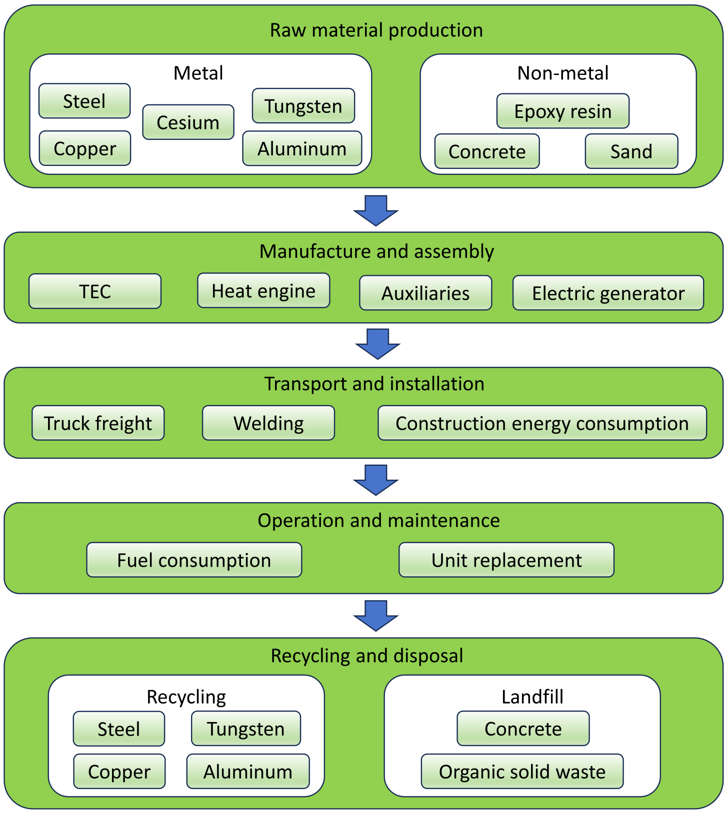

Figure 22. Carbon footprint boundary of thermionic topping system.

On the other hand, thermionics-integrated hybrid systems require tailored designs that balance application-specific adaptability, lifecycle costs, and carbon footprints. Incorporating a thermionic topping cycle can reduce the levelized cost of electricity (LCOE) relative to standalone heat engines. Current integration strategies mainly encompass cascading with conventional heat engines or with solid-state thermal converters. According to our previous assessments, a thermionic-Stirling power system can theoretically achieve an LCOE as low as 50–87 $ MWh^{-1} in typical Chinese regions, whereas traditional Dish-Stirling systems often exceed 115 $ MWh^{-1} and mature utility-scale solar PV range between 38–78 $ MWh^{-1} [214]. Thermionics-PVs usually employ GaSb cells (0.72 eV bandgap) to convert infrared radiation from 1500 K broadband heat sources into electricity. However, their scalability is hindered by costly GaSb PV cell and low-efficiency single-junction structures of merely 3%–5%, resulting in a unit power cost of $50–100/W [215]. While efficiency gains are achievable through tandem architectures or nanostructured selective emitters, process complexity exacerbates both emissions and costs. Besides, for thermionics-thermoelectrics, one promising heat-resisting material is SiGe alloys (up to 900 °C). However, their fabrication processes, such as CVD, emit 500–800 kg CO_2/kg, far exceed mid-low-temperature thermoelectrics like Bi_2Te_3 [216]. Hence, except for energy efficiency maximization, tailored designs must consider lifecycle costs and carbon impacts to ensure that the thermionic based systems are adaptable to specific applications.

Advances in science and technology to meet challenges

Breakthroughs in computational modeling and life cycle analysis tools provide more accurate assessments of carbon footprints and economic viability, guiding material selection and system optimization. The existing carbon emissions and economic analyses of components like PVs and gas turbines provide valuable insights for optimizing the design and packaging processes of thermionic topping systems [217]. Advances in cutting-edge material science have enabled the development of high-performance thermionic components, such as nano-engineered cathodes and anodes with enhanced thermal and electrical properties. Low WF materials such as graphene, doped diamond, and nanostructured surfaces, offer promising improvements in TE while enhancing thermal and chemical stability [190]. The Innovations in the related fabrication processes, including advanced coating techniques and recycling protocols, have significantly reduced the energy intensity of production while reducing the carbon footprint and economics of TEC components for large-scale applications.

The low-carbon operation of integrated energy systems can be achieved by incorporating demand response strategies and carbon trading mechanisms to offset the initial costs of thermionic systems [218]. Demand response leverages price incentives to shift load demand, improving the alignment between energy supply and consumption. This helps stabilize load peaks and valleys, enhance economic efficiency and deliver additional environmental benefits. Carbon trading provides an additional revenue stream, allowing the system to generate income through the sale of carbon credits or savings on carbon allowances. The implementation of tiered carbon trading can significantly reduce the integrated energy system's carbon footprint—by as much as 6.7% [219]. For instance, in coal-fired power plants, the higher upfront costs of thermionic systems can be offset by fuel savings and reduced emissions, particularly in regions with established carbon pricing policies. These benefits are further amplified when combined with government incentives and carbon credit schemes.

Concluding remarks

The thermionic topping cycle offers a promising pathway for increasing the efficiency and reducing carbon emissions of heat-to-electricity terrestrial application, particularly in CSP and fossil fuel-fired power plants. The current economic and environmental challenges need to be addressed to unlock the full potential of this technology. Future research should focus on material innovation, particularly in finding alternatives to expensive and rare materials like cesium, and on improving the durability of thermionic converters. Additionally, policy mechanisms such as carbon pricing and subsidies for high-efficiency technologies will be critical in incentivizing the adoption of thermionic systems at scale. By balancing carbon reduction benefits with economic feasibility, thermionic topping systems could play a key role in the global transition to cleaner energy solutions.

17. Present and future applications of thermionics

Gang Xiao[1,*] *and Hao Qiu*[2]

[1]State Key Laboratory of Clean Energy Utilization, Zhejiang University, Hangzhou 310027, People's Republic of China
[2]School of Energy and Power Engineering, Shandong University, Jinan 250061, People's Republic of China

E-mail: xiaogangtianmen@zju.edu.cn

Keywords: space nuclear power thermionic system, hybrid CSP-PETE, efficiency

Status

TE, essentially, provides an electron source in the form of a heated cathode. Broadly speaking, it encompasses various forms such as PETE, electric field-enhanced TE, and Cs ion-enhanced thermionic transport. Given the outstanding advantages such as simple structure, high efficiency and flexibility, thermionics has a wide range of applications. A historical trajectory and expansion of thermionics applications are summarized in figure 23.

In the power generation and supply field, the Soviet Union, the United States, and Western European countries began to explore the space applications of thermionic devices in the mid-20th century. Typical applications included the TOPAZ and TOPAZ-II space nuclear power thermionic systems [220]. However, this technology has not been used for a long time. Up to now, the applications related to thermionic electric generation mainly include space nuclear power systems, CSP systems, and industrial waste heat power generation. However, due to issues such as vacuum sealing, continuous and long-term stable operation, and cost, most of the above-mentioned scenarios are still at the laboratory stage and have not achieved large-scale implementation. Once these problems are overcome, these scenarios will be commercially implemented on a large scale, and this will give rise to even more potential application scenarios, including lunar surface power supply units, deep-space probes (such as Jupiter and Mars probes), and power supply for deep-sea exploration equipment (or bases). In addition, thermionics can provide power for extreme environment monitoring. For example, it can supply high-temperature-resistant and maintenance-free power to sensors inside nuclear reactors.

In the fields of microscopy and measurement, hot-cathode ionization vacuum gauges [221] and transmission electron microscopy [222] have achieved mature commercial applications and there are corresponding commercial products available. The corresponding potential applications, which are thermionic heat flux meters and thermometers, are proposed by the author of this section for the first time. The thermionic current is directly related to temperature and the heat flux of the heat source, and it has a rapid response. These can be used for heat flux and temperature measurement in high-temperature environments, such as in high-temperature furnace equipment and for measuring the temperature of metals in a smelting furnace.

In addition, TE cooling is still in the research stage, yet it holds potential application prospects in certain specific fields. For instance, it could be applied to the local cooling of microelectronic devices, experiments in low-temperature physics, and the cooling systems of space probes.

Current and future challenges

This subsection focuses on the engineering bottlenecks in the application scenarios and summarizes the research issues and challenges for different application scenarios respectively. For thermionic devices in space missions, cost is often not a limiting factor. Space-based equipment typically cannot be maintained manually. Thus, the most critical requirement is its long-term stable operation, with an extremely stringent demand for the device lifespan, which must exceed 10 years. Jupiter/Mars probes are required to operate stably in an environment where ultra-low temperatures and intense radiation alternate. Existing thermionic materials may fail under such conditions. Current thermionic devices rely on a high-vacuum environment (or filling Cs vapor in the high-vacuum environment) to maintain the electron transfer across the electrode gap. However, the vacuum packaging technology is vulnerable to issues such as material thermal expansion and micro-leakage, which will lead to performance degradation during long-term operation. Low WF hot cathodes (such as dispenser cathode materials) are prone to performance degradation under continuous high temperatures (>1200 °C), shortening the lifespan of the equipment. For deep-sea equipment, the impact of high pressure on the vacuum chamber needs to be addressed.

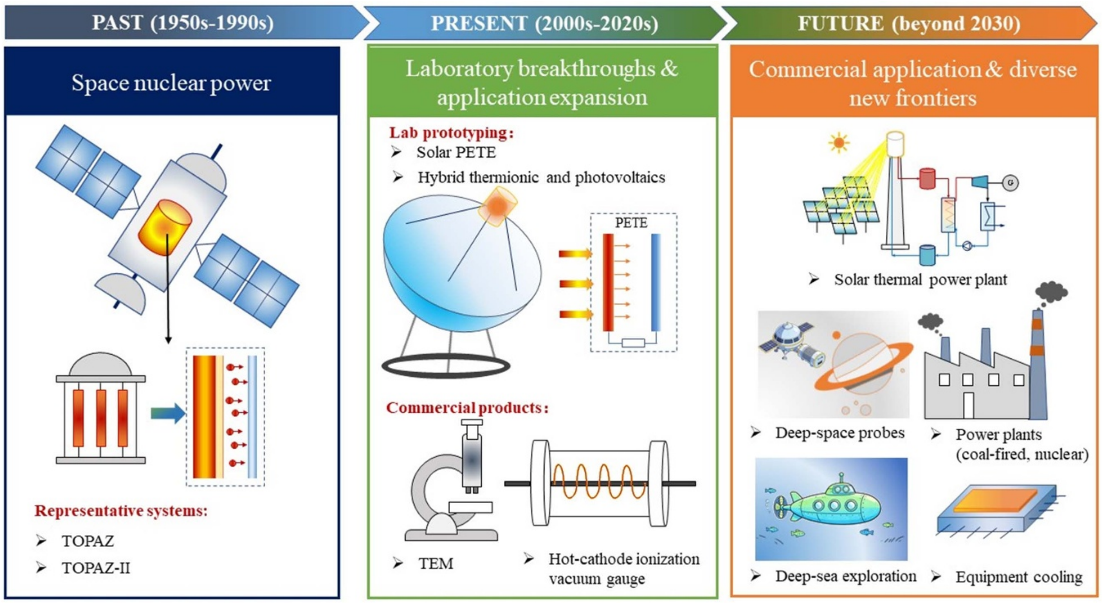

Figure 23. The evolutionary roadmap of thermionics: from space power to multi-domain applications.

For thermionics in the civilian power generation field, the most crucial common issues are to improve efficiency and reduce costs. Three major challenges need to be addressed. Firstly, the limitation of the space-charge effect on inter-electrode electron transport. Secondly, the preparation of high-performance, long-life, and low-cost electrode materials. Thirdly, the effective packaging and maintenance of vacuum devices in non-stable high-temperature environments. The most promising market application in the civilian power generation field is the combination with current CSP plants. Although the proposal of the PETE has increased the comprehensive ideal efficiency of the system to nearly 50% [13], when it comes to the combination with current CSP plants, there are still some specific challenges. The sunlight penetration loss and electron diffusion loss of the cathode are in conflict. To overcome this issue, a suitable cathode thickness usually needs to be selected to achieve a trade-off between these two conflicting factors [147, 223]. The operating temperature of existing CSP plants is generally lower than 1200 °C, making it difficult to achieve the ignition mode Cs ionization and thus making it hard to overcome the space-charge effect. The temperature of the anode waste heat is limited, which makes it difficult to efficiently couple with existing advanced thermodynamic cycle power generation (as discussed in section 11). Finally, the structural and system design of thermionic converter to be potentially used from kilowatt-level to megawatt-level production needs to be considered.

Advances in science and technology to meet challenges

Recent advancements have focused on improving the efficiency, reliability, and scalability of thermionics. Due to space limitations, this subsection focuses on a potential approach to achieving the efficient coupling of PETE technology with CSP plants in the future. The anode-incident PETE can effectively address the conflict between sunlight penetration loss and electron diffusion loss. As shown in figure 24, concentrated solar photons first penetrate the transparent anode and are absorbed by the cathode after passing through the gap. In this way, the incident surface for collecting photons is the emission surface for releasing electrons, reducing the recombination loss during the electron diffusion process. In such a configuration, either a bulk cathode or a cathode with a black substrate can be employed to substitute the thin-film cathode in traditional PETE systems, thereby averting the transmission loss of solar photons. In addition, existing research has demonstrated that sunlight can enhance the ionization of Cs atoms [224, 225]. Therefore, sufficient ionization of Cs can be achieved without the need for a high-temperature ignition mode, thereby overcoming the adverse effects of the space-charge effect.

Figure 24 presents a coupling mode of PETE and CSP plants. The PETE unit is designed as a standardized ‘heat-absorbing tube’, in which the working fluid (such as supercritical CO_2) of the thermodynamic cycle flows, and the inner wall of the tube directly exchanges heat with the cathode of PETE. Part of the sunlight absorbed by the cathode is used for PETE power generation, and part is absorbed by the working fluid. Compared with using the anode waste heat, the heat source temperature of the thermodynamic cycle system is significantly increased. In this way, it can also be well integrated with energy

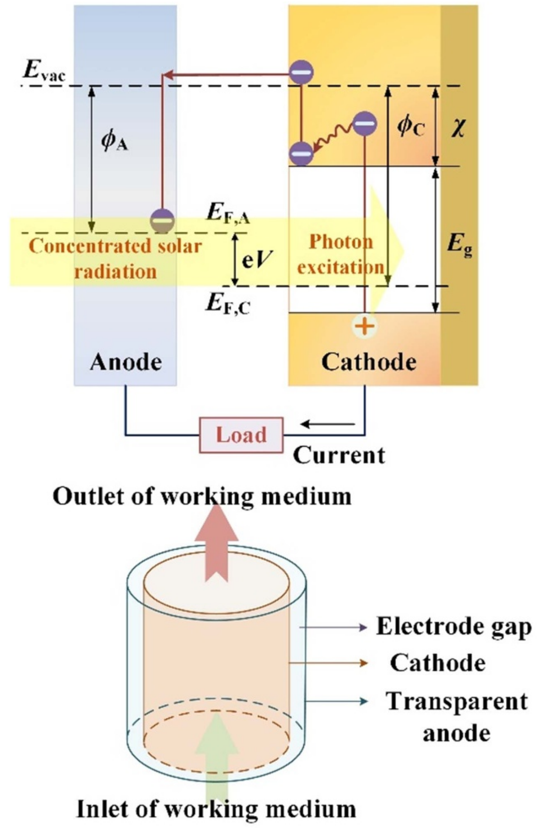

Figure 24. Band diagram of anode-incident PETE and schematic diagram of its coupling structure with CSP .plant's heat-absorbing tube [204, 226].

storage. Through reasonable design and control, the coordinated optimal operation of the PETE module and the thermodynamic cycle power generation module can be achieved respectively.

Concluding remarks

Thermionics, with its characteristics of simple structure, high efficiency and flexibility, shows unique potential in fields such as space energy, industrial waste heat recovery, and solar power generation. Although current technologies are still restricted by challenges such as material degradation, vacuum packaging costs, and the space-charge effect, through collaborative breakthroughs in materials science and engineering innovation (such as the CSP-PETE hybrid system), the dawn of its commercial application has emerged.

Data availability statement

The data that support the findings of this study are available upon reasonable request from the authors.

Acknowledgments

1. Introduction

Alessandro Bellucci, Gideon Segev and Daniele M Trucchi

The work described in this publication was subsidized by the European Union under the Horizon Europe Work programme–Cluster 5 managed by CINEA-European Climate Infrastructure and Environment Executive Agency through the BLAZETEC project, Grant Agreement No. 101160724. Views and opinions expressed are however those of the author(s) only and do not necessarily reflect those of the European Union or CINEA. Neither the European Union nor the granting authority can be held responsible for them. We would like to thank Ms Caroline Mitchell, Ms Elin Morris and

Dr Róisín Guthrie of IOP Publishing for the continuous and very appreciated support in the production of this roadmap.

2. Perovskites as next generation thermionic emitter materials
Ryan Jacobs, Dane Morgan and John Booske

Our initial work was funded by Defense Advance Research Project Agency (DARPA) through the Innovative Vacuum Electronic Science and Technology (INVEST) project [18, 23, 27]. For later work the authors would like to thank the Wisconsin Alumni Research Foundation (WARF) for providing financial support for this work [25–27].

3. Hexaborides materials for thermionic cathodes
Muhammad M Hasan

The author gratefully acknowledges the financial support given by the Australian Renewable Energy Agency (ARENA), Grant No. 1-A065, and the SUST Research Centre, Shahjalal University of Science and Technology, Sylhet, Bangladesh.

4. Functionalized CVD diamond and other NEA materials for electron emission
Ramiz Zulkharnay, Neil A Fox and Paul W May

R Z wishes to thank the UK Atomic Energy Authority for postdoctoral funding through the Studying Tritium in Diamond Energy Structures (STRIDES) Phase II programme, and the Royal Society of Chemistry for funding support through a Researcher Collaborations Grant (C25-8928513904). This work was supported by the Engineering and Physical Sciences Research Council (EPSRC) under Grant No. EP/K030302/1/46623.

5. 2D materials for thermionic electrodes (theoretical models)
L K Ang

L K A would like to acknowledge the support of Singapore A*STAR IRG (M23M6c0102).

6. Engineering of electrode surfaces to enhance TEC performance
Chace Franey and Mohammad Ghashami

This work was supported by NSF/EPSCoR RII Track-1: Emergent Quantum Materials and Technologies (EQUATE), Grant No. OIA-2044049.

7. Characterization methods of low WF coatings
Alessio Mezzi

The author would like to warmly thank Professor Saulius Kaciulis for his collaboration and inspiration on many research activities, like the study of WF, over the last 25 years.

8. Thermionic devices using cesium
Jared W Schwede

The author gratefully acknowledges discussions with and input from P Schindler, A Lietz, J McVey, I Hamilton, N Cook, C Hall, F Schmitt, and L Hess.

9. Spacers for the inter-electrode gap in thermionic devices
Nicolas A Loubet, Katie Bezdjian, Esther López and Alejandro Datas

This work is part of the projects TED2021-131778B-C21 (funded by MCIN/AEI/10.13039/501100011033 and the European Union 'NextGenerationEU'/PRTR) and PID2020-115719RB-C22 (funded by MICIU/AEI/10.13039/501100011033). Funded by the European Union through Grant Agreement 101160724 (BLAZETEC project). Views and opinions expressed are however those of the authors only and do not necessarily reflect those of the European Union. Neither the European Union nor the granting authority can be held responsible for them.

10. Space-charge in thermionic energy conversion
Mohammadamin Jalili and Alireza Nojeh

We thank the Natural Sciences and Engineering Research Council of Canada, the Canada Foundation for Innovation, the British Columbia Knowledge Development Fund, BCFRST/the British Columbia Innovation Council, the Canada First Research Excellence Fund Quantum Materials and Future Technologies Program, CMC Microsystems, Compute Canada, and the University of British Columbia for financial support of our thermionics research.

11. Thermodynamic approaches of thermionic-based converters
Ehsanur Rahman and Xin Zhang

Ehsanur Rahman acknowledges a basic research grant from BUET, and Xin Zhang acknowledges the financial support from the Natural Science Foundation of Jiangsu Province (BK20221063).

12. Recent progress in data-driven discovery of stable low WF materials
Peter Schindler

P S gratefully acknowledges the start-up funds from Northeastern University, Department of Mechanical and Industrial Engineering.

13. New methods for the prediction of performance of thermionic materials and devices
Elizabeth D Juette, Van P Carey and Jean-Pierre Fleurial

This work was supported by a NASA Space Technology Graduate Research Opportunity (Grant No. 80NSSC22K1220) and the endowment of the A. Richard Newton Chair in Engineering at UC Berkeley. Part of the research was carried out at the Jet Propulsion Laboratory, California Institute of Technology, under a contract with the National Aeronautics and Space Administration (80NM0018D0004).

14. Development of PETE converters
Matteo Mastellone, Alessandro Bellucci and Daniele M Trucchi

The authors gratefully acknowledge the TECHPRO 'Thermionic Energy Conversion for High Power RadiatiOn' PRIN2022 Project No. 2022KXKR3S funded by the Italian Ministry of University and Research (MUR) within the framework of the EU Programme Next Generation Europe, and the SPEEDHY ('Solar PhotoElectrochEmical black Diamond converters for HYdrogen and ammonia production') project, funded by the European Union-Next Generation EU, Mission 4 Component 1, CUP B53D23015370006, MUR project 2022J9CEFM. This work reflects only the authors' views and opinions, neither the MUR nor the European Commission can be considered responsible for them.

15. Advances in hybrid TIPV energy converters
Alejandro Datas

This work is part of the Projects TED2021-131778B-C21, funded by MCIN/AEI/10.13039/501100011033 and the European Union ('NextGenerationEU'/PRTR), and BLAZETEC, funded by the European Union through Grant Agreement 101160724. The views and opinions expressed in this work are solely those of the authors and do not necessarily reflect those of the European Union. Neither the European Union nor the granting authority assumes responsibility for them.

16. Carbon footprint and economics of thermionic topping system
Guanghua Zheng and Lili Wang

The authors gratefully acknowledge the support by the National Natural Science Foundation of China (No. 52406231), the Baima Lake Laboratory Joint Funds of the Zhejiang Provincial Natural Science

Foundation (Nos. LBMHY25E060004, LBMHY24E060014) and the Zhejiang Educational Committee Foundation (No. Y202351883).

17. Present and future applications of thermionics
Gang Xiao and Hao Qiu

The authors gratefully acknowledge the support from the National Natural Science Foundation of China (No. 52406258) and the Natural Science Foundation of Shandong Province (Nos. ZR2024QE199 and ZR2025MS819).

ORCID iDs

Alessandro Bellucci 0000-0001-7509-3318
Daniele M Trucchi 0000-0001-8278-4707
Gideon Segev 0000-0002-6175-3458
Ryan Jacobs 0000-0003-2229-6730
John Booske 0000-0001-5051-602X
Muhammad M Hasan 0000-0003-4472-2681
Ramiz Zulkharnay 0000-0002-7420-399X
L K Ang 0000-0003-2811-1194
Mohammad Ghashami 0000-0001-5033-0495
Nicolas A Loubet 0009-0005-4197-6995
Esther López 0000-0003-4256-9329
Alejandro Datas 0000-0001-5964-3818
Mohammadamin Jalili 0000-0002-6732-4785
Alireza Nojeh 0000-0001-8683-1195
Ehsanur Rahman 0000-0003-0757-3285
Peter Schindler 0000-0002-1319-6570
Elizabeth D Juette 0009-0000-9483-6383
Matteo Mastellone 0000-0002-4291-6477
Hao Qiu 0000-0001-8290-1467

References

[1] Trucchi D M and Melosh N A 2017 Electron-emission materials: advances, applications, and models *MRS Bull.* **42** 488–92
[2] Hatsopoulos G N and Gyftopoulos E P 1973 *Thermionic Energy Conversion: Processes and Devices* (MIT Press)
[3] Eindhoven N, Wolff L R, Veltkamp W B, Schoonen J M W M and Hendriksen H A M (eds) 1990 *Thermionic Energy Conversion* (Eindhoven University of Technology)
[4] Gryaznov G M, Zhabotinskii E E, Zrodnikov A V, Nikolaev Y V, Ponomarev-Stepnoi N N, Pupko V Y, Serbin V I and Usov V A 1989 Thermoemission reactor-converters for nuclear power units in outer space *Sov. At. Energy* **66** 414–8
[5] Campbell M F, Celenza T J, Schmitt F, Schwede J W and Bargatin I 2021 Progress toward high power output in thermionic energy converters *Adv. Sci.* **8** 2003812
[6] Trucchi D M, Bellucci A, Girolami M, Calvani P, Cappelli E, Orlando S, Polini R, Silvestroni L, Sciti D and Kribus A 2018 Solar thermionic-thermoelectric generator (ST^2G): concept, materials engineering, and prototype demonstration *Adv. Energy Mater.* **8** 1802310
[7] Khalid K A A, Leong T J and Mohamed K 2016 Review on thermionic energy converters *IEEE Trans. Electron Devices* **63** 2231–41
[8] Hasan M M, Cuskelly D, Sugo H and Kisi E H 2015 Low temperature synthesis of low thermionic work function $(La_xBa_{1-x})B_6$ *J. Alloys Compd.* **636** 67–72
[9] Kirkwood D M *et al* 2018 Frontiers in thermionic cathode research *IEEE Trans. Electron Devices* **65** 2061–71
[10] Seif N, Zhou Q, Liu X, Balk T J and Beck M J 2022 Sc-containing (scandate) thermionic cathodes: fabrication, microstructure, and emission performance *IEEE Trans. Electron Devices* **69** 3513–22
[11] Seif M N, Zhou Q, Liu X, Balk T J and Beck M J 2022 Sc-containing (scandate) thermionic cathodes: mechanisms for Sc enhancement of emission *IEEE Trans. Electron Devices* **69** 3523–34
[12] Liang S J, Liu B, Hu W, Zhou K and Ang L K 2017 thermionic energy conversion based on graphene van der Waals heterostructures *Sci. Rep.* **7** 46211
[13] Schwede J W *et al* 2010 Photon-enhanced thermionic emission for solar concentrator systems *Nat. Mater.* **9** 762–7
[14] Bellucci A, García-Linares P, Martí A, Trucchi D M and Datas A 2022 A three-terminal hybrid thermionic-photovoltaic energy converter *Adv. Energy Mater.* **12** 2200357
[15] Bellucci A, Girolami M, Mastellone M, Orlando S, Polini R, Santagata A, Serpente V, Valentini V and Trucchi D M 2021 Novel concepts and nanostructured materials for thermionic-based solar and thermal energy converters *Nanotechnology* **32** 024002
[16] Rahman E and Nojeh A 2020 Harvesting solar thermal energy with a micro-gap thermionic-thermoelectric hybrid energy converter: model development, energy exchange analysis, and performance optimization *Energy* **204** 117947
[17] Wang Y, Su S, Liu T, Su G and Chen J 2015 Performance evaluation and parametric optimum design of an updated thermionic-thermoelectric generator hybrid system *Energy* **90** 1575–83

[18] Lin L, Jacobs R, Ma T, Chen D, Booske J and Morgan D 2023 Work function: fundamentals, measurement, calculation, engineering, and applications *Phys. Rev. Appl.* **19** 037001

[19] Chen X F, Lu H, Zhu W G and Tan O K 2005 Enhanced field emission of silicon tips coated with sol–gel-derived $(Ba_{0.65}Sr_{0.35})TiO_3$ thin film *Surf. Coat. Technol.* **198** 266–9

[20] Yang T-H, Harn Y-W, Chiu K-C, Fan C-L and Wu J-M 2012 Promising electron field emitters composed of conducting perovskite $LaNiO_3$ shells on ZnO nanorod arrays *J. Mater. Chem.* **22** 17071

[21] Jacobs R, Booske J and Morgan D 2016 Understanding and controlling the work function of perovskite oxides using density functional theory *Adv. Funct. Mater.* **26** 5471–82

[22] Zhong Z and Hansmann P 2016 Tuning the work function in transition metal oxides and their heterostructures *Phys. Rev. B* **93** 1–9

[23] Lin L, Jacobs R, Chen D, Vlahos V, Lu-Steffes O, Alonso J A, Morgan D and Booske J 2022 Demonstration of low work function perovskite $SrVO_3$ using thermionic electron emission *Adv. Funct. Mater.* **32** 2203703

[24] Bundaleski N, Trigueiro J, Silva A G, Moutinho A M C and Teodoro O M N D 2013 Influence of the patch field on work function measurements based on the secondary electron emission *J. Appl. Phys.* **113** 183720

[25] Sheikh M S, Jacobs R, Morgan D and Booske J 2024 Time dependence of $SrVO_3$ thermionic electron emission properties *J. Appl. Phys.* **135** 055104

[26] Sheikh M S, Lin L, Jacobs R, Kordesch M E, Sadowski J T, Charpentier M, Morgan D and Booske J 2024 Direct evidence of low work function on $SrVO_3$ cathode using thermionic electron emission microscopy and high-field ultraviolet photoemission spectroscopy *APL Mater.* **12** 061105

[27] Lin L, Jacobs R, Morgan D and Booske J 2023 Investigating thermionic emission properties of polycrystalline perovskite $BaMoO_3$ *IEEE Trans. Electron Devices* **70** 1871–7

[28] Ren Z, Ren Z, Zhang Z, Buonassisi T and Li J 2023 Autonomous experiments using active learning and AI *Nat. Rev. Mater.* **8** 563–4

[29] Montoya J H *et al* 2022 Toward autonomous materials research: recent progress and future challenges *Appl. Phys. Rev.* **9** 011405

[30] Schindler P, Antoniuk E R, Cheon G, Zhu Y and Reed E J 2024 Discovery of stable surfaces with extreme work functions by high-throughput density functional theory and machine learning *Adv. Funct. Mater.* **34** 2401764

[31] Deng B, Zhong P, Jun K, Riebesell J, Han K, Bartel C J and Ceder G 2023 CHGNet: pretrained universal neural network potential for charge-informed atomistic modeling *Nat. Mach. Intell.* **5** 1031–41

[32] Barroso-Luque L *et al* 2024 Open materials 2024 (OMat24) inorganic materials dataset and models (arXiv: 2410.12771)

[33] Jain A 2024 Machine learning in materials research: developments over the last decade and challenges for the future *Curr. Opin. Solid State Mater. Sci.* **33** 101189

[34] Lafferty J M 1951 Boride cathodes *J. Appl. Phys.* **22** 299–309

[35] Goebel D M and Katz I 2008 *Fundamental of Electric Propulsion* (Wiley) 10.1002/9780470436448

[36] Futamoto M, Nakazawa M and Kawabe U 1980 Thermionic emission properties of hexaborides *Surf. Sci.* **100** 470–80

[37] Olsen G H and Cafiero A V 1978 Single-crystal growth of mixed (La, Eu, Y, Ce, Ba, Cs) hexaborides for thermionic emission *J. Cryst. Growth* **44** 287–90

[38] Bellucci A, Mastellone M, Girolami M, Serpente V, Sani E, Sciti D and Trucchi D M 2021 Thermionic emission measurement of sintered lanthanum hexaboride discs and modelling of their solar energy conversion performance *Ceram. Int.* **47** 20736–9

[39] Hasan M M, Kisi E and Sugo H 2021 Synthesis of nanostructured lanthanum hexaboride via simple borothermal routes at low temperatures *Ceram. Int.* **47** 29295–302

[40] Hasan M M, Kisi E and Sugo H 2022 Single-step low-temperature synthesis routes for (Ba, Ce, Gd) hexaborides and their thermionic emission properties *J. Alloys Compd.* **916** 165474

[41] Ma M, Yang X, Meng H, Zhao Z, He J and Chu Y 2023 Nanocrystalline high-entropy hexaboride ceramics enable remarkable performance as thermionic emission cathodes *Fundam. Res.* **3** 979–87

[42] Wang Y, Xu J, Luo S, Bao Y, Zhang J, Han C, Yang X and Zhang J 2023 Spark plasma sintering and characterization of bulk $La_{1-x}Sr_xB_6$ hexaborides *Ceram. Int.* **49** 22882–9

[43] Ma T, Jacobs R, Booske J and Morgan D 2021 Work function trends and new low-work-function boride and nitride materials for electron emission applications *J. Phys. Chem. C* **125** 17400–10

[44] Nakazawa M, Futamoto M, Usami K and Kawabe U 1981 Surface compositions of hexaborides at high temperatures *J. Appl. Phys.* **52** 6917–20

[45] Bellucci A *et al* 2020 Nanocrystalline lanthanum boride thin films by femtosecond pulsed laser deposition as efficient emitters in hybrid thermionic photovoltaic energy converters *Appl. Surf. Sci.* **513** 145829

[46] Storms E K and Mueller B A 1979 A study of surface stoichiometry and thermionic emission using LaB_6 *J. Appl. Phys.* **50** 3691–8

[47] Jacobson D L and Storms E K 1978 Work function measurement of lanthanum—boron compounds *IEEE Trans. Plasma Sci.* **6** 191–9

[48] Back T C, Schmid A K, Fairchild S B, Boeckl J J, Cahay M, Derkink F, Chen G and Sayir A 2017 Work function characterization of directionally solidified LaB_6–VB_2 eutectic *Ultramicroscopy* **183** 67–71

[49] Hasan M M, Kisi E and Sugo H 2023 Structural and thermionic emission investigations of perovskite $BaHfO_3$ based low work function emitters *Mater. Sci. Eng. B* **296** 116679

[50] Scheer J J and van Laar J 1965 GaAs-Cs: a new type of photoemitter *Solid State Commun.* **3** 189–93

[51] James M C, Fogarty F, Zulkharnay R, Fox N A and May P W 2021 A review of surface functionalisation of diamond for thermionic emission applications *Carbon* **171** 532–50

[52] Zulkharnay R, Fox N A and May P W 2024 Enhanced electron emission performance and air-surface stability in sco-terminated diamond for thermionic energy converters *Small* **20** 2405408

[53] Martinelli R U and Fisher D G 1974 The application of semiconductors with negative electron affinity surfaces to electron emission devices *Proc. IEEE* **62** 1339–60

[54] Xiao G, Zheng G, Qiu M, Li Q, Li D and Ni M 2017 Thermionic energy conversion for concentrating solar power *Appl. Energy* **208** 1318–42

[55] Koeck F A M and Nemanich R J 2017 Advances in thermionic energy conversion through single-crystal n-type diamond *Front. Mech. Eng.* **3** 1–11

[56] Zulkharnay R and May P W 2024 Applications of diamond films: a review *Funct. Diam.* **4** 2410160

[57] Zulkharnay R and May P W 2023 Experimental evidence for large negative electron affinity from scandium-terminated diamond *J. Mater. Chem. A* **11** 13432–45

[58] Nebel C E 2003 Electronic properties of CVD diamond *Semicond. Sci. Technol.* **18** S1
[59] Yoshida R, Miyata D, Makino T, Yamasaki S, Matsumoto T, Inokuma T and Tokuda N 2018 Formation of atomically flat hydroxyl-terminated diamond (1 1 1) surfaces via water vapor annealing *Appl. Surf. Sci.* **458** 222–5
[60] Zulkharnay R, Greenwood W, Wood A, Laverock J and Fox N A 2026 Achieving a large net 'negative electron affinity' on diamond (100) via molecular oxygen and lithium functionalization *ACS Appl. Mater. Interfaces* **18** 9032–42
[61] Bellucci A, Girolami M, Mastellone M, Mezzi A, Serpente V, Orlando S, Santagata A, Polini R, Kribus A and Trucchi D M 2026 Demonstrating black-diamond-based high-temperature solar cells *Joule* **10** 102223
[62] Croot A, Wan G, Rowan A, Andrade H D, Smith J A and Fox N A 2017 Beta radiation enhanced thermionic emission from diamond thin films *Front. Mech. Eng.* **3** 1–8
[63] Jensen K L 2017 *Introduction to the Physics of Electron Emission* (Wiley)
[64] Liang S-J and Ang L K 2015 Electron thermionic emission from graphene and a thermionic energy converter *Phys. Rev. Appl.* **3** 014002
[65] Trushin M 2018 Theory of thermionic emission from a two-dimensional conductor and its application to a graphene-semiconductor Schottky junction *Appl. Phys. Lett.* **112** 171109
[66] De D K and Olawole O C 2019 A three-dimensional model for thermionic emission from graphene and carbon nanotube *J. Phys. Commun.* **3** 015004
[67] Ang Y S, Yang H Y and Ang L K 2018 Universal scaling laws in Schottky heterostructures based on two-dimensional materials *Phys. Rev. Lett.* **121** 056802
[68] Wei X, Chen Q and Peng L 2013 Electron emission from a two-dimensional crystal with atomic thickness *AIP Adv.* **3** 042130
[69] Ang Y S, Chen Y, Tan C and Ang L K 2019 Generalized high-energy thermionic electron injection at graphene interface *Phys. Rev. Appl.* **12** 014057
[70] Ang L K, Ang Y S and Lee C H 2023 Universal model for electron thermal-field emission from two-dimensional semimetals *Phys. Plasmas* **30** 033103
[71] Luo Y, Yang H Y, Ang Y S and Ang L K 2024 Analytical model of optical-field-driven sub-cycle electron tunneling pulses from two-dimensional materials *Nano Lett.* **24** 3882
[72] Hernandez N, Cahay M, O'Mara J, Ludwick J, Walker D E Jr, Back T and Hall H 2024 Field emission characteristics of AlGaN/GaN nanoscale lateral vacuum diodes *J. Appl. Phys.* **135** 204305
[73] Lepetit B 2021 A quantum mechanical model of electron field emission from two dimensional materials. Application to graphene *J. Appl. Phys.* **129** 144302
[74] Chan W J, Ang Y S and Ang L K 2021 Thermal-field electron emission from three-dimensional Dirac and Weyl semimetals *Phys. Rev. B* **104** 245420
[75] Kahaly M U, Misra S and Mishra S K 2017 Photo-assisted electron emission from illuminated monolayer graphene *J. Appl. Phys.* **121** 205110
[76] Massicotte M, Schmidt P, Vialla F, Watanabe K, Taniguchi T, Tielrooij K J and Koppens F H L 2016 Photo-thermionic effect in vertical graphene heterostructures *Nat. Commun.* **7** 12174
[77] Hassan M O, Takahata K and Nojeh A 2021 Space charge in a vacuum diode: from macroscopic to microscopic gaps *J. Appl. Phys.* **130** 024502
[78] Jassem A, Chernin D, Petillo J J and Lau Y Y 2021 Analysis of anode current from a thermionic cathode with a 2D work function distribution *IEEE Trans. Plasma Sci.* **49** 749
[79] Devon Jensen A N M T E, Ghashami M and Park K 2021 Submicrometer-gap thermionic power generation based on comprehensive modeling of charge and thermal transport *Phys. Rev. Appl.* **15** 024062
[80] Smith J R, Nemanich R J and Bilbro G L 2006 The effect of Schottky barrier lowering and nonplanar emitter geometry on the performance of a thermionic energy converter *Diam. Relat. Mater.* **15** 870
[81] Franey C, Al-Ameri B M, Acosta G I and Ghashami M 2024 Enhancement of thermionic power generation via engineered microstructures *Phys. Rev. Appl.* **21** 024004
[82] Barmina E V, Serkov A A, Stratakis E, Fotakis C, Stolyarov V N, Stolyarov I N and Shafeev G A 2012 Nano-textured W shows improvement of thermionic emission properties *Appl. Phys. A* **106** 1
[83] Lim I T, Lambert S A, Vay J-L and Schwede J W 2018 Electron reflection in thermionic energy converters *Appl. Phys. Lett.* **112** 073906
[84] Dahdolan M and Ghashami M 2021 Comprehensive theoretical framework for the analysis of microgap thermionic energy conversion under constant heat inputs *Energy Convers. Manage.* **245** 114600
[85] Islam M, Inal O T and Luke J R 2006 Development of electron reflection suppression materials for improved thermionic energy converter performance using thin film deposition techniques *J. Appl. Phys.* **100** 084903
[86] Cauduro A L F, Hess L H, Ogletree D F, Schwede J W and Schmid A K 2019 Tailoring low energy electron absorption via surface nano-engineering of cesiated chromium films *Appl. Phys. Lett.* **115** 071602
[87] Jin F and Beaver A 2017 High thermionic emission from barium strontium oxide functionalized carbon nanotubes thin film surface *Appl. Phys. Lett.* **110** 213109
[88] Zhang Z M 2020 *Nano/Microscale Heat Transfer* (Springer International Publishing)
[89] Florian C, Kirner S V, Krüger J and Bonse J 2020 Surface functionalization by laser-induced periodic surface structures *J. Laser Appl.* **32** 022063
[90] Kim J W and Kim A 2021 Absolute work function measurement by using photoelectron spectroscopy *Curr. Appl. Phys.* **31** 52–9
[91] Yoshitake M 2021 *Work Function and Band Alignment of Electrode Materials: The Art of Interface Potential for Electronic Devices, Solar Cells, and Batteries, NIMS Monographs* (Springer) (https://doi.org/10.1007/978-4-431-56898-8)
[92] Pakhira N and Mahato R 2023 Role of work function distribution on field emission effects *Physica B* **670** 415394
[93] Yoshitake M 2021 *Work Function and Band Alignment of Electrode Materials, NIMS Monographs* (Springer) (https://doi.org/10.1007/978-4-431-56898-8)
[94] Mishra K C, Garner R and Schmidt P C 2004 Model of work function of tungsten cathodes with barium oxide coating *J. Appl. Phys.* **95** 3069
[95] Zurcher P and Bauer R S 1983 Photoemission determination of dipole layer and VB-discontinuity formation during the MBE growth of GaAs on Ge(110) *J. Vac. Sci. Technol. A* **1** 695
[96] Olawolea O C *et al* 2022 Progress in the experimental and computational methods of work function evaluation of materials: a review *Heliyon* **8** e11030
[97] Bellucci A 2026 The quest for low work function materials: advances, challenges, and opportunities *Crystals* **16** 47

[98] Kim J S, Lägel B, Moons E, Johansson N, Baikie I D, Salaneck W R, Friend R H and Cacialli F 2000 Kelvin probe and ultraviolet photoemission measurements of indium tin oxide work function: a comparison *Synth. Met.* **111–2** 311–4
[99] Martinez E, Guedj C, Mariolle D, Licitra C, Renault O, Bertin F, Chabli A, Imbert G and Delsol R 2008 Electronic and chemical properties of the TaN/*a*-SiOC:H stack studied by photoelectron spectroscopy for advanced interconnects *J. Appl. Phys.* **104** 073708
[100] Mezzi A, Soltani P, Kaciulis S, Bellucci A, Girolami M, Mastellone M and Trucchi D M 2018 Investigation of work function and chemical composition of thin films of borides and nitrides *Surf. Interface Anal.* **50** 1138–44
[101] Bellucci A *et al* 2019 Lanthanum (oxy)boride thin films for thermionic emission applications *Appl. Surf. Sci.* **479** 296–302
[102] Mezzi A, Bolli E, Kaciulis S, Mastellone M, Girolami M, Serpente V, Bellucci A, Carducci R, Polini R and Trucchi D M 2020 Work function and negative electron affinity of ultrathinbarium fluoride films, Surf *Interface Anal.* **52** 968–74
[103] Mezzi A, Bolli E, Kaciulis S, Bellucci A, Paci B, Generosi A, Mastellone M, Serpente V and Trucchi D M 2023 Multi-technique approach for work function exploration of Sc_2O_3 thin films *Nanomaterials* **13** 1430
[104] Rasor N S and Warner C 1964 Correlation of emission processes for adsorbed alkali films on metal surfaces *J. Appl. Phys.* **35** 2589–600
[105] Hatsopoulos G N and Gyftopoulos E P 1979 *Thermionic Energy Conversion* vol 2 (MIT Press)
[106] Becker R A 1967 Thermionic space power systems review *J. Spacecr. Rockets* **4** 847–51
[107] Fitzpatrick G O and Britt E J 1978 Thermionics and its application to the SPS *Radiation Energy Conversion in Space* (American Institute of Aeronautics and Astronautics) pp 211–21
[108] Gryaznov G M 2000 *30th Anniversary of the Startup of Topaz—The First Thermionic Nuclear Reactor in the World* (Springer Nature) (https://doi.org/10.1007/BF02673508)
[109] Rasor N 1991 Thermionic energy conversion plasmas *IEEE Trans. Plasma Sci.* **19** 1191–208
[110] Rasor N S 2017 Hybrid mode cesium diode thermionic converter *J. Appl. Phys.* **121** 203304
[111] Rasor N S 1993 The collector enigma *The Thermioinc Conversion Specialist Conf.* p 22
[112] Rahman E and Nojeh A 2020 Interplay between near-field radiative coupling and space-charge effects in a microgap thermionic energy converter under fixed heat input *Phys. Rev. Appl.* **14** 24082
[113] Dick R S, McVey J B, Fitzpatrick G O and Britt E J 1983 High performance, close-spaced thermionic converters *Proc. Intersociety Energy Conversion Engineering Conf.* pp 198–201
[114] Fitzpatrick G, Lawless J, Nikolaev Y and Klinkov A 1993 Demonstration of close-spaced thermionic converters (ACS)
[115] Lietz A M, Groenewald R E, Scherpelz P and Hopkins M M 2023 Kinetic simulations of ignited mode cesium vapor thermionic converters *J. Appl. Phys.* **133** 023301
[116] Campanell M, Wang C and Nguyen K 2025 Two mechanisms limiting the emitted electron current from a cathode to an anode *Phys. Rev. Lett.* **134** 145301
[117] King D B 2001 The microminiature thermionic converter *AIP Conf. Proc.* **552** 1152–7
[118] Lee J-H, Bargatin I, Vancil B K, Gwinn T O, Maboudian R, Melosh N A and Howe R T 2014 Microfabricated thermally isolated low work-function emitter *J. Microelectromech. Syst.* **23** 1182–7
[119] Campbell M F *et al* 2020 Nanostructured spacers for thermionic and thermophotovoltaic energy converters *J. Microelectromech. Syst.* **29** 637–44
[120] Geller C B *et al* 1996 *Final Reports of the High Efficiency Thermionics (HET-IV) and Converter Advancement (CAP) Programs* (West Mifflin) (https://doi.org/10.2172/225989)
[121] Mustafaev A S, Yarygin V I, Soukhomlinov V S, Tsyganov A B and Kaganovich I D 2018 Nano-size effects in graphite/graphene structure exposed to cesium vapor *J. Appl. Phys.* **124** 123304
[122] Chou S H, Voss J, Bargatin I, Vojvodic A, Howe R T and Abild-Pedersen F 2012 An orbital-overlap model for minimal work functions of cesiated metal surfaces *J. Phys.: Condens. Matter* **24** 445007
[123] Lee J-H, Bargatin I, Melosh N A and Howe R T 2012 Optimal emitter-collector gap for thermionic energy converters *Appl. Phys. Lett.* **100** 173904
[124] Beggs J E 1963 Vacuum thermionic energy converter *Adv. Energy Convers.* **3** 447–53
[125] Loubet N A, Bezdjian K, López E and Datas A 2025 Micro/nanoscale spacers for enhanced thermophotovoltaic and thermionic energy conversion: a comprehensive review *Sol. Energy Mater. Sol. Cells* **289** 113673
[126] Belbachir R Y, An Z and Ono T 2014 Thermal investigation of a micro-gap thermionic power generator *J. Micromech. Microeng.* **24** 085009
[127] Belbachir R Y, An Z and Ono T 2016 Impact of thermal contact resistances on micro-gap heat losses for microthermionic power generators *Microsyst. Technol.* **22** 2811–20
[128] Nicaise S M *et al* 2019 Micron-gap spacers with ultrahigh thermal resistance and mechanical robustness for direct energy conversion *Microsyst. Nanoeng.* **5** 31
[129] Lang S, Sharma G, Molesky S, Kränzien P U, Jalas T, Jacob Z, Petrov A Y and Eich M 2017 Dynamic measurement of near-field radiative heat transfer *Sci. Rep.* **7** 13916
[130] Sabbaghi P, Long L, Ying X, Lambert L, Taylor S, Messner C and Wang L 2020 Super-Planckian radiative heat transfer between macroscale metallic surfaces due to near-field and thin-film effects *J. Appl. Phys.* **128** 025305
[131] Ito K, Miura A, Iizuka H and Toshiyoshi H 2015 Parallel-plate submicron gap formed by micromachined low-density pillars for near-field radiative heat transfer *Appl. Phys. Lett.* **106** 083504
[132] Bellucci A *et al* 2021 Dielectric micro- and sub-micrometric spacers for high-temperature energy converters *Energy Technol.* **9** 2000788
[133] Zeneli M, Bellucci A, Sabbatella G, Fotopoulou M, Apostolopoulos V, Stamatopoulos P, Trucchi D M, Nikolopoulos A and Rakopoulos D 2023 Thermal assessment of dielectric microspacer technology using an advanced three-dimensional simulation model *Sustainability* **15** 1786
[134] Littau K A, Sahasrabuddhe K, Barfield D, Yuan H, Shen Z-X, Howe R T and Melosh N A 2013 Microbead-separated thermionic energy converter with enhanced emission current *Phys. Chem. Chem. Phys.* **15** 14442–6
[135] Alvarez-Quintana J, Ll. Peralba-Garcia J L L and Rodríguez-Viejo J 2009 Ultra-low thermal conductivity in nanoscale layered oxides *J. Heat Transfer* **132** 032402
[136] DeSutter J, Tang L and Francoeur M 2019 A near-field radiative heat transfer device *Nat. Nanotechnol.* **14** 751–5
[137] Wanke R, Voesch W, Rastegar I, Kyriazis A, Braun W and Mannhart J 2017 Thermoelectronic energy conversion: concepts and materials *MRS Bull.* **42** 518–24
[138] Zhang P, Valfells Á, Ang L K, Luginsland J W and Lau Y Y 2017 100 years of the physics of diodes *Appl. Phys. Rev.* **4** 011304

[139] Rahman E and Nojeh A 2023 Micro-gap thermo-photo-thermionics: an alternative approach to harvesting thermo-photons and its comparison with thermophotovoltaics *Appl. Therm. Eng.* **224** 119993

[140] Zhao M, Fang S, Jiang Z and Yu J 2024 Effect of near-field evanescent wave heat transfer on the performance of a cesium thermionic energy converter with graphene anode *J. Power Sources* **605** 234519

[141] Edelen J P, Cook N M, Hall C C, Hu Y, Tan X and Vay J-L 2020 Advanced modeling of field enhanced thermionic emission *J. Vac. Sci. Technol. B* **38** 043201

[142] Chen D, Jacobs R, Petillo J, Vlahos V, Jensen K L, Morgan D and Booske J 2022 Physics-based model for nonuniform thermionic electron emission from polycrystalline cathodes *Phys. Rev. Appl.* **18** 054010

[143] Zhang P and Pan T 2017 Exact analytical theory for inverse tunneling of free vacuum electrons into a solid *AIP Adv.* **7** 065307

[144] Dehnavi A *et al* 2023 Application of machine learning and artificial intelligence in design, optimization, and control of power electronics converters for renewable energy-based technologies *Power Electronics Converters and Their Control for Renewable Energy Applications* (Elsevier) pp 283–300

[145] Datas A and Vaillon R 2019 Thermionic-enhanced near-field thermophotovoltaics *Nano Energy* **61** 10–17

[146] Garg P, Kumar P and Srinivasan K 2013 Supercritical carbon dioxide Brayton cycle for concentrated solar power *J. Supercrit. Fluids* **76** 54–60

[147] Rahman E and Nojeh A 2021 Semiconductor thermionics for next generation solar cells: photon enhanced or pure thermionic? *Nat. Commun.* **12** 4622

[148] Bellucci A *et al* 2020 Photovoltaic anodes for enhanced thermionic energy conversion *ACS Energy Lett.* **5** 1364–70

[149] Zhang X, Ye Z, Su S and Chen J 2018 Thermionic-thermoradiative converters *IEEE Electron Device Lett.* **39** 1429

[150] Wang S, Zheng G, Ding N, Wang G and Xu J 2025 Thermodynamic analysis of combustion based photon enhanced thermionic emission-gas turbine energy conversion *Appl. Therm. Eng.* **258** 124669

[151] Kongtragool B and Wongwises S 2003 A review of solar-powered Stirling engines and low temperature differential Stirling engines *Renew. Sustain. Energy Rev.* **7** 131–54

[152] Chen H, Goswami D Y and Stefanakos E K 2010 A review of thermodynamic cycles and working fluids for the conversion of low-grade heat *Renew. Sustain. Energy Rev.* **14** 3059–67

[153] Smith J R, Bilbro G L and Nemanich R J 2006 Using negative electron affinity diamond emitters to mitigate space charge in vacuum thermionic energy conversion devices *Diam. Relat. Mater.* **15** 2082–5

[154] Wang Y *et al* 2023 Machine learning study on the electron emission properties of the thermionic cathode impregnants *2023 24th Int. Vacuum Electronics Conf. (IVEC)* (IEEE) pp 1–2

[155] Juette E D, Carey V P and Fleurial J P 2024 Physical versus data-driven modeling of thermionic device performance over the full range of power generation operating conditions *Energy Sustain.* **87899** V001T10A002

[156] Fernandez J G *et al* 2023 Optimization of thermionic cooling semiconductor heterostructures with deep learning techniques *2023 Int. Conf. Simulation of Semiconductor Processes and Devices (SISPAD)* (IEEE) (https://doi.org/10.23919/SISPAD57422.2023.10319607)

[157] De Waele S, Lejaeghere K, Sluydts M and Cottenier S 2016 Error estimates for density-functional theory predictions of surface energy and work function *Phys. Rev. B* **94** 235418

[158] Patra A, Bates J E, Sun J and Perdew J P 2017 Properties of real metallic surfaces: effects of density functional semilocality and van der Waals nonlocality *Proc. Natl Acad. Sci.* **114** E9188–E96

[159] Palizhati A, Zhong W, Tran K, Back S and Ulissi Z W 2019 Toward predicting intermetallics surface properties with high-throughput DFT and convolutional neural networks *J. Chem. Inf. Model.* **59** 4742–9

[160] Focassio B, Freitas L P M and Schleder G R 2025 Performance assessment of universal machine learning interatomic potentials: challenges and directions for materials' surfaces *ACS Appl. Mater. Interfaces* **17** 1311–2

[161] Mehdizadeh A and Schindler P 2025 Surface stability modeling with universal machine learning interatomic potentials: a comprehensive cleavage energy benchmarking study *AI Sci.* **1** 025002

[162] Owen C J, Xie Y, Johansson A, Sun L and Kozinsky B 2024 Low-index mesoscopic surface reconstructions of Au surfaces using Bayesian force fields *Nat. Commun.* **15** 3790

[163] Rønne N, Aspuru-Guzik A and Hammer B 2024 Generative diffusion model for surface structure discovery *Phys. Rev. B* **110** 235427

[164] Antoniuk E R, Schindler P, Schroeder W A, Dunham B, Pianetta P, Vecchione T and Reed E J 2021 Novel ultrabright and air-stable photocathodes discovered from machine learning and density functional theory driven screening *Adv. Mater.* **33** 2104081

[165] Witman M D and Schindler P 2025 MatFold: systematic insights into materials discovery models' performance through standardized cross-validation protocols *Digit. Discovery* **4** 625–35

[166] Hsu C, Schlesinger C, Mudaliar K, Leung J, Walters R and Schindler P 2025 FIRE-GNN: force-informed, relaxed equivariance graph neural network for rapid and accurate prediction of surface properties *Adv. Intell. Discovery* **0** e202500162

[167] Shi G, Wang Y, Yang K, Qiu Y, Zhu H and Zeng X 2026 A surface emphasized multi-task learning framework for surface property predictions: a case study of magnesium intermetallics *J. Magn. Alloys* **14** 101622

[168] Roy P, Rekhi L, Koh S W, Li H and Choksi T S 2023 Predicting the work function of 2D MXenes using machine-learning methods *J. Phys. Energy* **5** 034005

[169] Hatsopoulos G N and Gyftopoulos E P 1979 *Thermionic Energy Conversion. Volume II. Theory, Technology, and Application* (MIT Press)

[170] Zavadil K R, Battaile C C, Marshall A C, King D B and Jennison D R 2004 Low work function material development for the microminiature thermionic converter

[171] Khoshaman A H and Alireza N 2016 A self-consistent approach to the analysis of thermionic devices *J. Appl. Phys.* **119** 044902

[172] Go D B, Haase J R, George J, Mannhart J, Wanke R, Nojeh A and Nemanich R 2017 Thermionic energy conversion in the twenty-first century: advances and opportunities for space and terrestrial applications *Front. Mech. Eng.* **3** 296537

[173] Juette E D, Carey V P and Fleurial J-P 2024 Physical versus data-driven modeling of thermionic device performance over the full range of power generation operating conditions *ASME 2024 18th Int. Conf. Energy Sustainability* p V001T10A002

[174] Hula G 2015 *Atomic Power in Space II: A History of Space Nuclear Power and Propulsion in the United States* (Idaho National Laboratory (INL))

[175] Raissi M, Perdikaris P and Karniadakis G E 2019 Physics-informed neural networks: a deep learning framework for solving forward and inverse problems involving nonlinear partial differential equations *J. Comput. Phys.* **378** 686–707

[176] Wu C, Zhu M, Tan Q, Kartha Y and Lu L 2023 A comprehensive study of non-adaptive and residual-based adaptive sampling for physics-informed neural networks *Comput. Methods Appl. Mech. Eng.* **403** 115671

[177] Smestad G P 2004 Conversion of heat and light simultaneously using a vacuum photodiode and the thermionic and photoelectric effects *Sol. Energy Mater. Sol. Cells* **82** 227–40
[178] Su S, Zhang H, Chen X, Kang J and Chen J 2013 Parametric optimum design of a photon-enhanced thermionic solar cell *Sol. Energy Mater. Sol. Cells* **117** 219–24
[179] Wang Y, Liao T, Zhang Y, Chen X, Su S and Chen J 2016 Effects of nanoscale vacuum gap on photon-enhanced thermionic emission devices *J. Appl. Phys.* **119** 45106
[180] Xiao G, Zheng G, Ni D, Li Q, Qiu M and Ni M 2018 Thermodynamic assessment of solar photon-enhanced thermionic conversion *Appl. Energy* **223** 134–45
[181] Varpula A and Prunnila M 2012 Diffusion-emission theory of photon enhanced thermionic emission solar energy harvesters *J. Appl. Phys.* **112** 044506
[182] Segev G, Rosenwaks Y and Kribus A 2015 Limit of efficiency for photon-enhanced thermionic emission vs. photovoltaic and thermal conversion *Sol. Energy Mater. Sol. Cells* **140** 464–76
[183] Liu L, Diao Y and Xia S 2019 High-performance GaAs nanowire cathode for photon-enhanced thermionic emission solar converters *J. Mater. Sci.* **54** 5605–14
[184] Schindler P, Riley D C, Bargatin I, Sahasrabuddhe K, Schwede J W, Sun S, Pianetta P, Shen Z-X, Howe R T and Melosh N A 2019 Surface photovoltage-induced ultralow work function material for thermionic energy converters *ACS Energy Lett.* **4** 2436–43
[185] Schwede J W *et al* 2013 Photon-enhanced thermionic emission from heterostructures with low interface recombination *Nat. Commun.* **4** 1576
[186] Reck K, Dionigi F and Hansen O 2014 Photon-enhanced thermionic emission in cesiated p-type and n-type silicon *29th European Photovoltaic Solar Energy Conf. Exhibition* pp 328–30
[187] Koeck F A, Nemanich R J, Lazea A and Haenen K 2009 Thermionic electron emission from low work-function phosphorus doped diamond films *Diam. Relat. Mater.* **18** 789–91
[188] Sun T, Koeck F A M, Rezikyan A, Treacy M M J and Nemanich R J 2014 Thermally enhanced photoinduced electron emission from nitrogen-doped diamond films on silicon substrates *Phys. Rev. B* **90** 121302
[189] Salerno R *et al* 2024 Low electron affinity silicon/nanocrystalline diamond heterostructures for photon-enhanced thermionic emission *ACS Appl. Energy Mater.* **7** 868–73
[190] Calvani P, Bellucci A, Girolami M, Orlando S, Valentini V, Polini R and Trucchi D M 2016 Black diamond for solar energy conversion *Carbon* **105** 401–7
[191] Segev G, Kribus A and Rosenwaks Y 2013 High performance isothermal photo-thermionic solar converters *Sol. Energy Mater. Sol. Cells* **113** 114–23
[192] Bellucci A, Caposciutti G, Antonelli M and Trucchi D M 2023 Techno-economic evaluation of future thermionic generators for small-scale concentrated solar power systems *Energies* **16** 1190
[193] Datas A 2016 Hybrid thermionic-photovoltaic converter *Appl. Phys. Lett.* **108** 143503
[194] Bellucci A, Linares P G, Villa J, Martí A, Datas A and Trucchi D M 2022 Hybrid thermionic-photovoltaic converter with an $In_{0.53}Ga_{0.47}As$ anode *Sol. Energy Mater. Sol. Cells* **238** 111588
[195] Qiu H, Lin S, Xu H, Hao G and Xiao G 2022 Hybrid thermionic-photovoltaic converter with graphene-on-semiconductor heterojunction anode for efficient electricity generation *iScience* **25** 105051
[196] Bellucci A, García-Linares P, Martí A, Trucchi D M and Datas A 2022 A three-terminal hybrid thermionic-photovoltaic energy converter *Adv. Energy Mater.* **12** 2200357
[197] Qiu H, Lin S, Xu H, Hao G and Xiao G 2023 Experimental and theoretical study on hybrid thermionic-photovoltaic energy converters with graphene/semiconductor Schottky junction *Energy Convers. Manage.* **276** 116584
[198] Liao T, Zhang X, Chen X and Chen J 2019 Near-field thermionic-thermophotovoltaic energy converters *J. Appl. Phys.* **125** 203103
[199] Datas A and Vaillon R 2019 Thermionic-enhanced near-field thermophotovoltaics for medium-grade heat sources *Appl. Phys. Lett.* **114** 133501
[200] Liao T, Du J, Guo J, Chen X and Chen J 2019 Schottky junction-based thermophotovoltaic-thermionic devices *J. Phys. D: Appl. Phys.* **53** 055503
[201] Li W, Peng W, Yang Z, Su G, Su S and Chen J 2020 Performance improvements and parametric design strategies of an updated thermionic-photovoltaic converter *Phys. Scr.* **95** 035208
[202] Xiao J, Du J, Su S and Chen J 2021 The maximum efficiency and parametric optimum selection of a solar-driven thermionic-photovoltaic integrated device *IEEE Trans. Electron Devices* **68** 632–7
[203] Rahman E and Nojeh A 2022 The effects of electronic and photonic coupling on the performance of a photothermionic-photovoltaic hybrid solar device *Sol. Energy Mater. Sol. Cells* **247** 111945
[204] Qiu H, Xu H and Xiao G 2023 Hybrid photon-enhanced thermionic emission and photovoltaic converter with concentrated solar power *Sol. Energy Mater. Sol. Cells* **254** 112279
[205] Zhang X, Ang Y S, Du J-Y, Chen J and Ang L K 2020 Graphene-based thermionic-thermoradiative solar cells: concept, efficiency limit, and optimum design *J. Clean. Prod.* **242** 118444
[206] Zheng G, Chen Y, Ding N and Xu J 2023 Inner-cascaded photovoltaic-thermionic-thermoradiative conversion for concentrated solar power *Sol. Energy* **264** 112063
[207] Fitzpatrick G O and Allen D T 1990 Thermionic converter: normal and transparent collectors *Energy Conversion Engineering Conf., 1990. IECEC-90. Proc. 25th Intersociety* pp 283–9
[208] Barrigón E, García I, Barrutia L, Rey-Stolle I and Algora C 2014 Highly conductive p++-AlGaAs/n++-GaInP tunnel junctions for ultra-high concentrator solar cells *Prog. Photovolt. Res. Appl.* **22** 399–404
[209] Song J, Han J, Choi M and Lee B J 2022 Modeling and experiments of near-field thermophotovoltaic conversion: a review *Sol. Energy Mater. Sol. Cells* **238** 111556
[210] Zhang Z, Zheng G, Wang L, Ding N and Xu J 2025 Environmental, energy and economic assessment of thermionic enhanced solar dish–Stirling power generation *Sol. Energy* **285** 113125
[211] Musacchio A, Bartocci P, Serra A, Cencioni L, Colantoni S and Fantozzi F 2021 Decarbonizing materials sourcing and machining in the gas turbine sector, through a cost-carbon footprint nexus analysis *J. Clean. Prod.* **310** 127392
[212] Reddy V S, Kaushik S C, Ranjan K R and Tyagi S K 2013 State-of-the-art of solar thermal power plants—a review *Renew. Sustain. Energy Rev.* **27** 258–73
[213] Souza D, Basquiroto F, Gao W and Duan W 2022 Graphene opens pathways to a carbon-neutral cement industry *Sci. Bull.* **67** 5–8

[214] Lazard 2025 Levelized cost of energy + (available at: www.lazard.com/research-insights/levelized-cost-of-energyplus-lcoeplus/)
[215] Bett A W and Sulima O V 2003 GaSb photovoltaic cells for applications in TPV generators *Semicond. Sci. Technol.* **18** S184
[216] Kishita Y, Ohishi Y, Uwasu M, Kuroda M, Takeda H and Hara K 2016 Evaluating the life cycle CO_2 emissions and costs of thermoelectric generators for passenger automobiles: a scenario analysis *J. Clean. Prod.* **126** 607–19
[217] Stylos N and Koroneos C 2014 Carbon footprint of polycrystalline photovoltaic systems *J. Clean. Prod.* **64** 639–45
[218] Yang P, Jiang H, Liu C, Kang L and Wang C 2023 Coordinated optimization scheduling operation of integrated energy system considering demand response and carbon trading mechanism *Int. J. Electr. Power Energy Syst.* **147** 108902
[219] Yang M and Liu Y 2023 Research on multi-energy collaborative operation optimization of integrated energy system considering carbon trading and demand response *Energy* **283** 129117
[220] Xie L, Qiu Z, He Y, Tian R, Meng T, Tan S and Zhao F 2024 Physical optimization and safety analysis of space thermionic reactor *Prog. Nucl. Energy* **168** 105010
[221] Jousten K, Boineau F, Bundaleski N, Illgen C, Setina J, Teodoro O M N D, Vicar M and Wüest M 2020 A review on hot cathode ionisation gauges with focus on a suitable design for measurement accuracy and stability *Vacuum* **179** 109545
[222] Song Z and Xie Z 2018 A literature review of *in situ* transmission electron microscopy technique in corrosion studies *Micron* **112** 69–83
[223] Qiu H, Xu H, Ni M and Xiao G 2022 Photo-thermo-electric modeling of photon-enhanced thermionic emission with concentrated solar power *Sol. Energy Mater. Sol. Cells* **246** 111922
[224] Inaguma T, Tsuda N and Yamada J 2010 Short circuit current of thermionic energy converter by resonance light irradiation *Electr. Eng. Japan* **158** 14–21
[225] Ito T and Cappelli M A 2012 Optically pumped cesium plasma neutralization of space charge in photon-enhanced thermionic energy converters *Appl. Phys. Lett.* **101** 213901
[226] Qiu H, Hao M, Meng B, Sun A and Xiao G 2023 Theories, advances, challenges, and innovations in photon-enhanced thermionic emission technology for concentrating solar systems *Renew. Sustain. Energy Rev.* **227** 116558